FIRST Payload Module/Focal Plane Unit Straylight Model:

Final Report

Prepared by: A.G.Richards (APART analysis)
M.Caldwell (ASAP analysis)

Address: Optical Systems Group
Space Science Department
Rutherford Appleton Laboratory
Chilton, Didcot, Oxfordshire OX11 0QX
United Kingdom

Date: May 11 2001

Issue: 1.1

RAL Document Ref: SPIRE/RAL/N/0101.01
RAL Contract Ref: 023/94

ESA Document Ref:
ESA Contract Ref: ESTEC 10975/94/NL/CC.

CONTENTS

FIGURES

TABLES

0. CHANGES

Issue	Date	Changes
1.0	April 29, 1999	First issue.
1.1	May 11, 2001	Corrected some typos and mislabelled table and figure references; Corrected sign error in equation for Y axis shift in table 6.4-1

1. INTRODUCTION

This report describes the work carried out for ESA specified in the statement of work, PT-SW-06020, and the proposal SSD-PROP-06020 issued in response to it. The main task was to construct and verify, using the Breault Research Organisation's (BRO) APART straylight analysis software package, a mathematical model that will allow the determination of the straylight entering a Focal Plane Unit (FPU) from the FIRST payload module (PLM). Strictly speaking, the PLM consists of the FIRST instrument cryostat but for the purposes of this work, representative APART models of the FIRST sunshield, the FIRST telescope (primary mirror, secondary mirror and secondary support structure) are also required. Because a detailed APART model existed for it, the SPIRE instrument was specified to be the representative 'real' FPU. A second task was to do a preliminary ASAP analysis of the beam pattern at the main optical components.

2. DOCUMENTS

The following documents (and documents referenced therein) and listings were the sources of geometrical, optical, surface and thermal properties included in the APART PLM/FPU straylight models described in this report:

#1 FIRST PLM/FPU Straylight model Statement of work, PT-SW-06020, issue 1, 2/11/98

#2 Zip file DSS97MODEL.ZIP containing APART scripts that formed the basis of earlier straylight analyses.

#3 Fax PT-06275, 19 January 1999, giving sunshield dimensions and telescope optical parameters

#4 Fax PT-06294, 25 January 1999, confirming tripod leg location and mechanical envelope data.

#5 SPIRE/RAL/N0044 issue 1, September 1998, 'Descriptions of CODEV and APART models of FIRST-SPIRE'

3. APART MODELLING – SOME CONSTRAINTS AND LIMITATIONS

3.1 Overview

APART is a deterministic stray radiation analysis program capable of predicting both the irradiance at any surface due to scattering and diffraction of unwanted radiation and predicting radiative thermal loads on surfaces. It consists of three programs:

Program 1 defines and verifies the geometry of objects. Each object is assigned and identified by an object number. Up to 300 objects may be defined. The co-ordinate system used forces the Z-axis to be always along the optical axis (see later section on the difficulties that this raises). Input files for this program must have .IN1 file type. A geometry definition file in binary format is output, along with a vector plot data file.

Program 2 is used to identify the objects that can be illuminated by external point sources, and the objects (critical objects) that can transfer radiation to the detector. It calculates 'Transfers'

between user-specified pairs of surfaces. This consists in determining projected solid angles and angular information relating sections of one surface to sections of another, which may be in different optical spaces. In these calculations, obscuring objects lying between two surfaces must be included and the user must specify the obscuring objects. Command input files for program 2 must have .IN2 file type. The geometry definition file output by program 1 is also used as input. A transfer file is updated and output in binary format.

Program 3 takes the successful (non-zero) transfers calculated by program 2 and combines them into user-specified scattering paths in order to determine the straylight power (in watts) reaching the specified 'final' surface (which is normally the FPU detector, but not always). In order to calculate these power transfers each surface is assigned a coating with specific scattering characteristics. For thermal emission, one or more wavebands can be specified and each surface is assigned a temperature and emissivity for a specific waveband. Input files for program 3 have .IN3 file type. Data on energy reaching the target surface is output in various forms.

3.2 APART Co-ordinate system

APART uses a standard co-ordinate break system. The Z-axis always follows the local optical axis. The Y-Z plane is then the meridional plane, X-Z is the sagittal plane. The Z-axis direction may change at an optical surface, if the optic is reflecting or refracting. Rotations of the optical surface also cause changes in the orientation of the Z-axis, and the orientation of either or both X- and Y-axes may also change. Figure 3.2-1 shows how the APART co-ordinate system will change as a result of a gut ray being reflected at point P on the primary mirror.

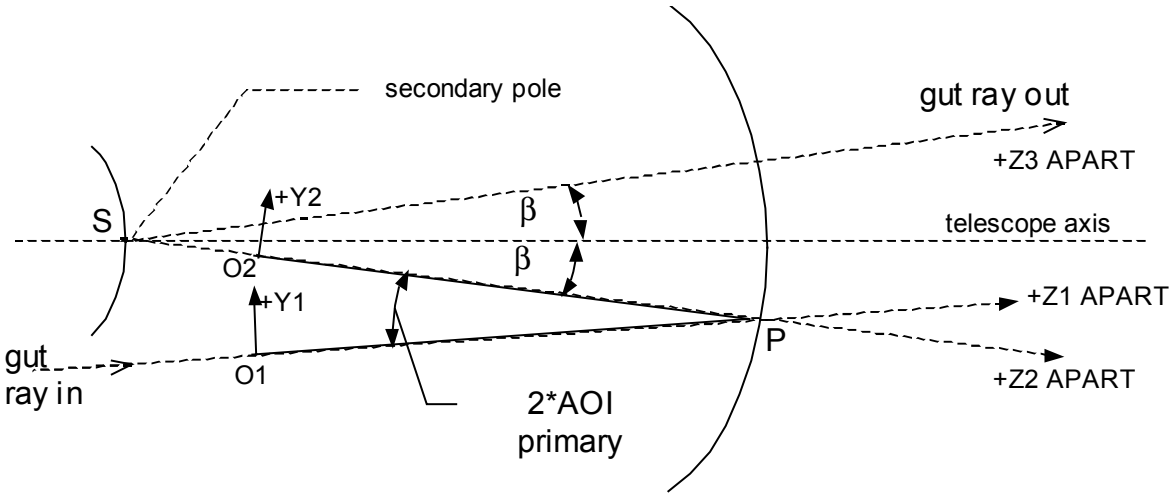

Figure 3.2-1 Change of APART co-ordinate frame at reflection point P

The APART Z-axis is rotated through an angle equal to twice the angle of incidence at the primary (AOI primary). The origin O2 of the rotated frame is located such that the distance O2P = distance O1P. In order to locate O2 at the pole of the secondary mirror, the distance O1P must be chosen equal to the path length PS of the gut ray between primary and secondary mirrors. In this example, the aperture stop is located at the secondary so the gut ray passes through S, the pole of the secondary mirror.

This type of co-ordinate break system makes it impossible for APART to output object geometry in the ESA specified co-ordinate system (see FIRST Telescope Assembly Specifications, FIRST PT-RQ-03832, 01.02.97) shown in figure 3.2-2. This calls for the origin to be at the centre of the telescope interface triangle, which must be on the telescope axis 125 mm from the pole of the primary. The +X axis must point towards target space at 90 degrees to the interface plane. The +Z axis must point toward the sun, which is nominally in the XZ plane at zero roll-angle, and be in the plane normal to the X-axis. The +Y axis completes a right-handed orthogonal reference frame.

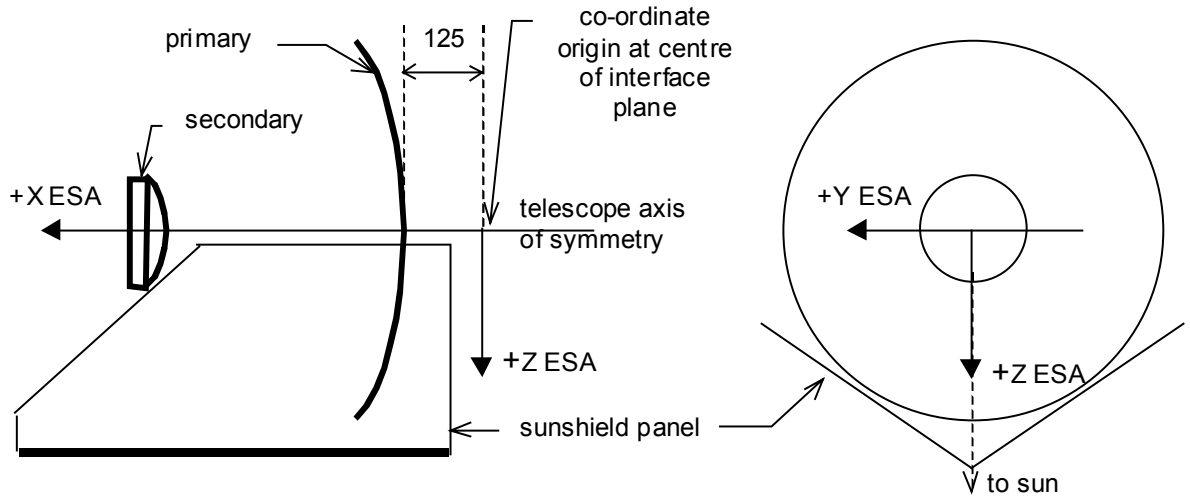

Figure 3.2-2 ESA co-ordinate system for FIRST

Because the gut ray direction determines APART's co-ordinate system, the location and orientation of the objects making up the optical surfaces and structure cannot be finally specified until the direction of this 'gut' ray is known. Even though the optics and the surrounding structure may have a natural co-ordinate system (e.g. one with the +Z axis along the telescope axis of symmetry), a gut ray to an off-axis viewing FPU detector will define a co-ordinate system which is tilted with respect to this 'natural' co-ordinate system. The FIRST telescope/PLM structure and optics must therefore be capable of being easily redefined in any co-ordinate system that may result from selecting a particular FPU detector's off-axis view direction for the gut ray.

Therefore a scheme was developed whereby as much use as possible was made of a 'natural' co-ordinate system. The geometry of every non-FPU object (and some of the FPU surfaces) is initially set up in a 'natural' co-ordinate system that has its origin at the centre of the secondary mirror and its +Z direction along the telescope axis towards the primary mirror (see figure 3.2-3). The +Y axis of this co-ordinate system is parallel to the ESA-specified –Z direction and the +X direction is parallel to the ESA-specified +Y direction. The task of transforming the object's location and orientation to the APART co-ordinate system was given to a specially written macro called XYZSHIFT. For correct operation, the macro must be supplied with the co-ordinate offsets of the centre of the secondary and the azimuth and elevation angles that transform from the 'natural' co-ordinate system to the APART gut ray co-ordinate system in the first optical space. A reference point is selected for each object which, when transformed using XYZSHIFT, orients and locates the object correctly in the APART system.

Although the APART co-ordinate system will change after a reflection at one of the optical surfaces, an object can be correctly positioned in a subsequent optical space by means of the APART 'REPEAT' command.

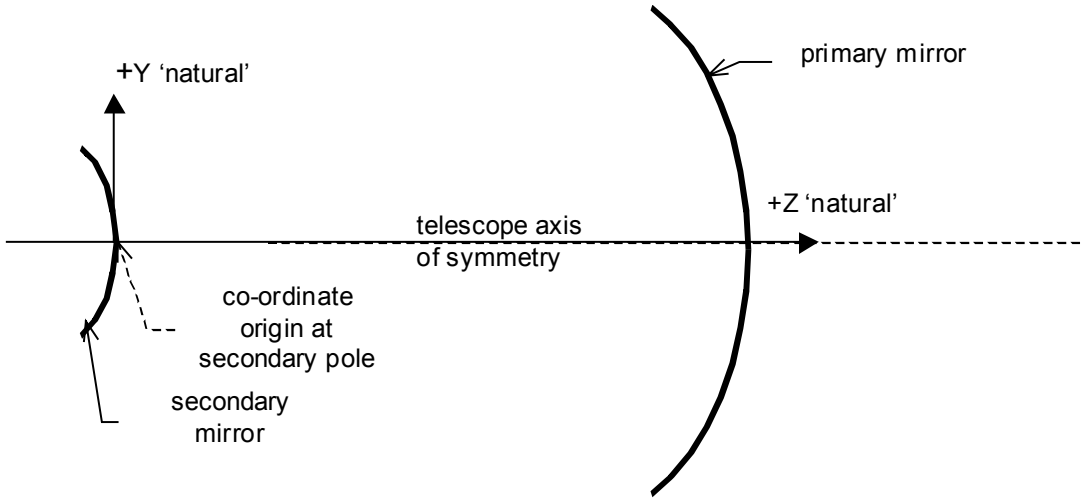

Figure 3.2-3 'Natural' co-ordinate system for defining telescope surfaces to APART

The 'origin' of the APART system in space 1 is chosen to be the point O1 located at a distance PS in front of the point of intersection P of the gut ray with the primary mirror (see figure 3.2-4b). The Z co-ordinate of the optical surface located at the primary is then equal to +PS. This selection ensures that O2 will be located at S, the pole of the secondary, making the APART Z2 co-ordinate of the secondary equal to zero. The plane of incidence of the gut ray will in general be inclined to the 'natural' YZ-plane by some azimuth angle ϕ (see figure 3.2-4a). In the plane of incidence, the angle that the input gut ray makes with the telescope axis direction is the elevation angle mentioned above (angle α in figure 3.2-4b). The gut-ray data (see table 3.2-1) are determined by using other special macros which essentially ray trace the system in reverse from the selected FPU detector to the telescope object space. These macros are collected in the file FIRSTEL.MAC. The macro XYZSHIFT is defined in the APART program 1 file TELINIT.IN1. Table 3.2-1 summarises the important parameters used to set up the space 1 co-ordinate frame, together with their APART identifiers.

Parameter	APART Identifier	Derivation or Link to other parameters
Gut ray path length between primary and secondary	PATH	
Azimuth of plane of incidence, ϕ	AZ_PRIME	Derived from FPU boresight
Elevation in plane of incidence, α	EL_PRIME	Derived from β and ray-tracing
Angle of incidence at secondary, β	AOISEC	Derived from FPU boresight
Angle of incidence at primary	AOIPRI	Derived from β and ray-tracing
Y-offset of pole of secondary in space 1	PS	PATH*SIN(2*AOIPRI)
Z-offset of pole of secondary in space 1	PC	PATH*(1-COS{2*AOIPRI})

Table 3.2-1 Parameters used to set up the APART space 1 co-ordinate frame

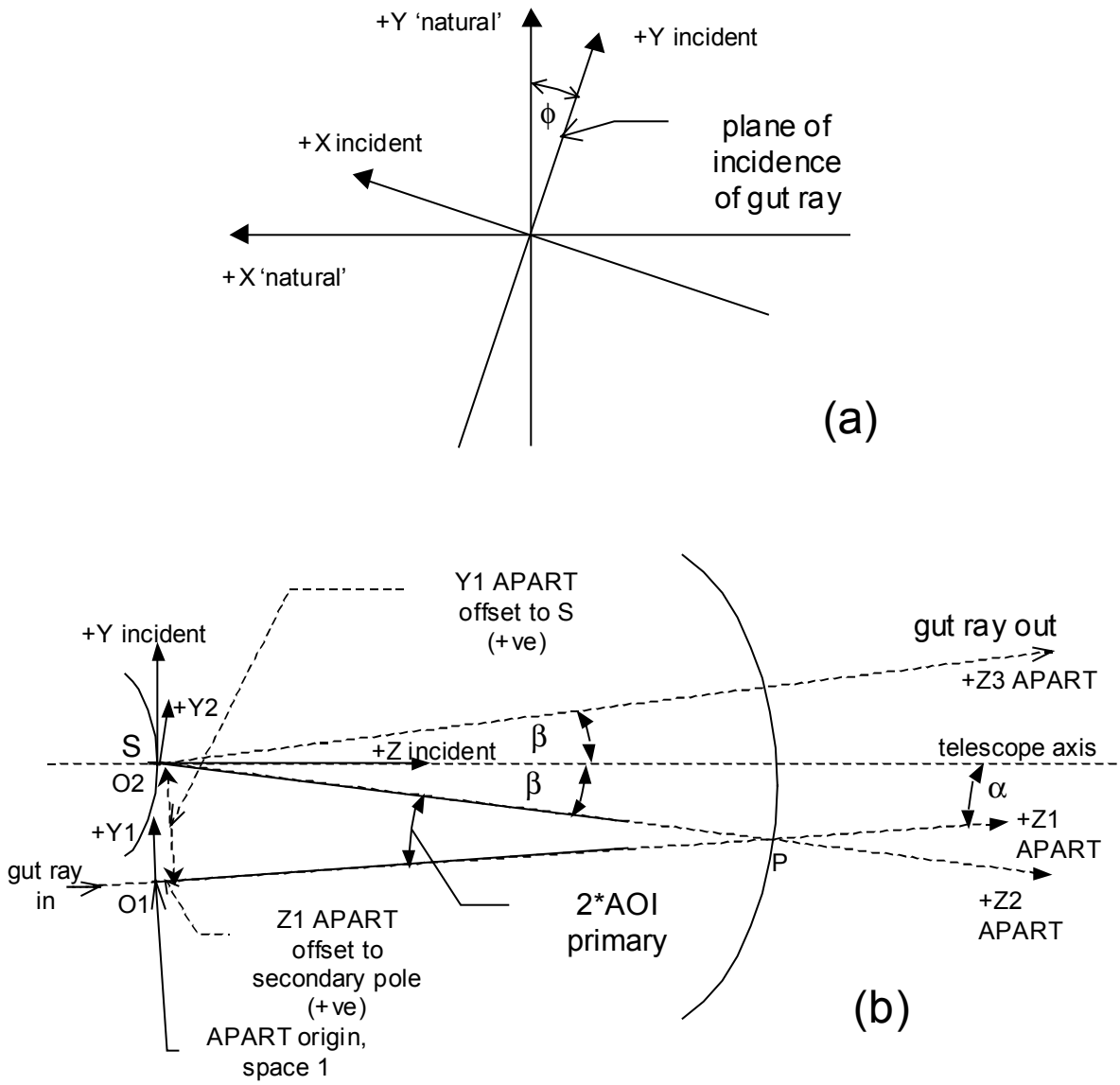

Figure 3.2-4 APART space 1, 2 and 3 co-ordinate frames for the FIRST telescope model

3.3 APART optical spaces

APART considers objects as existing in so-called optical spaces. These are regions which, when viewed from an external source, can be reached by passage through one or more 'optical' surfaces. An optical space must not be confused with a physical space. An optical space (apart from the first optical space) is physical space that is reached by passage through an optical surface. Separate optical spaces may involve identical or overlapping physical spaces. Figure 3.3-1 illustrates this. The physical space in front of the primary mirror covers part or all of optical spaces 1,2 and 3. The physical space behind the primary mirror covers part of optical spaces 1,2 and 4.

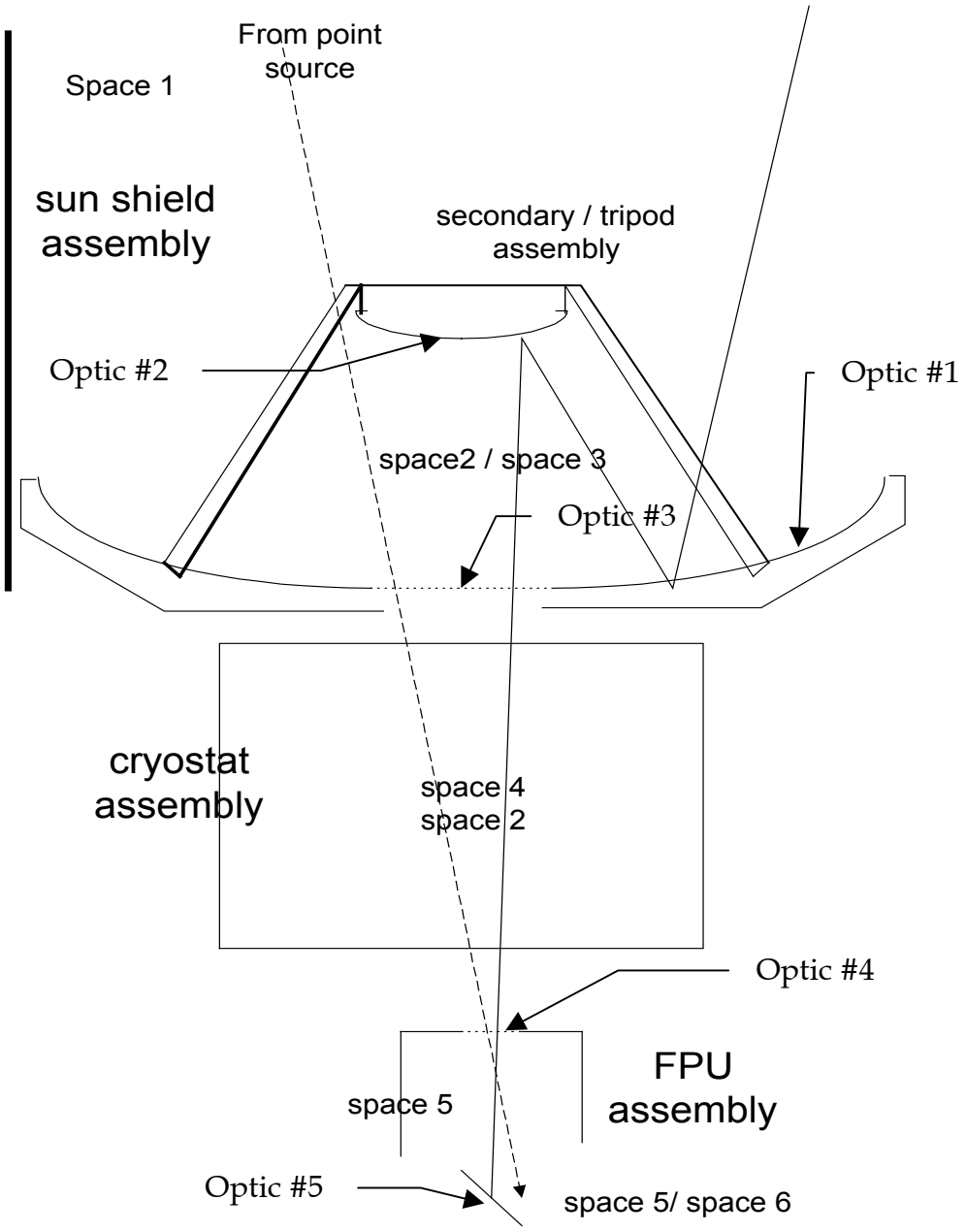

Figure 3.3-1 APART optical spaces for the FIRST PLM/FPU model

An APART 'optical' surface is one where a refraction or reflection may take place. It may be a 'real' surface, one that has optical and thermal properties attached to it, or it may be a dummy surface. The 'optical' surfaces are specified in the order in which they are intersected by the gut ray. In general, optical space N+1 is reached by passing through optic #N. Here, the first optical surface is located at the primary mirror, so an object in space 1 which transfers energy to an object in space 2 must send the radiation by reflection from the primary mirror. Equally, transfers from space 1 to space 3 involve reflections at the primary and secondary mirrors, in that order, whereas transfers from space 2 to space 3 involve a reflection from the secondary mirror only.

A dummy optical surface is often used to compartmentalise a complicated system in order to reduce the number of 'REPEAT's. In the present model, dummy optical surfaces are placed at the primary, at the front of the hole in the primary mirror and at the entrance aperture of each

FPU (other dummy surfaces are used within the detailed SPIRE FPU model). An optical surface is the only surface that is automatically included in two optical spaces and so it does not need to be repeated. There is an APART upper limit of 900 to the sum of the number of separate objects defined in the model (300 maximum) and twice the total number of times any surface is REPEATed into other spaces. This limit is almost reached with the present FIRST PLM/SPIRE FPU model, mainly due to the necessity of defining most of the objects in space 1 and repeating many of them into several subsequent spaces.

Taking one particular structure as an example, consider the tripod assembly, which supports the secondary mirror. This structure consisting of more than 20 objects 'exists' in the first optical space, in that it can theoretically be illuminated by radiation from an external point source without the light having to be reflected from the primary mirror. However, the tripod can also be illuminated by light that has been reflected by the primary, so the tripod must also 'exist' in optical space 2. The tripod can also be illuminated by light which starts in space 2 (say at the sunshield) and which is reflected by the secondary. So, the tripod structure must also 'exist' in space 3. Therefore, the tripod structure must be 'REPEAT'ed into spaces 2 and 3. Since radiation which enters space 4 by passing through the dummy optical surface at the front of the hole in the primary mirror is travelling behind the primary, it cannot reach the tripod and so the tripod does not need to be 'REPEAT'ed into subsequent spaces.

Taking the cryostat structure as an example, radiation from any surfaces suspended in front of the primary mirror can theoretically reach it by passing through the hole in the primary without being reflected from the primary or the secondary, so the cryostat surfaces must be defined in space 1. On the other hand, radiation originating at or being scattered by the cryostat surfaces can reach the secondary mirror directly, without reflection from the primary, so the cryostat surfaces must also 'exist' in optical space 2. The cryostat surfaces need not be repeated into space 3 but they do need to be 'REPEAT'ed into space 4, behind the hole in the primary. Similarly, FPU surfaces that can 'see' secondary mirror and tripod surfaces through the hole in the primary must also be defined in space 2. This means in practice that some FPU surfaces must be defined in space 1 and then REPEATed into space 2.

The need to consider and plan for repeating surfaces that make up major modules of the FIRST telescope/PLM/FPU into other optical spaces was intimately involved in the way that the APART program files were finally structured. Each time a new optical surface was specified and a new optical space defined, REPEAT commands for surfaces in each module had to be executed. The input file for each module was therefore split into sections flagged (using a variable SPACEARG) according to the optical space to which they applied. For space 1 (SPACEARG=1), the APART commands define surface geometry and in most cases the APART commands for subsequent spaces are just REPEAT commands.

4. THE ORIGINAL APART GEOMETRY CODE

4.1 Display of the Original model

The original APART program 1 code for the telescope /PLM geometry was received as a single file, FIRST.IN1. This file was input to APART97, the latest PC version of APART from the Breault Research Organisation (BRO) and the resulting vector plot file displayed and rotated using a wireframe display application WIREFRAME.EXE specially written by the author for displaying APART vector files. A view of the telescope model was saved in HPGL graphic format and it is displayed in figure 4.1-1.

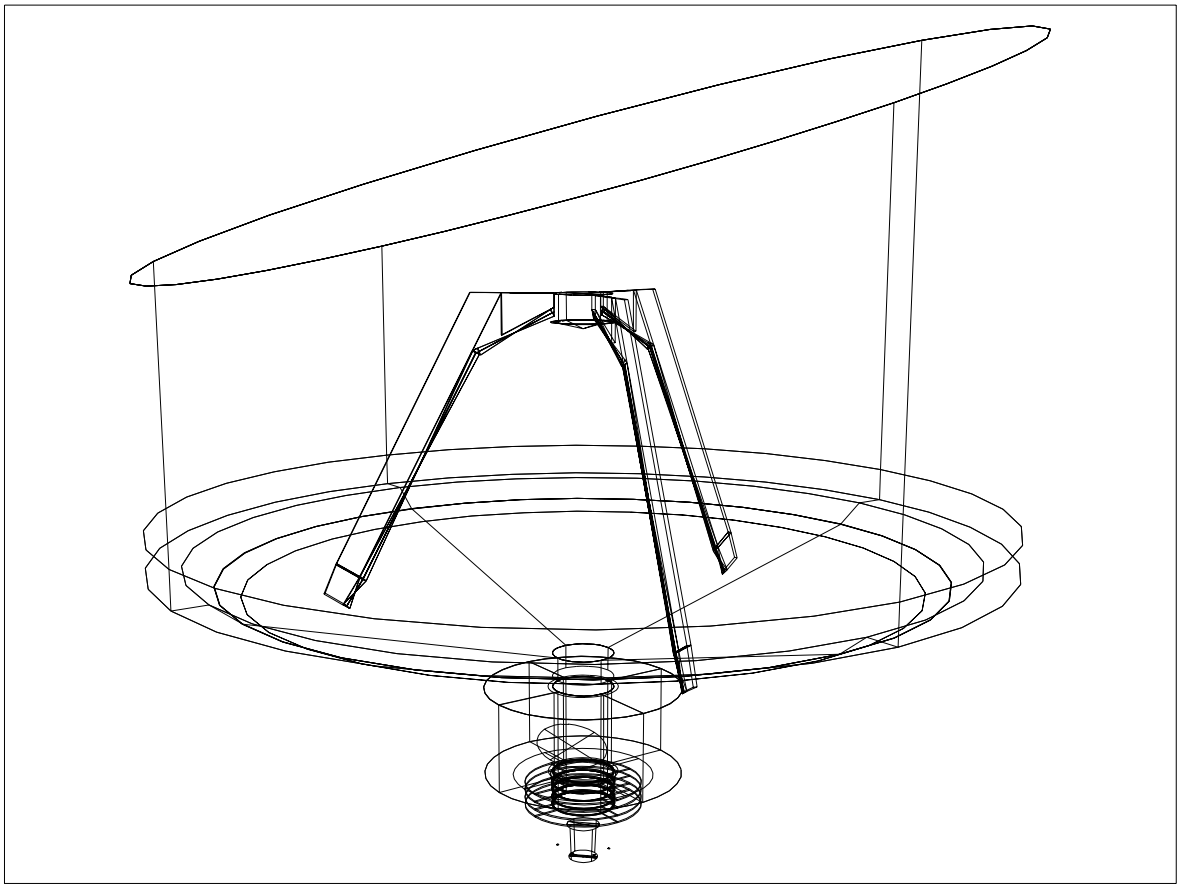

Figure 4.1-1 Original FIRST telescope / PLM model

Figure 4.1-1 shows that in the original geometry, the telescope has a sliced cylindrical sun shade, a tripod support for the secondary mirror, a representation of the inside of the cryostat and a detector located on-axis in the telescope focal plane.

After successfully running and displaying the original model, the next step was to list all of the APART object numbers used. It then became possible to identify numbers in the range 1-300 that remained available for any new objects that may need to be. This data is collected in the file FIRST_SURFACE_NUMBERS_OLD.DOC, part of which is reproduced in figure 4.1-2.

Object#	Type	ObjectLabel	SUN SHIELD	TRIPOD	SECON DARY	PRIM ARY	CRYO STAT	OPTIC	FPU
1	EDGE	ENTR.WINDOW	*						
2	CONE	SUN SHIELD	*						
3	DISK	SMOBSCURATION			*				
4	CONE	SMBACKSIDECONE			*				
5	RECT	TRIPOD1RECT		*					
6	RECT	TRIPOD2RECT		*					
7	RECT	TRIPOD3RECT		*					
8	EDGE	M2EDGEOBSC.			*				
9	EDGE	SUN SHIELDEDGE	*						
10	PYRAMID	LEG#1 BODY		*					
11	PYRAMID	LEG#1 INSERT		*					
12	FLAT	LEG#1 EDG.FAC#1		*					
13	FLAT	LEG#1 EDG.FAC#2		*					
14	PYRAMID	STRUT#1.INNER SECT		*					
15	PYRAMID	STRUT#1.OUTER SECT		*					
16	FLAT	STRUT#1 EDG.FAC1#		*					
17	FLAT	STRUT#1.EDG.FAC2#		*					
18	FLAT	INSERT#1EDG.FAC1#		*					
19	FLAT	INSERT#1EDG.FAC2#		*					
20	PYRAMID	LEG#2 BODY		*					
21	PYRAMID	LEG#2 INSERT		*					
22	FLAT	LEG#2.EDG.FAC#1		*					
23	FLAT	LEG#2.EDG.FAC#2		*					
24	PYRAMID	STRUT#2.INNER SECT		*					
25	PYRAMID	STRUT#2.OUTER SEC T		*					
26	FLAT	STRUT#2.EDG.FAC1#		*					
27	FLAT	STRUT#2.EDG.FAC2#		*					
28	FLAT	INSERT#2EDG.FAC1#		*					
29	FLAT	INSERT#2EDG.FAC2#		*					
30	PYRAMID	LEG#3 BODY		*					
31	PYRAMID	LEG#3 INSERT		*					
32	FLAT	LEG#3.EDG.FAC#1		*					
33	FLAT	LEG#3.EDG.FAC#2		*					
34	PYRAMID	STRUT#3.INNER SECT		*					
35	PYRAMID	STRUT#3.OUTER SECT		*					
36	FLAT	STRUT#3.EDG.FAC1#		*					
37	FLAT	STRUT#3.EDG.FAC2#		*					
38	FLAT	INSERT#3EDG.FAC1#		*					
39	FLAT	INSERT#3EDG.FAC2#		*					
40→104	-	(NOT USED)							
105	EDGE	Secondary 110% edge			*				
106→109		(NOT USED)							
110	RECT	PHOC detector							*
111	DISK	detector at fov=0°							*
112	DISK	detector at fov=0.1°							*
113	DISK	detector at fov=0.25°							*
114	DISK	detector at fov=-0.1°							*
115	DISK	detector at fov=-0.25°							*

Figure 4.1-2 Excerpt from FIRST_SURFACE_NUMBERS_OLD.DOC

The APART object numbers, object type and the text label for each object in the original model are given in the first three columns. Subsequent columns are used to flag the major subsystem with which the object is associated and whether the object is an APART optical surface.

4.2 Initial re-organisation of the Original model

After examining the geometry data in FIRST.IN1, the following steps were taken:

- The sun shield and associated objects were deleted from the model.
- The focal plane objects and associated surfaces were deleted from the model.
- The main parameters that determine the geometry of each of the main subsystems were identified and given an APART identifier.
- The APART code defining the geometry of all the remaining objects/surfaces was rewritten in terms of the main geometry parameters.
- The APART code defining all the remaining objects/surfaces was re-organised to express the geometry in the natural co-ordinate frame centred at the pole of the secondary and to give each object a reference point in this frame.

5. THE NEW GEOMETRY – ADDITIONS + MODIFICATIONS

We detail here the main parameters defining the geometry of the major modules and any major changes made to them.

5.1 Sun shield

The original sun shield design, which existed in the received model, was a sliced cone. The FIRST telescope design for L2 orbit involves a completely redesigned sun shield. The new design features two trapezium-shaped identical panels, joined along their long edge at an angle of 120 degrees. The assembly is located on the sunward side of the telescope with the junction aligned parallel to the telescope axis and at 90 degrees to the nominal telescope – sun line. Figures 5.1-1 and 5.1-2 show the main dimensions either taken directly from data in RD#3 or derived from such data. In these figures, all numbers enclosed by rectangular borders are to be considered given quantities from which all other dimensions follow by calculation. The numbers are used to define the APART parameters listed in table 5.1-1.

Parameter	APART identifier	Value
Projected width of panel with margin	PROJ_WID	2053
Angle of panel	ANG_PANEL	30 degrees
Length of innermost edge forwards of fixation plane	L_INEDGE	3375
Length of outermost edge forwards of fixation plane	L_OUTEDGE	1682
y-offset of panel end projected to PROJ_WID	Y_PANEL	924
Major Width of panel	BIGW	2306
Minor width of panel	SMALLW	206
Depth of dividing line below primary edge	DROP	100
Depth of lower panel	NEWH	600
Level of fixation plane below primary pole level	TEL_FIX	125
Sag of primary at edge	SAG_PM	403 (depends on curvature)

Table 5.1-1 Sun shield APART model parameters

In the latest model, each of the two panels is divided into two parts. The lower part starts 100 mm below the level of the edge of the primary and the upper part extends forwards from this level to a limit 3250 mm forwards of the plane level with the pole of the primary mirror. The lower extreme of the lower panel is uncertain but has been set 700 mm below the level of the primary edge. This will allow it to cover the gap between the back of the primary mirror and the front aperture of the cryostat with a margin of around 100mm. This strategy enables the application of different temperatures to the sections below and behind the primary that theoretically can radiate into the gap between the rear of the primary and the front aperture of the cryostat. The location of the dividing level is linked to the location of the edge of the primary mirror. This will depend on the sag of the mirror at its edge, so it depends on the actual mirror shape. The APART model will automatically respond to any choice made for the primary shape, so long as it is a conic of revolution.

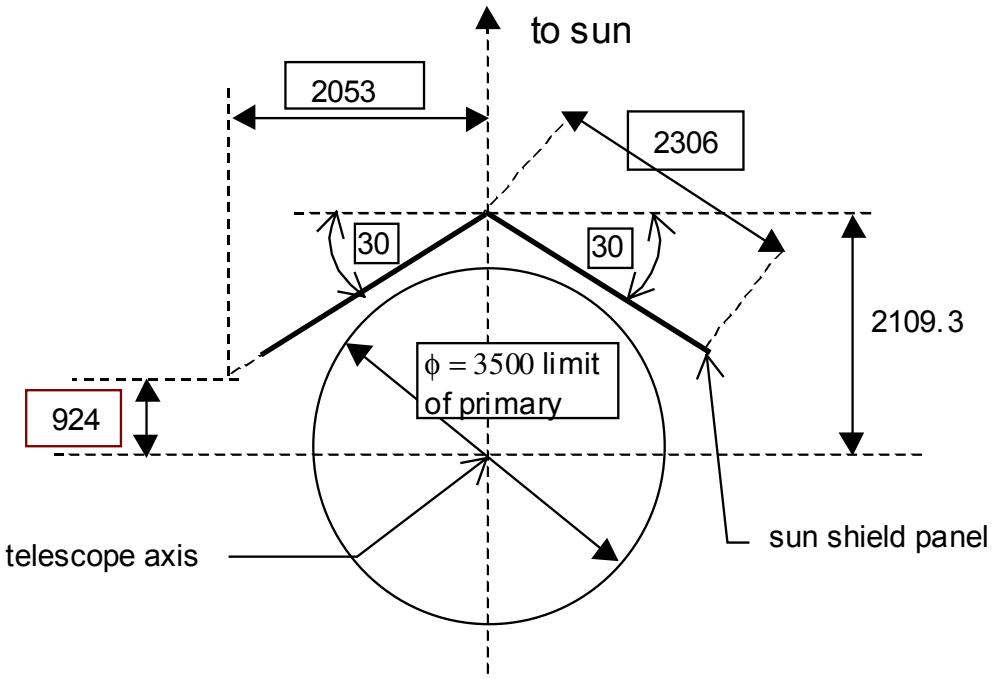

Figure 5.1-1 Location and orientation of the FIRST sun shield panels

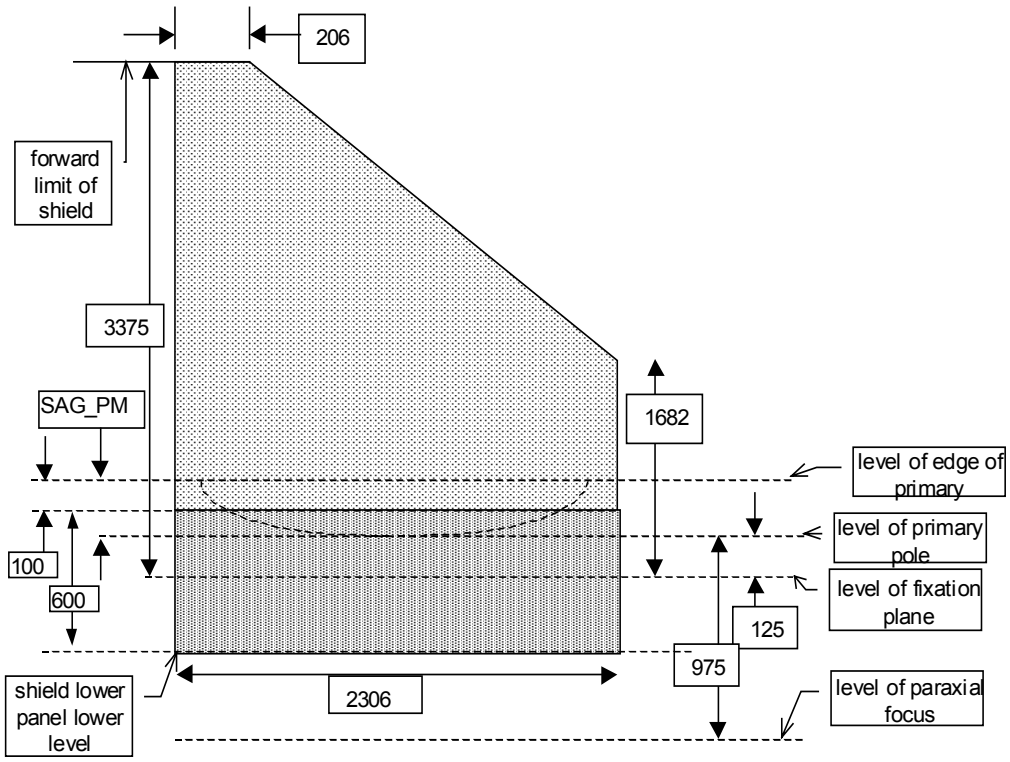

Figure 5.1-2 Dimensions of the modelled FIRST sun shield panels

Each of the main sun shield panels was represented initially using three surfaces/objects but each was also represented as a single object (a rectangle with one corner sliced off) as shown in figure 5.1-3. Diffracting edge objects were also added.

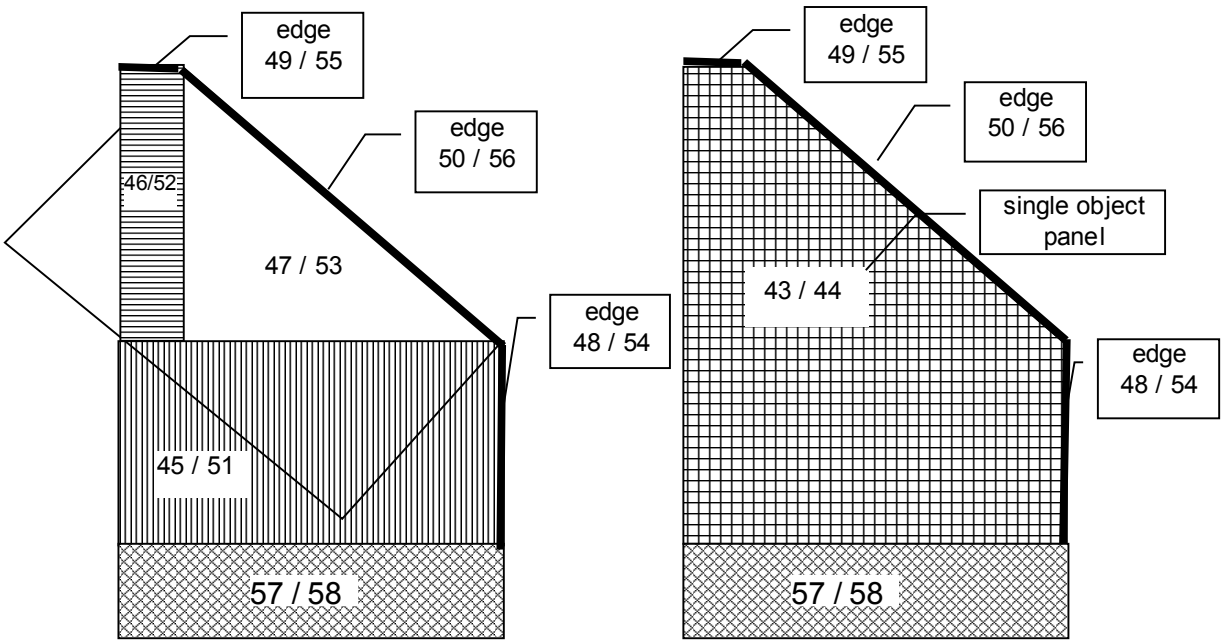

Figure 5.1-3 APART sunshield panel objects modelled two different ways

The pairs of numbers in each text box represent the numbering for the two separate halves of the sun shield. The reason for modelling the panels in two different ways was initial

uncertainty whether APART can use a sliced rectangle as an obscuration when modelling its action of shielding objects from outside radiation. Thermal emission from the sun shield used the single object model for each panel.

The diagrams in figure 5.1-4 show the shadowing effect of this sun shield design for sun angles equal to 65 and 60 degrees to the telescope axis at nominal roll and also for a roll as much as 10 degrees away from the nominal direction. The position of the secondary cell and its support struts above the primary used the latest telescope design parameters given in the next section. The MATHCAD file SUNSHADOW.MCD was used to produce these diagrams.

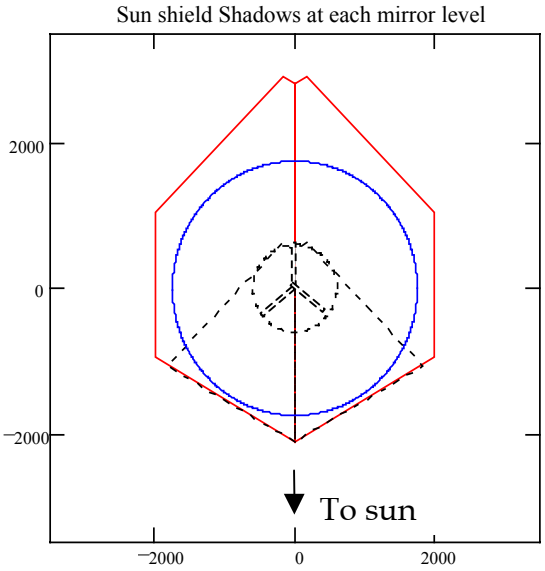

Sun elevation from telescope axis = 60 degrees
Sun azimuth = 0 deg from nominal

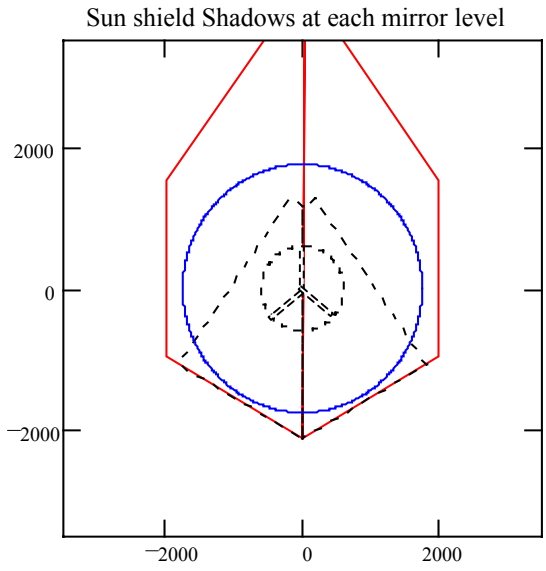

Sun elevation from telescope axis = 65 degrees
Sun azimuth = 0 deg from nominal

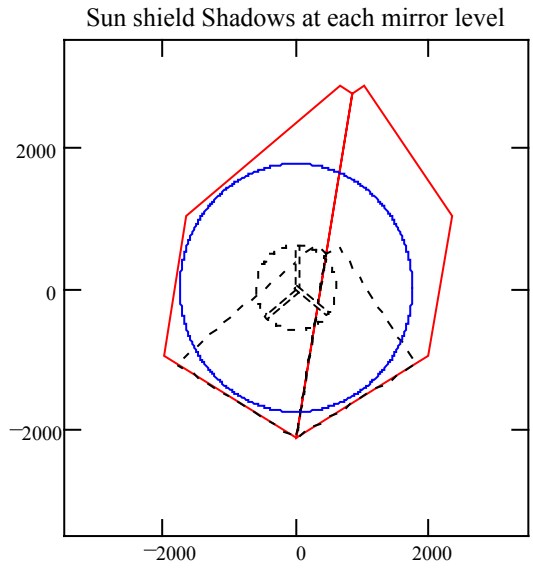

Sun elevation from telescope axis = 60 degrees
Sun azimuth = 10 deg from nominal

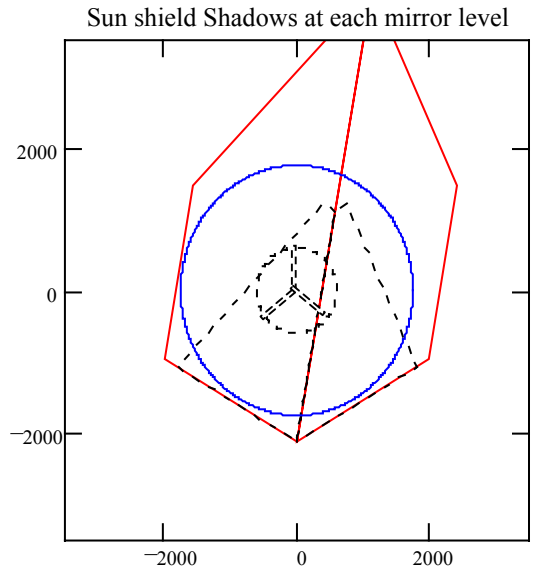

Sun elevation from telescope axis = 65 degrees
Sun azimuth = 10 deg from nominal

Figure 5.1-4 Shadowing effect of the sun shield

In each diagram in figure 5.1-4, the continuous outline shows the shadow thrown at the level of the edge of the primary, together with an outline of that edge. The dotted outline shows the shadow at the level of top of the tripod, together with a dotted circle marking the approximate extreme ends of the radial support struts at that level. The locations of the three support struts/legs are also approximately indicated as dotted rectangles.

5.2 Telescope

5.2.1 Optical surface data

The parameters defining the optical arrangement of the primary and secondary mirrors were taken from RD#3 and reproduced in table 5.2-1. The exception is the secondary conic constant, which was derived by raytracing using the other data together with the requirement to focus at 975 mm behind the primary. The values marked as 'old' are those used in the design modelled in the received APART files.

Parameter	APART identifier	Present value	Old value
Unvignetted FOV ½ angle	TELMAXANG	0.25	0.25
Level of the fixation plane below primary pole	TEL_FIX	125	125
Primary semi-diameter	RPRIEDGE	3500/2	3000/2
Primary radius of curvature	RADPRI	3800	3046.246
Primary conic constant	K_PRI	-1.000000	-1.000000
Hole semi-diameter	HOLRAD	296.23/2	260/2
Primary-secondary spacing	SPACMIRR	1720.3	1372.895
Secondary semi-diameter	RSECEDGE	314.7/2	241.56/2
Secondary radius of curvature	RADSEC	358.2	269.164
Secondary conic constant	K_SEC	-2.03629032	-1.249135
Secondary mirror axial thickness (between pole and edge)	THI_SM	50	50
Focal distance behind primary	ZBACKFOC	975	975

Table 5.2-1 Primary and secondary FIRST-order optical data

The main telescope parameters are defined in the APART file TELINIT.IN1 (look in TELINOLD.IN1 for an earlier model). There are no objects defined in this file, which is also responsible for computing sags at the primary and secondary edges and primary hole. It also calls specially written APART macros to check if the chosen combination of primary and secondary diameters is consistent with an unvignetted field of view up to TELMAXANG degrees from the telescope's axis. TELMAXANG is kept equal to 0.25 degrees.

5.2.2 Associated Primary mirror structure

The objects making up primary surfaces are collected into their own APART module in the file PRIMARY.IN1. The objects making up secondary surfaces are collected into their own APART module in the file SECONDRY.IN1 (note the spelling which keeps the filename at 8 characters – the DOS limit since APART runs in a DOS window).

The primary hole and other objects connected with the primary are shown dimensioned in figure 5.2.2-1. The object numbers are inside rectangular boxes, each with an arrow pointing to an object. The dimension data along with their APART identifiers is presented in table 5.2-2. Apart from the hole, these dimensions are only approximate estimates and do not indicate the final design. The central hole and the objects behind the primary outer edge are collected into their own APART module in the file HOLE.IN1. The main additions to the model of the primary are the annular rim level with the front edge of the primary, the cylindrical outer edge and the flat and conical parts of the rear surface of the primary. The rear surfaces are used for modelling transfers between the rear of the primary and the front of the cryostat.

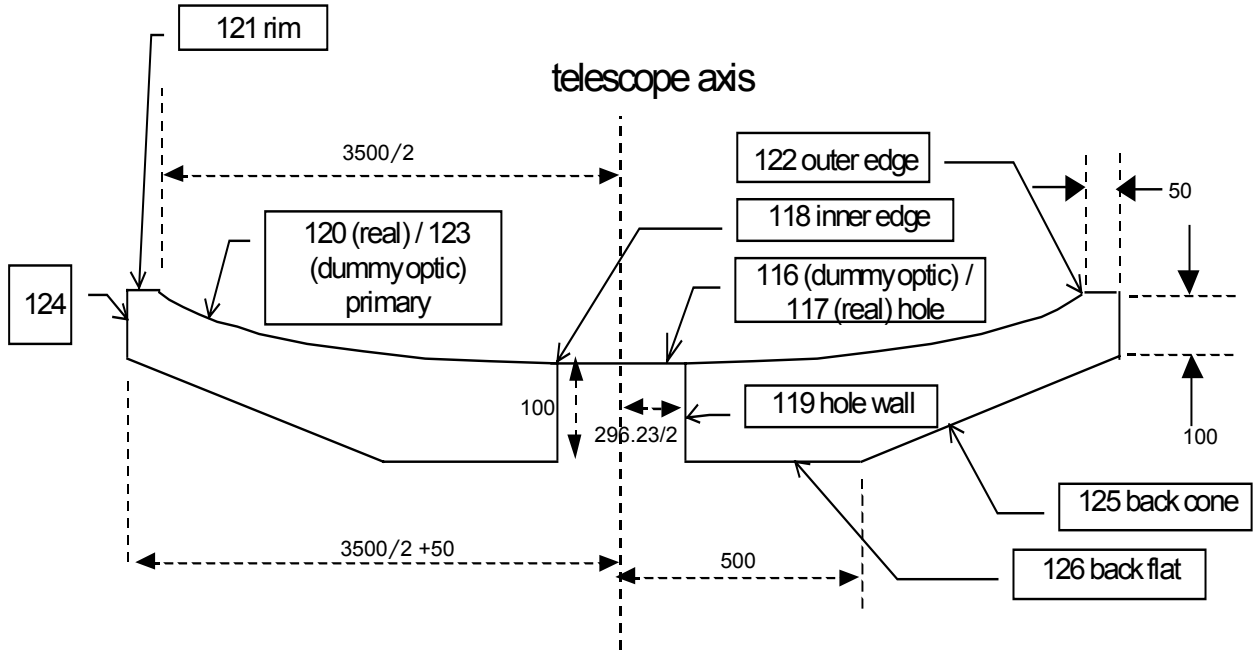

Figure 5.2-1 primary mirror object numbers and their major dimensions

parameter	APART identifier	Value
Primary hole semi-diameter	HOLRAD	296.23/2
Primary hole depth	THI_PM	100
Circular rim width	PRIRIM	50
Inner semi-diameter of circular rim	RPRIEDGE	3500/2
Thickness at rim	THI_PM	100
Outer radius of rear flat section	RPM_FLAT	500
Outer radius of rear conical section	RPM_CONE	RPRIEDGE+PRIRIM

Table 5.2-2 Primary mirror APART model parameters

5.3 Tripod and secondary mirror support cell

Figure 5.3-1 shows the way the tripod leg angle is derived from given quantities. The fixed dimensions are the radial locations of the foot point of the leg centre line on the primary (1000mm) and of the centreline at the level of the mechanical envelope (406.553mm). The mechanical envelope is set at the rear of the secondary cell. The axial separation of these two levels is determined by combining the axial mirror separation (that varies with telescope model), the thickness of the secondary plus its cell (presently held fixed) and the sag of the primary at the foot of the leg (that varies with primary curvature). It is the intention that the APART module be flexible and capable of responding quickly to telescope design changes involving mirror axial spacing and primary curvature. Table 5.3-1 shows data for the model as received and detailed in RD#2 and any changes subsequently made. The basic tripod leg and strut design is kept but the leg length and angle responds to the mirror spacing whilst keeping a fixed radial location on the primary for the tripod feet. Figure 5.3-2 shows a 3-D view of the tripod assembly. Figure 5.3-3 shows details of the leg design. This was obtained by exaggerating the leg thickness in the APART model by a large factor so that the sharp edges of the thin legs could be illustrated.

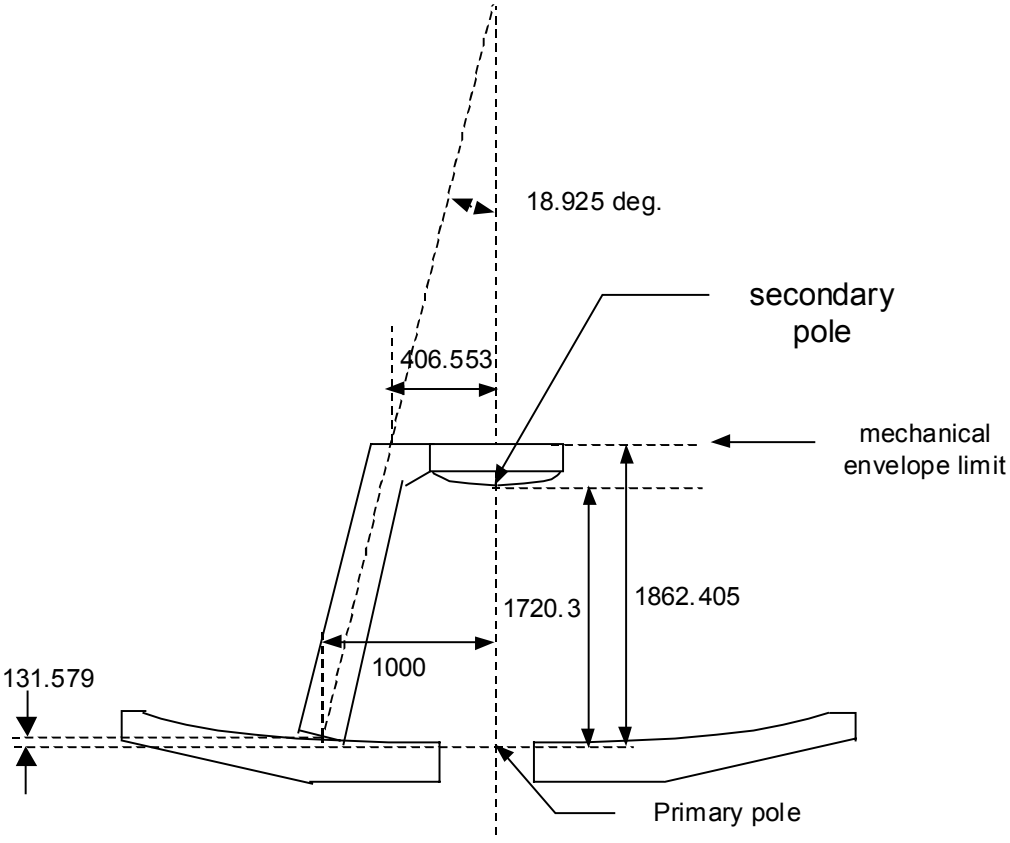

Figure 5.3-1 Tripod leg angle determination

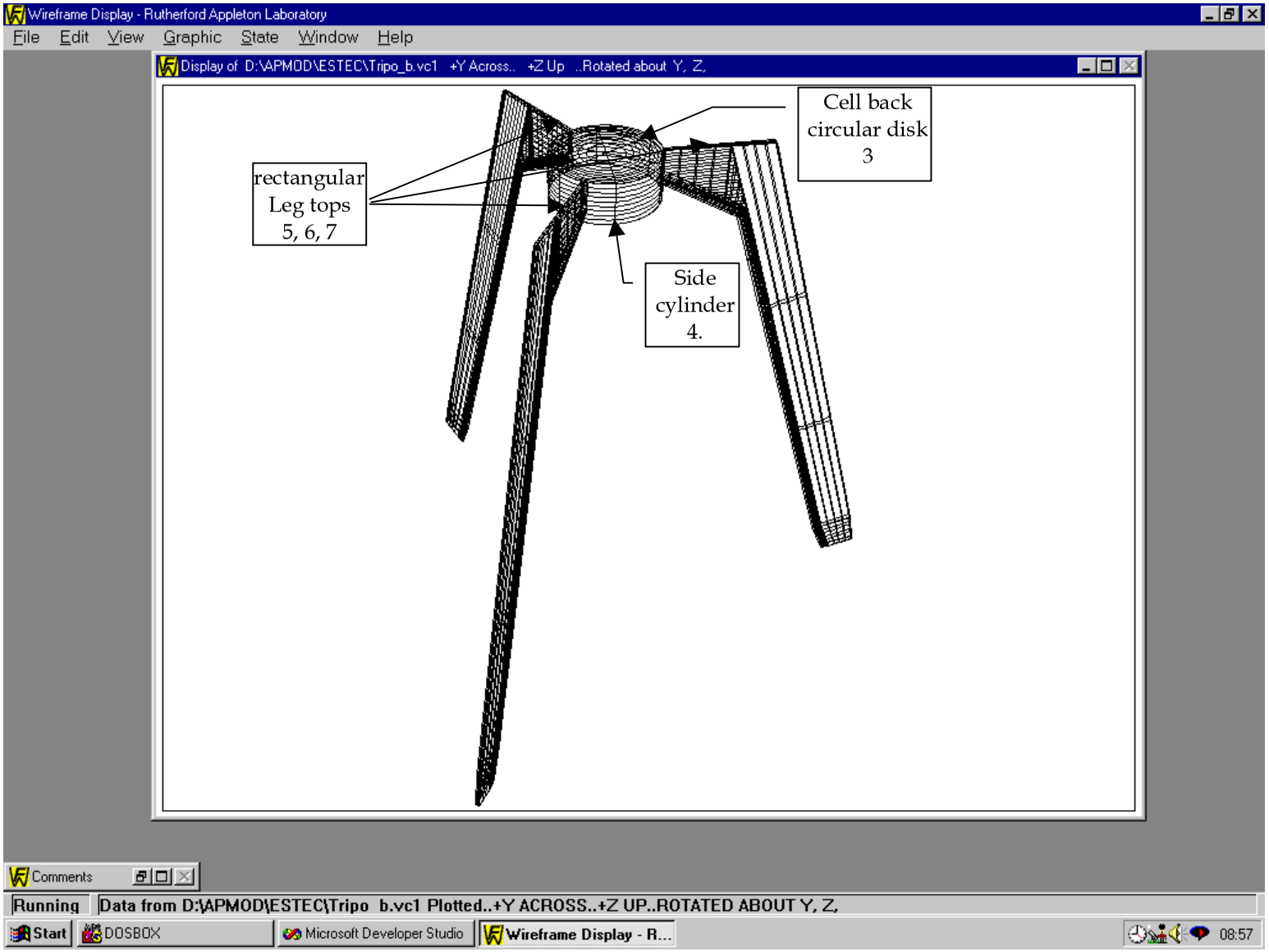

Figure 5.3-2 Tripod/ secondary mirror cell model with some APART object numbers

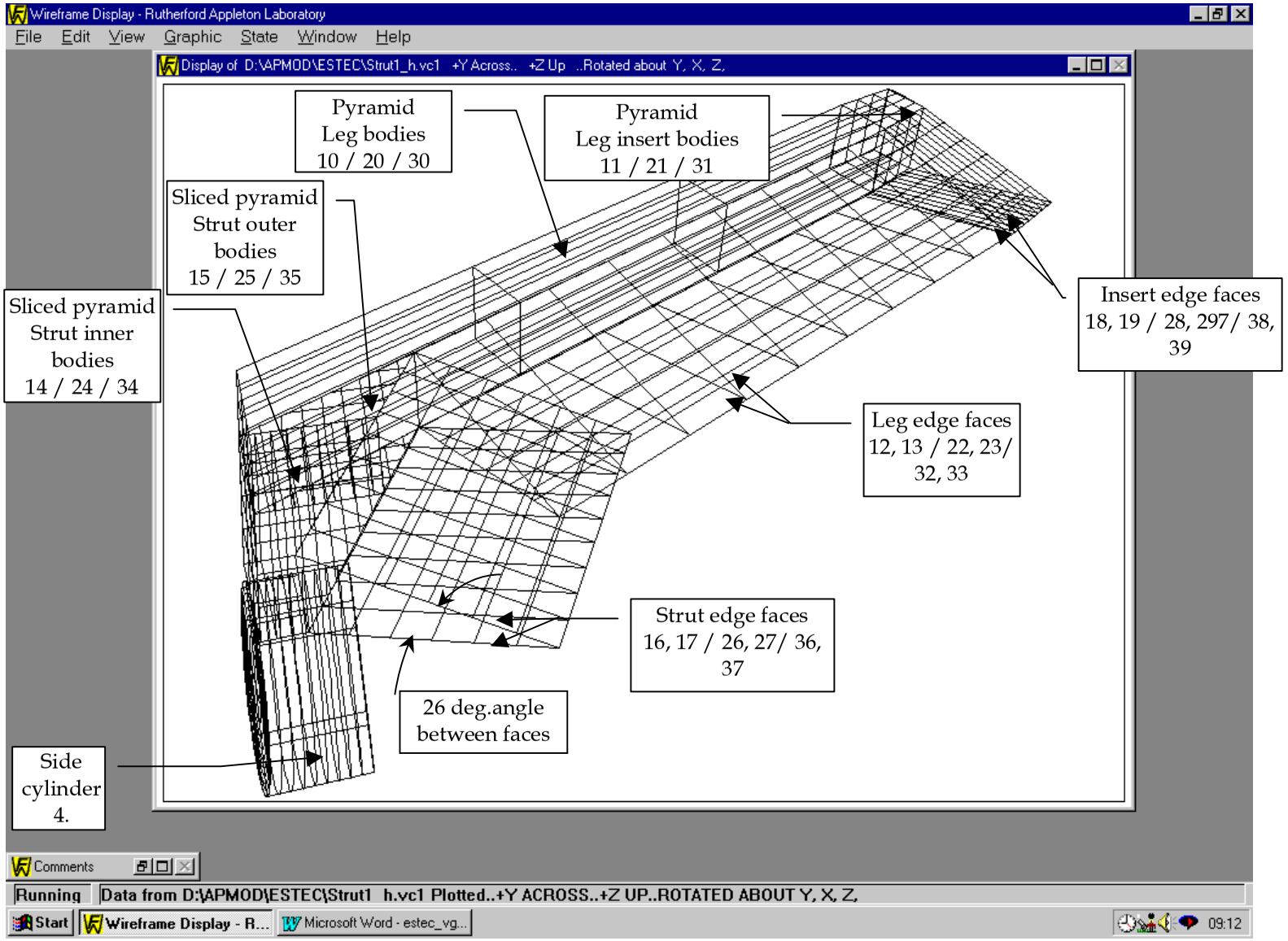

Figure 5.3-3 Detail of expanded Tripod leg (x10 thickness) with some APART object numbers

The ‘inserts’ that are modelled in the DSS design as tapered mini-leg extensions are kept in the present model but they are effectively removed from consideration by extending the main leg sections to the primary surface. This is done by equating to zero the fraction F_INSERT of the insert that exists above the surface of the primary. They can be recovered to their original length by changing the fraction F_INSERT back to a value of unity. All the main geometrical parameters that are mentioned in table 5.3-1 are defined in the APART program 1 file TRIPOD.IN1 that is devoted to the tripod module.

Parameter	APART identifier	‘Old’ value	‘New’ value
Azimuth angle of first leg	ANG_TRI1	-AZ_PRIME	-AZ_PRIME
Azimuth angle of second leg	ANG_TRI2	120-AZ_PRIME	120-AZ_PRIME
Azimuth angle of third leg	ANG_TRI3	-120-AZ_PRIME	-120-AZ_PRIME
Leg width	W_LEG	117.5	117.5
Leg thickness	T_LEG	15	15
Insert length	L_INSERT	145	145
Leg angle	A_LEG	27.5 deg.	18.925 deg.
Strut inside edge angle	B_LEG	62.1 deg.	62.1 deg.
½ angle between strut and leg edge faces	A_TRIANG	13 deg.	13 deg.
Radial distance to leg foot point on primary mirror	RSAG_LEG	1000	1000
Height of mechanical envelope above primary	HMECH	1515	1862.405

Table 5.3-1 Tripod APART model parameters

5.4 Cryostat

The main dimensions of the cryostat are shown in figure 5.4-1 along with the APART surface numbers. In that figure, object numbers are shown inside a rectangular box with single arrows leading from it. Dimensions are shown inside rectangles with double arrows leading from them. All surfaces represented in the figure as lines drawn parallel to the telescope axis of symmetry are to be understood to be cylinders co-axial with the telescope axis. All surfaces represented as lines drawn at 90 degrees to the telescope axis are to be taken to be annular disks.

The geometry of the cryostat model and the APART surface numbering has been kept unchanged from the original except that the inner radius of the apertures in all the inside surfaces has been assigned an APART variable RAD_CRY in file CRYOSTAT.IN1, allowing it to be easily altered if necessary. The APART code has been considerably reorganised so that the cryostat can be efficiently transformed in order to respond to any change in the choice of FPU boresight. The APART program 1 file CRYOSTAT.IN1 collects up all the cryostat objects and geometric parameter definitions. Table 5.4-1 shows the main APART parameters defining the geometry.

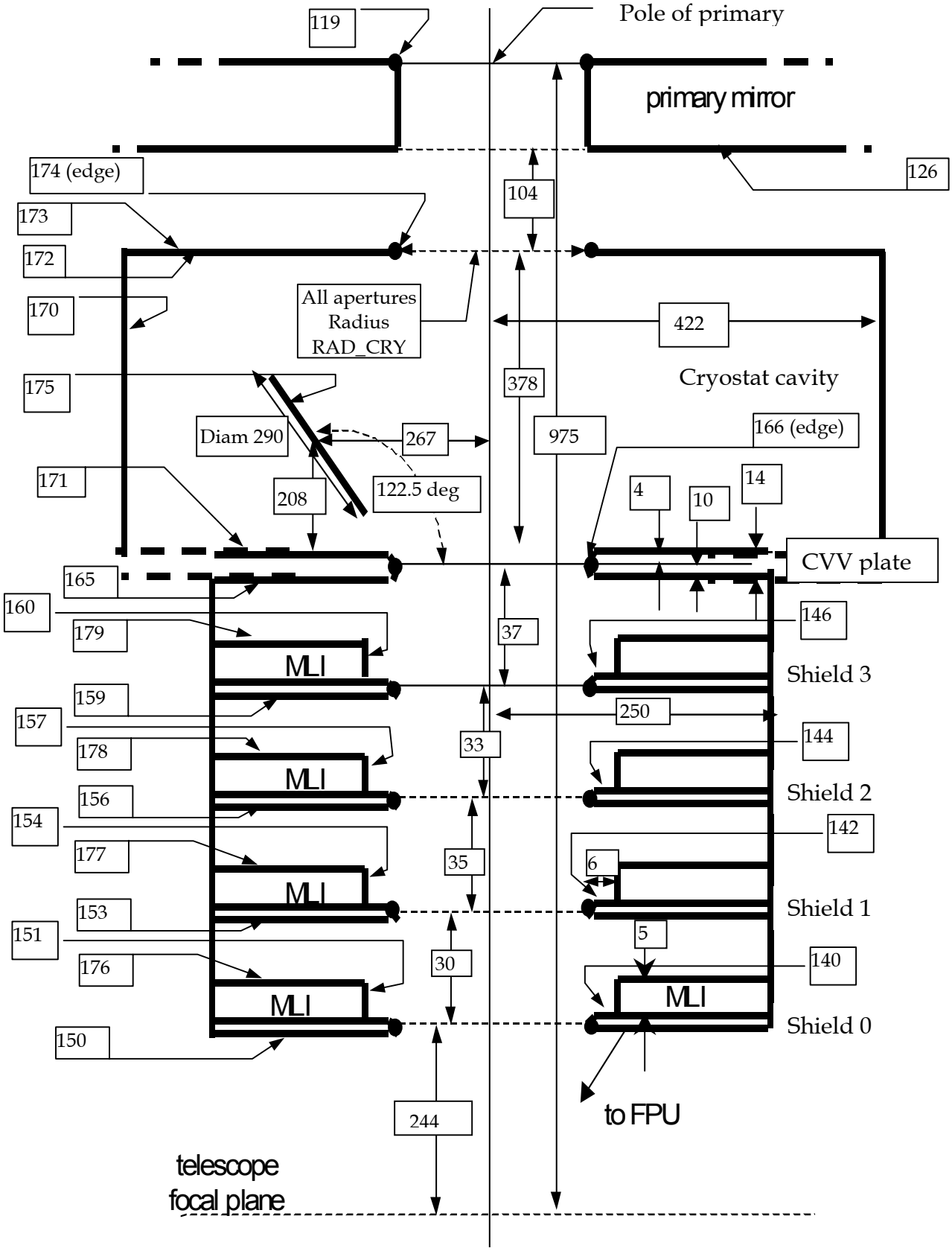

Figure 5.4-1 Cryostat geometry and APART surface numbers

Key to figure: Boxes with double arrows are dimensions. Boxes with single arrows are Object numbers.

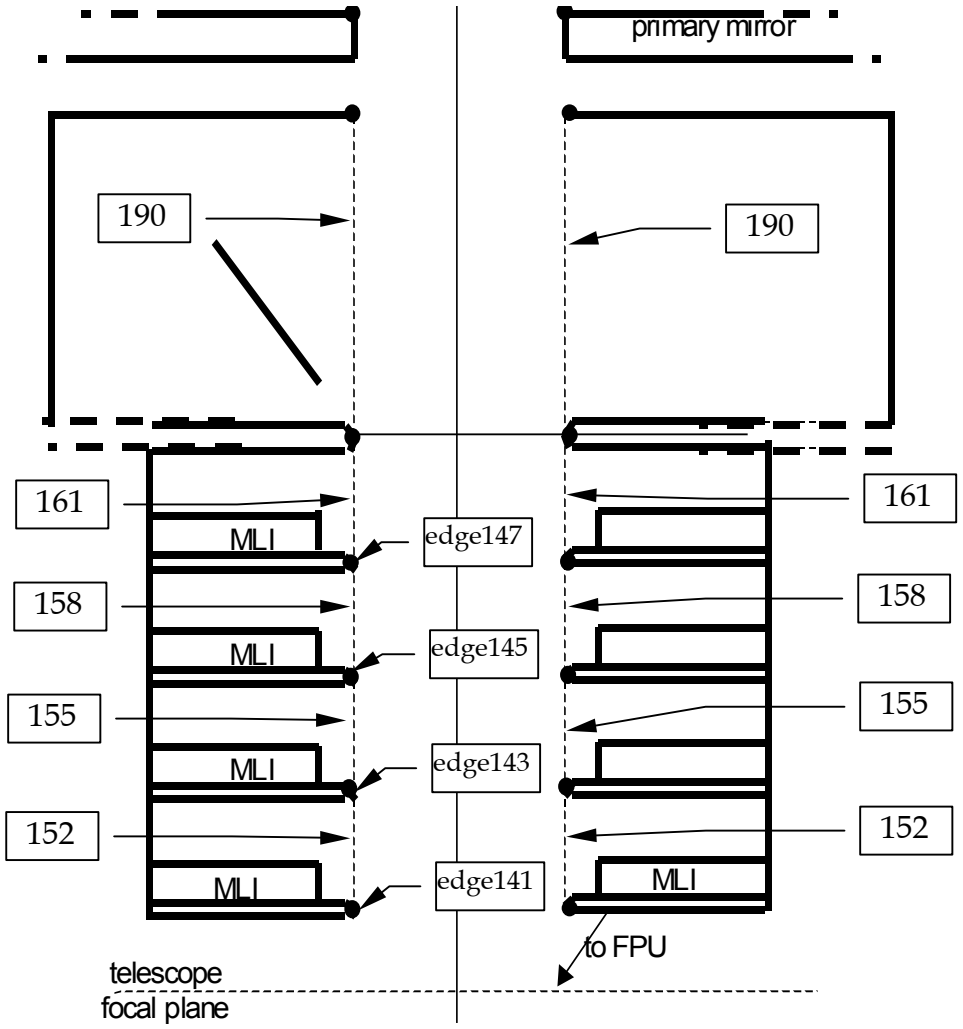

Figure 5.4-2 Additional surfaces included in the APART model of the cryostat

Parameter	APART identifier	Present Value
Radius of all apertures	RAD_CRY	130
Outer radius of shield surfaces	ROUT_SHLD	250
Axial location of centre of cover above CVV	DZ_COVER	208
Radial offset of opened cover	XCOVER	-267
Radius of circular cover	R_COVER	145
Opening angle of cover (0=closed)	ANG_COV	180-57.5
Edge radius on shield edges	R_SHLD	0.25
Radial width of lip on each shield	LIP_SHLD	6
Axial thickness of MLI on each shield	THICKML	5
Edge radius on CVV and CVV-cavity edges	R_CVV	0.5
Axial thickness of SHIELD 0	THICK0	30
Axial thickness of SHIELD 1	THICK1	35
Axial thickness of SHIELD 2	THICK2	33
Axial thickness of SHIELD 3	THICK3	37
Axial thickness of CVV	TH_CVV	14
Axial thickness of CVV inner conical edge face	TH_CVVIN	10
Axial thickness of cavity	THICKCAV	378
Radius of cavity wall cylinder	RAD_WALL	422
Axial location of SHIELD 0 above telescope focal plane	DZ_SHLD0	244

Table 5.4-1 Cryostat APART model parameters

The edge surfaces shown in figure 5.4-2 are real surfaces that are used to model edge scatter and emission. The cylindrical APART surfaces that are shown dotted in figure 5.4-2 are used for thermal emission studies. These do not correspond to real physical surfaces but they can be used as dummy sources of radiation from the inter-shield cavities. They are given emissivity values somewhat higher than that of a bare shield or MLI surface. This is to allow for the effects of multiple reflection of emitted radiation within the inter-shield cavities, which tends to boost the effective emissivity of each cavity towards unity.

5.5 Focal Plane Unit (FPU)

The detailed APART model that is used for a FPU was taken from the model for the SPIRE instrument. This model is described in RD#5. It is not the final optical design, but it is the only existing design that integrates structure with the optics. The APART objects were renumbered so as to be added to the FIRST telescope/PLM model using object numbers 200 and above. The APART file for this is SPIREFPU.IN1. This file forms the template for other FPU models that may be added in future. Figures 5.5-1→5.5-4, which are taken from RD#5, show the layout of the SPIRE model.

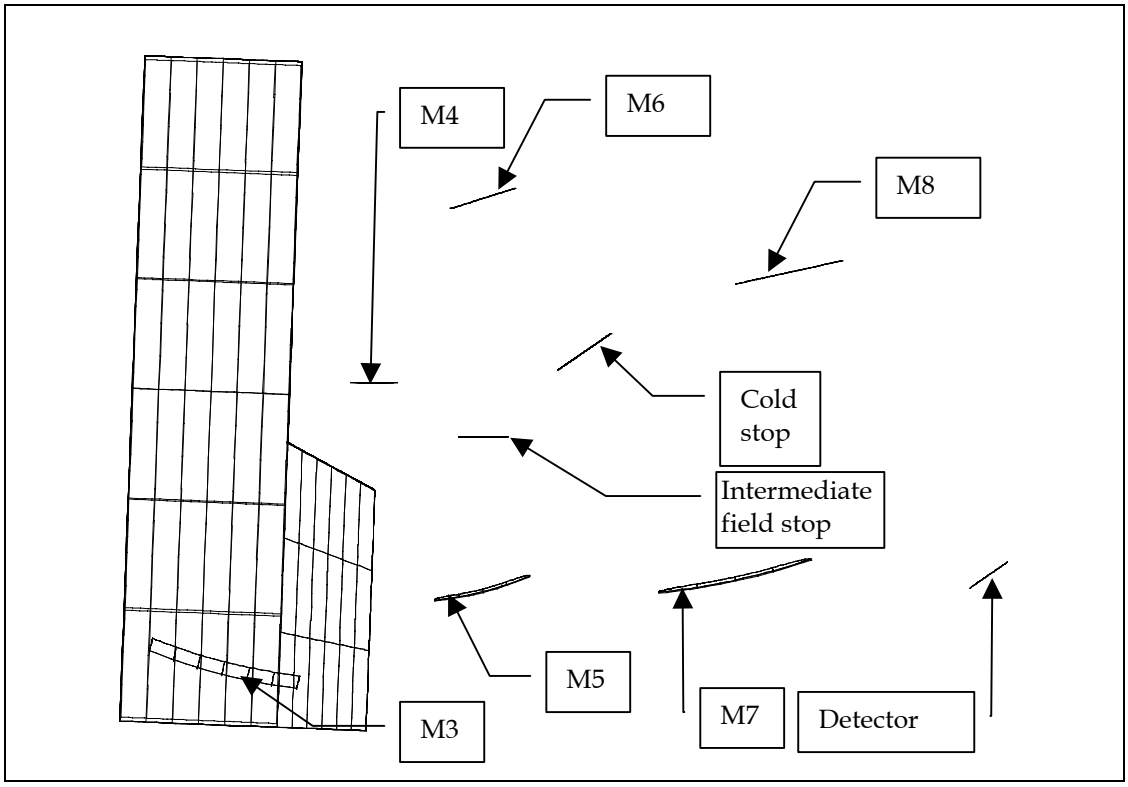

Figure 5.5-1 Y-Z plot of '15K' structure added to the APART model of SPIRE

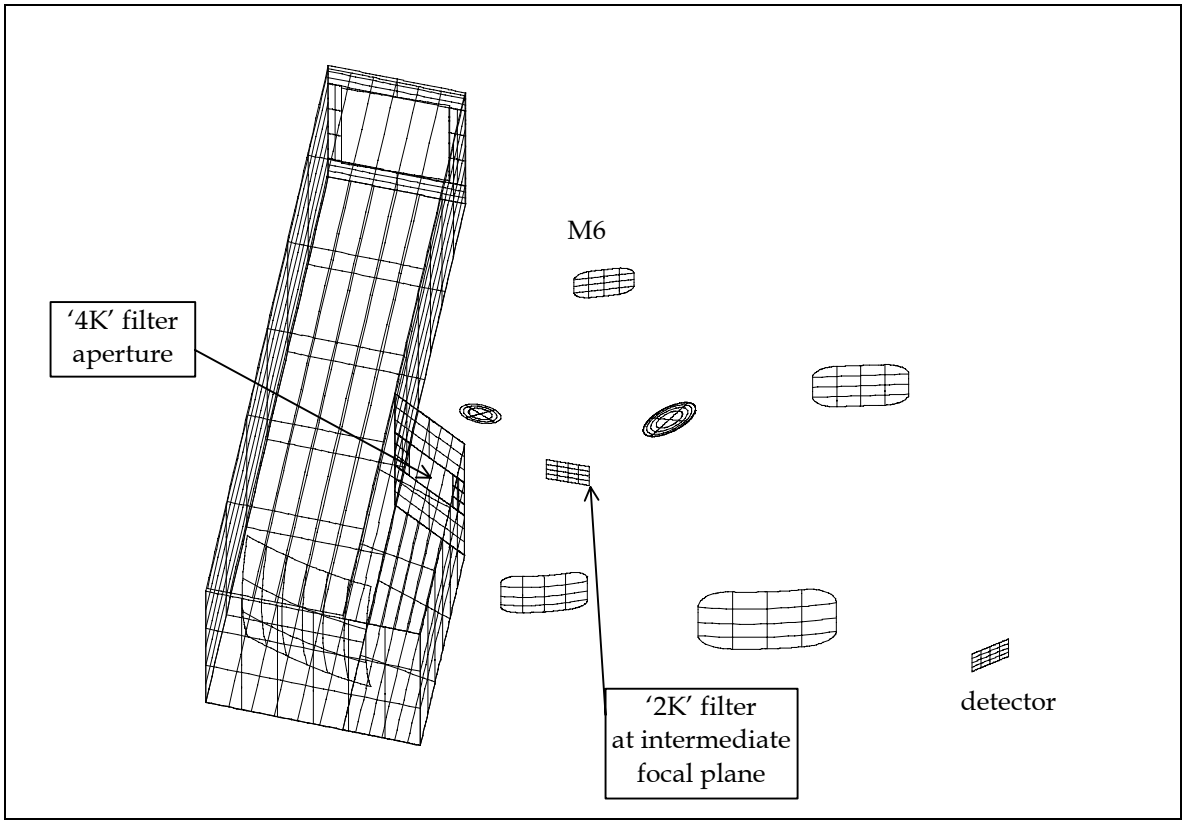

Figure 5.5-2 Isometric plot of SPIRE '15K' structure

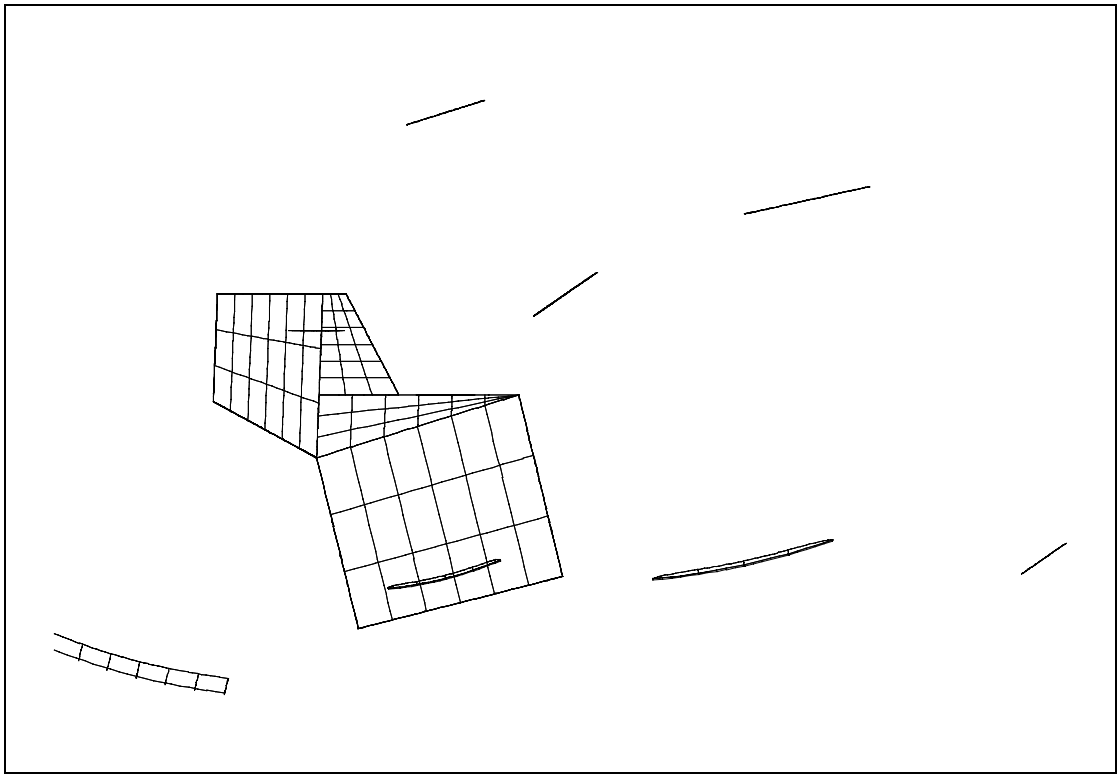

Figure 5.5-3 Y-Z plot of '4K' structure added to APART model of SPIRE

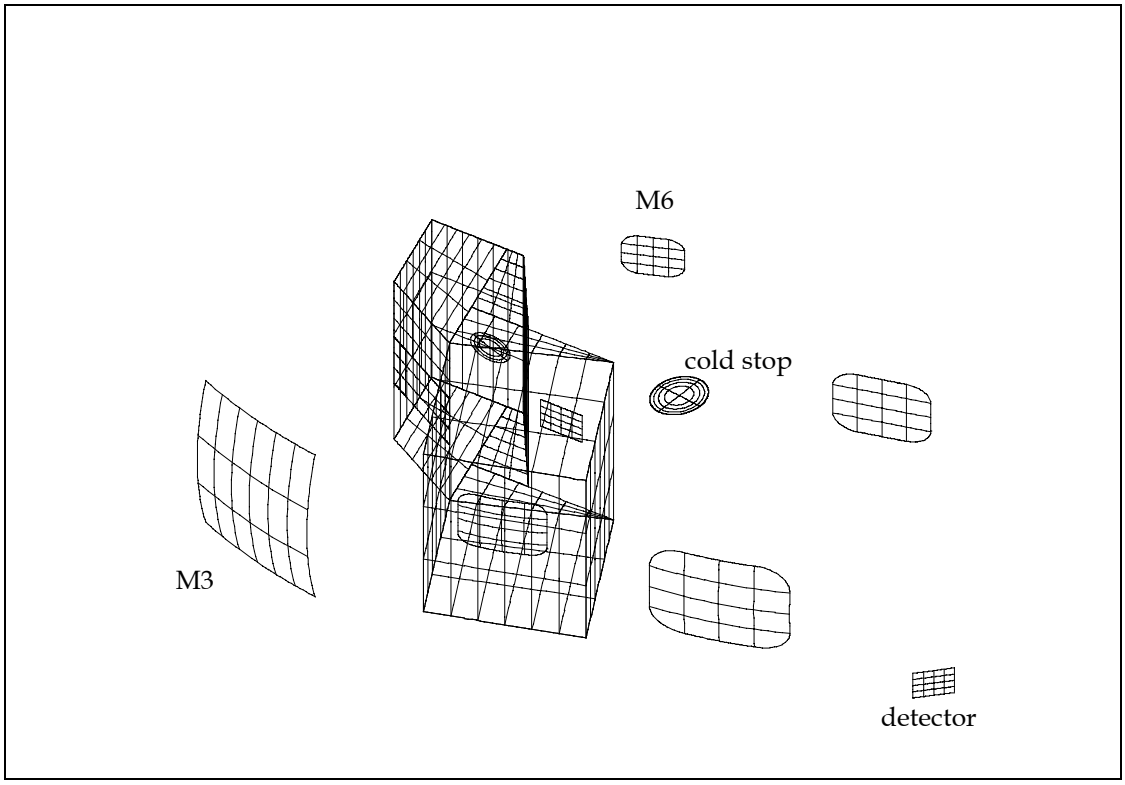

Figure 5.5-4 Isometric view of SPIRE '4K' structure

6. THE NEW MODULARISED APART MODEL

6.1 Generating the model from separate files

The first major change made to the code was to split the model into its major modules, assigning a separate APART file to each one. Additional files were created, such as TELINIT.IN1 for telescope parameter definition and consistency checking, and the text file FIRSTEL.MAC that contains specially written APART macros. A driver file called DRIVER.IN1 links the separate APART program 1 input files. The names and function of all the files that are required to define the geometry for the FIRST PLM model are presented in table 6.1-1

The other major area of work was the construction of a set of FPU files. These are also listed in table 6.1-1. The file SPIREFPU.IN1 is a detailed model of the FIRST SPIRE FPU design. The other FPU files have the same skeleton as the SPIREFPU.IN1 file but are presently lacking the detailed structure. The FPU files all have one thing in common: each of them has two objects defined in a special pre-space 1 section. These are a rectangular surface representing an entrance aperture and a rectangular surface that represents an aperture surround. The aperture surround is displaced slightly beyond the plane of the aperture surface. This is so that transfers to the surround can use the aperture surface as an obscuration, effectively creating a rectangular surround. Conversely, transfers involving radiation emitted or scattered forwards from the aperture surround surface can be obscured by the aperture surface so that only those sections outside the aperture surface contribute.

APART Program 1 file name	Function
DRIVER.IN1	Builds the APART geometry by adding all the sections from the data files listed below for each subsystem in the correct order.
TELINIT.IN1	Initialises the telescope geometry and defines a macro (XYZSHIFT) which is used to rotate and shift into the APART frame which is aligned to the gut ray which defines the boresight of a prime FPU. The prime FPU is selected in DRIVER.IN1 from one of the four available.
TELAXES.IN1	Adds 3 long thin cylinders to act as X, Y and Z-axes centred at the pole of the secondary mirror so that 3-D displays can be better interpreted.
SUNSHLD.IN1	Defines the sunshield structure detailed in section 5.1 that is based on the design data given in fax PT-06275, 19-January 199 from B. Guillaume, ESTEC
TRIPOD.IN1	Adds the tripod structure based on the original ESTEC APART file. Preserves the surface numbering used there. The model now incorporates the use of an in-line macro (XYZSHIFT, defined in TELINIT.IN1) to apply the azimuth (Z) and tilt (X) rotations and the shifts required to position surfaces in the co-ordinate frame defined by the off-axis view of a prime FPU (see TELINIT.IN1).
PRIMARY.IN1	Adds the APART model of the primary mirror structure. This is novel but uses some surface numbers previously used in the FIRST model. The 'real' primary is now numbered 120. It is defined in space 1 and repeated into spaces 2 and 3. A dummy optical primary numbered 123 is introduced as the boundary between spaces 1 and 2.
SECONDRY.IN1	Adds the APART model of the primary mirror structure. The 'real' secondary is now surface 129 and it is defined in space 1 and repeated into spaces 2 and 3. A separate dummy optical secondary is introduced, numbered 130, as the boundary between spaces 2 and 3.
HOLE.IN1	Adds the APART model of the primary hole structure. It uses some surface numbers used in the original FIRST model but it also adds new surfaces (125, 126) to represent the back of the primary mirror, facing the cryostat. The 'real' primary hole numbered 117 and it is defined in space 1 and repeated into spaces 2,3 and 4. A separate dummy optical hole (numbered 116) is introduced, as the optical boundary between spaces 3 and 4.
CRYOSTAT.IN1	Adds the model of the cryostat structure taken directly from the original FIRST APART file. The surface numbering has been preserved.
FIRSTEL.MAC	Contains APART macros required by other APART files
SPIREFPU.IN1	Adds the focal plane apertures and detailed model of SPIRE
PACSFPU.IN1	Adds focal plane apertures to represent PACS until a detailed model is available
HIFIFPU.IN1	Adds focal plane apertures to represent HIFI
DUMMYFPU.IN1	Adds the focal plane objects to represent an on-axis dummy FPU. Useful for obtaining vector plot files with data in a co-ordinate system with the Z-axis aligned parallel to the telescope axis of symmetry.
PLOTCOM.IN1	Adds the APART plot commands needed to output a 3-D vector plot file.

Table 6.1-1 APART program 1 files required for creating the APART geometry.

The co-ordinates of the gut ray defined in the telescope focal plane for each FPU determine the direction for the intended gut ray for that FPU. This data, in the form of X and Y co-ordinate values in the ‘natural’ co-ordinate system, is derived from an optical model of each FPU combined with the telescope. Figure 6.1-1 shows a 3-D plot obtained by selecting the DUMMYFPU as the prime FPU. The apertures that are modelled for each FPU are shown in their correct relative relationship near the focal plane.

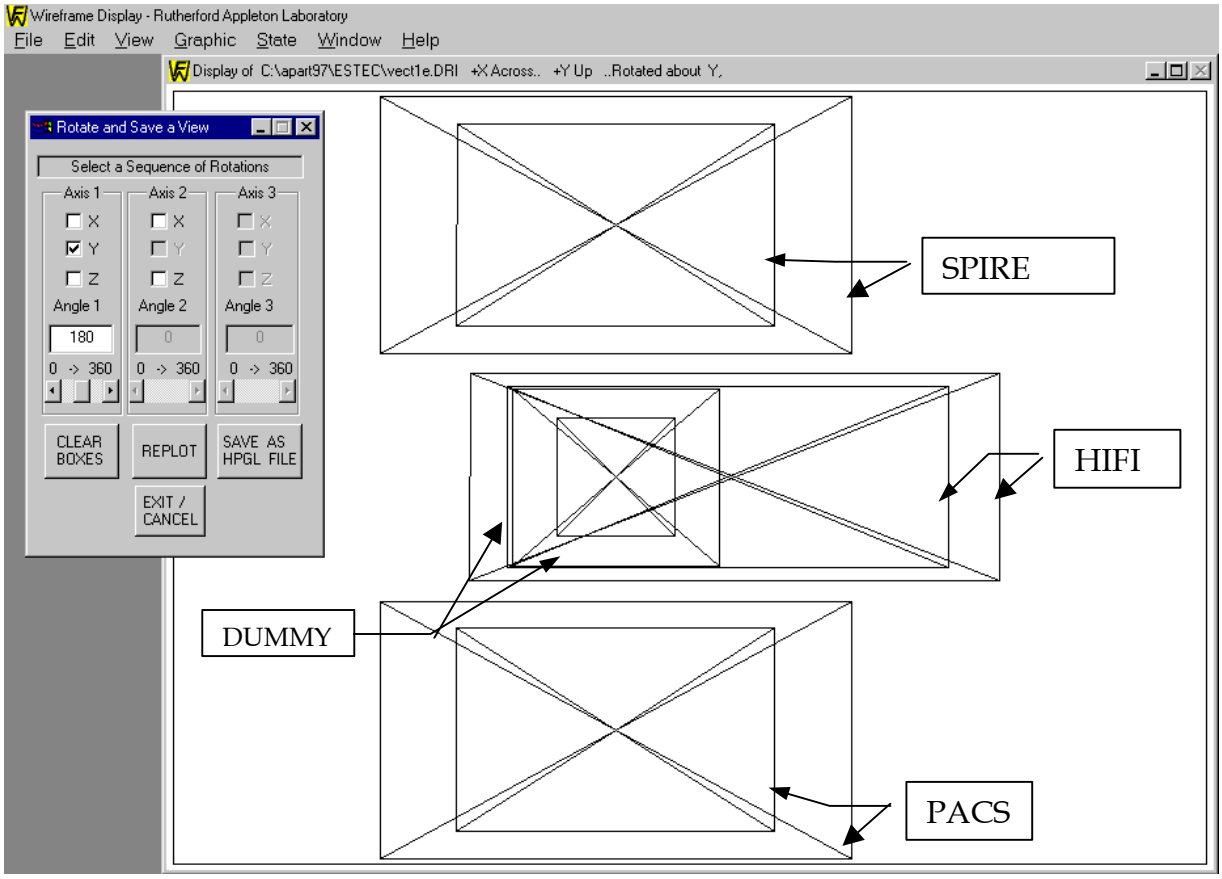

Figure 6.1-1 Apertures and aperture surrounds modelled for all four FPUs

6.2 Running the model

The driver file DRIVER.IN1 offers many options when it comes to producing a geometrical representation of the model. There are a number of switches which allow parts of the telescope / PLM-FPU structure to be excluded from the model and hence to be excluded from the 3D display. There is a switch that will determine which FPU determines the boresight and hence in which APART co-ordinate frame the model will be constructed. The text file DRIVER.IN1 details all these switches and they are presented in table 6.2-1.

To proceed with an APART program 1 run, the user first edits the switches in the DRIVER.IN1 file to select those subsystems that are to be included in that particular run. Setting ISYSTEM=1 will force the production of the geometry file for the whole system consisting of all the major subsystems, regardless of the settings for the other switches. The 'Prime' FPU is selected using the switch PRIMEFPU. After closing the file DRIVER.IN1 the program is executed using the command line

APART 1 DRIVER ext Y N N

In this command, 'ext' is the 3-character extension that will be added to all the APART files that are generated by program 1 to distinguish them from data produced by other runs.

Switch	value	Function
ISYSTEM	1	Overrides all other switches to force the inclusion of all subsystems.
ISYSTEM	0	Allows exclusion of sub-systems from the processed model
IAXES	1 or 0	Adds or omits 3 thin cylinders representing X,Y,Z axes centred at Secondary
ISUNSH	1 or 0	Includes or excludes sunshield model
ITRIPO	1 or 0	Includes or excludes tripod model
IPRIME	1 or 0	Includes or excludes primary model - Subject to IPRISEC value
ISECON	1 or 0	Includes or excludes secondary model- Subject to IPRISEC value
IPRISEC	1 or 0	Forces exclusion of primary/secondary if IPRIME or ISECON = 0
IHOLE	1 or 0	Includes or excludes primary hole structure and optic
ICRYO	1 or 0	Includes or excludes cryostat model
IFPU	1 or 0	Includes or excludes detailed FPU model. Only basic FPU apertures included if = 0
PRIMEFPU	1,2,3,4	Selects SPIRE, PACS, HIFI, DUMMY as the prime FPU, in that order.

Table 6.2-1 Switches available in the APART program 1 input file DRIVER.IN1

6.3 Selecting a FPU and finding the gut ray

When a particular FPU is selected as the 'prime' FPU by means of the APART parameter PRIMEFPU, then gut ray data (stored in a special 'SPACE 0' section of the APART file for that FPU) is accessed and used to set up the co-ordinate system.

Figure 6.3-1 illustrates the data programmed as a result of focal plane sharing arrangements made to date. The values are given in table 6.3-1. The data were extracted from SPIREFPU.IN1, PACSFPU.IN1, HIFIFPU.IN1 and DUMMYFPU.IN1. The way that the data is used to determine the gut ray direction is shown in figure 6.3-2. The Azimuth angle ϕFPU and elevation angle αFPU are determined using the co-ordinate values XFP, YFP and the spacing ZFOC from the focal plane to the secondary mirror. αFPU is always positive by definition. ϕFPU is measured from the +YFP direction and is shown negative in the figure. Note that the FPU gut ray co-ordinates in figure 6.3-1 are given in the telescope focal plane, which is located at ZFOC = SPACMIRR + ZBACKFOC along the telescope axis, measured from the pole of the secondary mirror. Refer to table 5.2-1 for the values of these APART parameters.

The SPIRE box aperture is provisionally located at 164.4mm back from the telescope focal plane measured parallel to the telescope axis, not along the gut ray. With no other information available, the aperture planes for the other instruments have been provisionally located at the same distance from the focal plane.

	SPIRE	PACS	HIFI	DUMMY
XFP	0.0		-40.5	0.0
YFP	+91.0547	-91.0547	0.0	0.0
ZFOC	1720.3+975	1720.3+975	1720.3+975	1720.3+975
α	1.9348743	1.9348743	0.860870	0.0
ϕ	0.0	180.0	0.0	0.0

Table 6.3-1 Provisional gut ray data for each FPU.

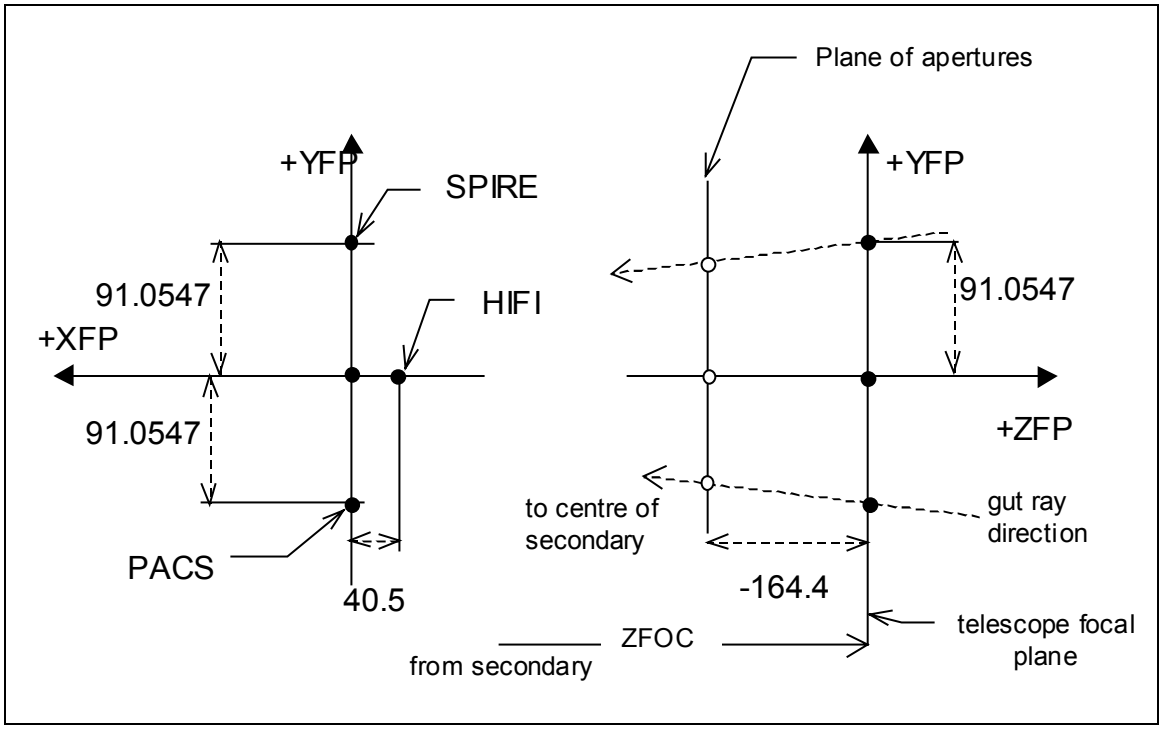

Figure 6.3-1 Provisional gut ray locations at the telescope focal plane

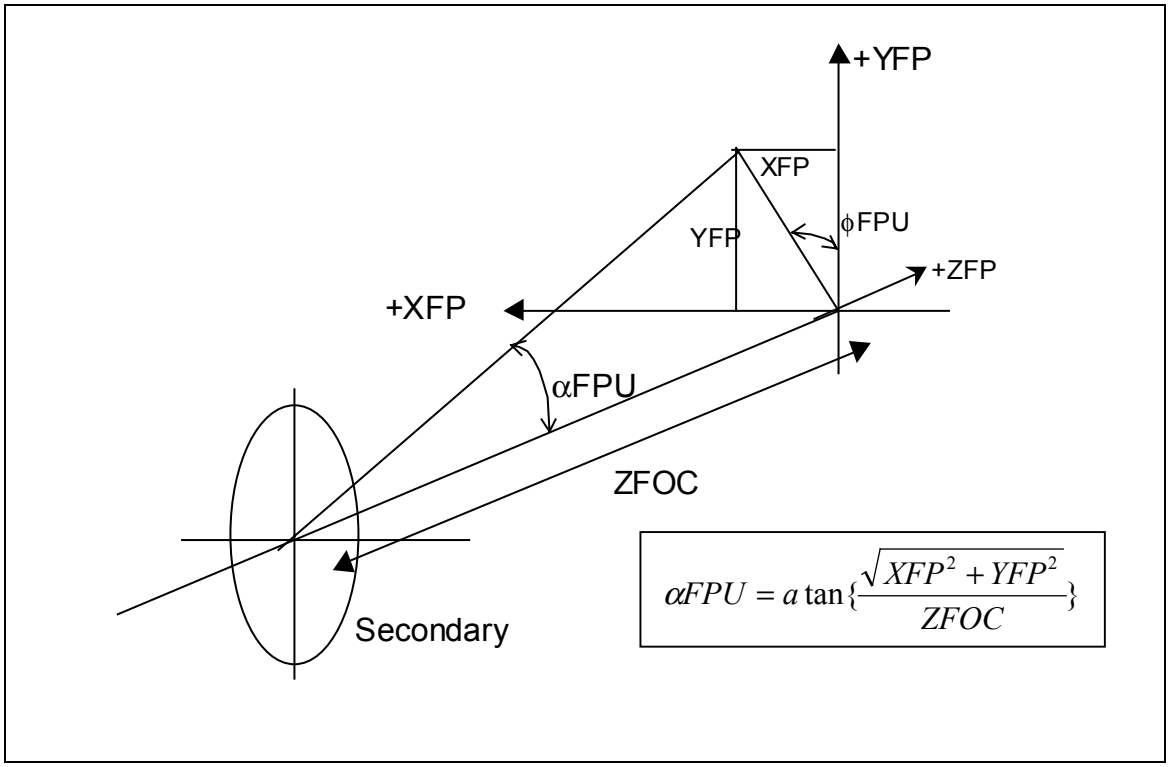

Figure 6.3-2 Calculating gut ray angles

6.4 Verifying the model geometry

6.4.1 Using APART vector plot data

If APART program 1 is run as described above, then a 3-D vector plot file called VECT1E.ext will be produced. This should show the geometry of the system as modelled, permitting some visual verification of the model. The vector plot data can be displayed and examined using the APART-supplied viewer or RAL viewer WIREFRAME.EXE. If the switch TELAXES=1 has been set, then the plot will show 3 objects representing lines along the 3 axes centred at the secondary mirror pole. This is useful for checking that the correct alignment of FPU and telescope has been selected. Figures 6.4-1→6.4-4 show plots of APART 3D vector data resulting from running DRIVER.IN1 through APART program 1 with various sub-systems switched on and off.

There are known bugs in the 3D vector plots that APART program 1 produces. For example, it is known that a sliced rectangle (a rectangle with part of it removed by slicing) is only approximately represented in the vector plot file. This explains the non-representative appearance of the sun shield panels in figure 6.4-1. Verification of the sun shield model requires more accurate representations, which are available by using the APART pre-processing program APMOD. Unfortunately, APMOD can deal with only a limited number of surfaces and it will not process user-written macros. This means that APART commands executed for the surfaces which are required to be checked must be extracted from the APART DRIVER.OT1 output listing and saved into a separate *.IN1 file. For this to work, all the commands executed within the macro XYZSHIFT must be made visible in the listing file by changing the command ECHO NONE to ECHO ALL inside the macro. As mentioned earlier, this macro is programmed in the file TELINIT.IN1. Figure 6.4-4 is a more accurate rendition of the sun shield obtained by extracting the sun shield definition commands from DRIVER.OT1, editing it and inputting it to APMOD. APMOD was then used to display the geometry and to output a vector plot file (*.VC1) which was subsequently displayed using the WIREFRAME.EXE application.

(This page intentionally left blank)

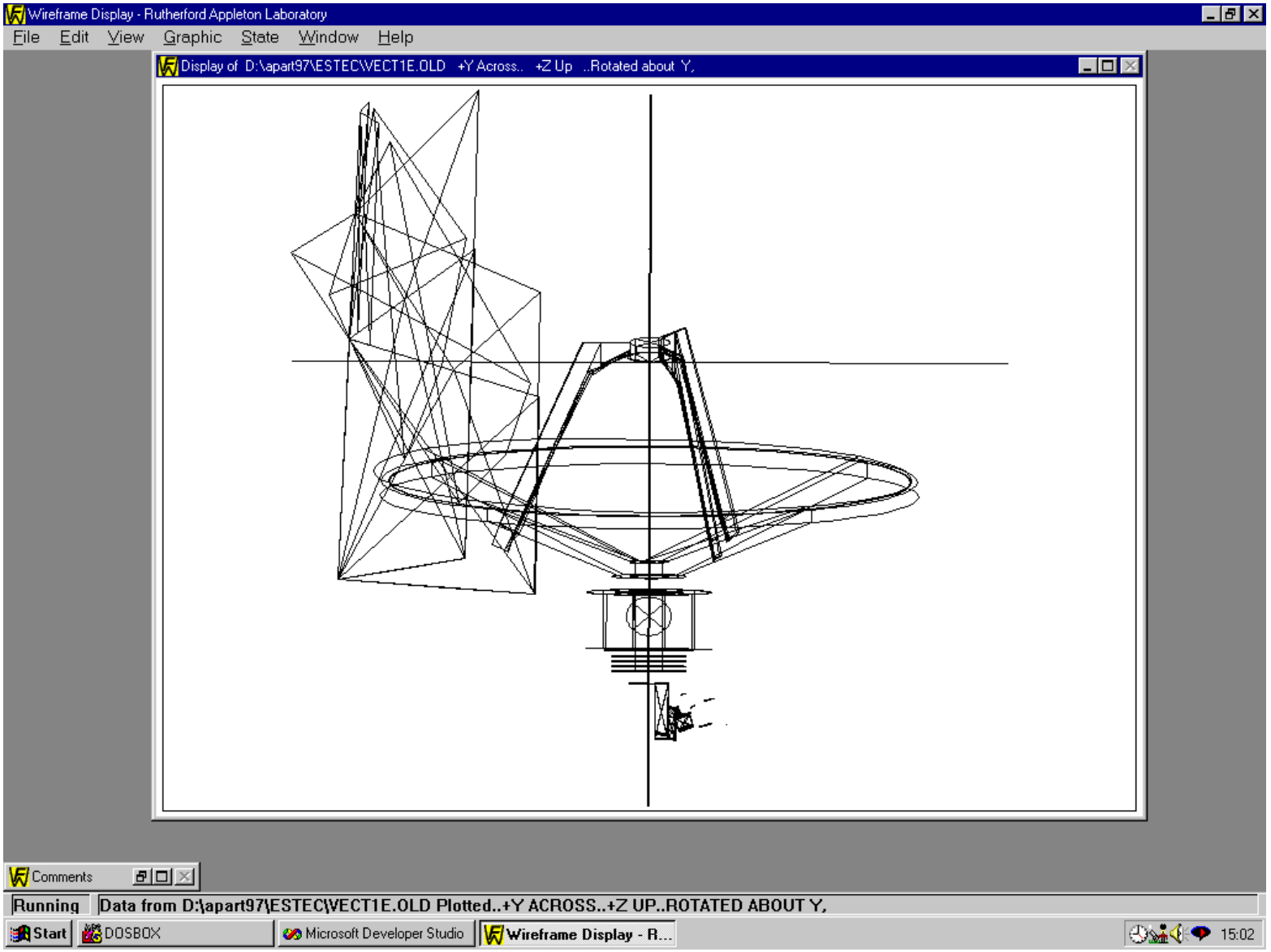

Figure 6.4-1 WIREFRAME display of the complete system, including X, Y, Z axes at secondary pole

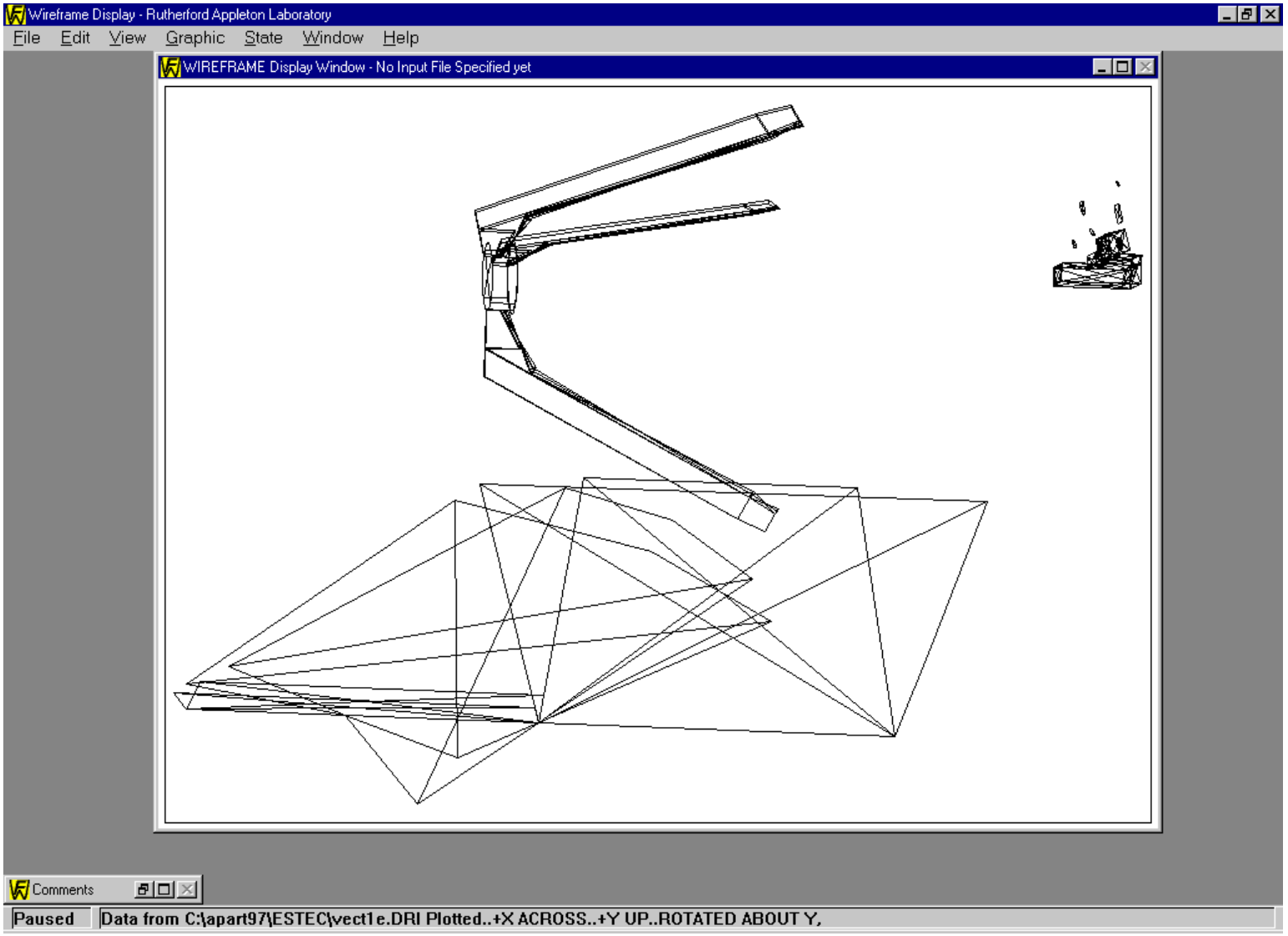

Figure 6.4-2 WIREFRAME display of the telescope without the primary mirror, the secondary mirror and the cryostat

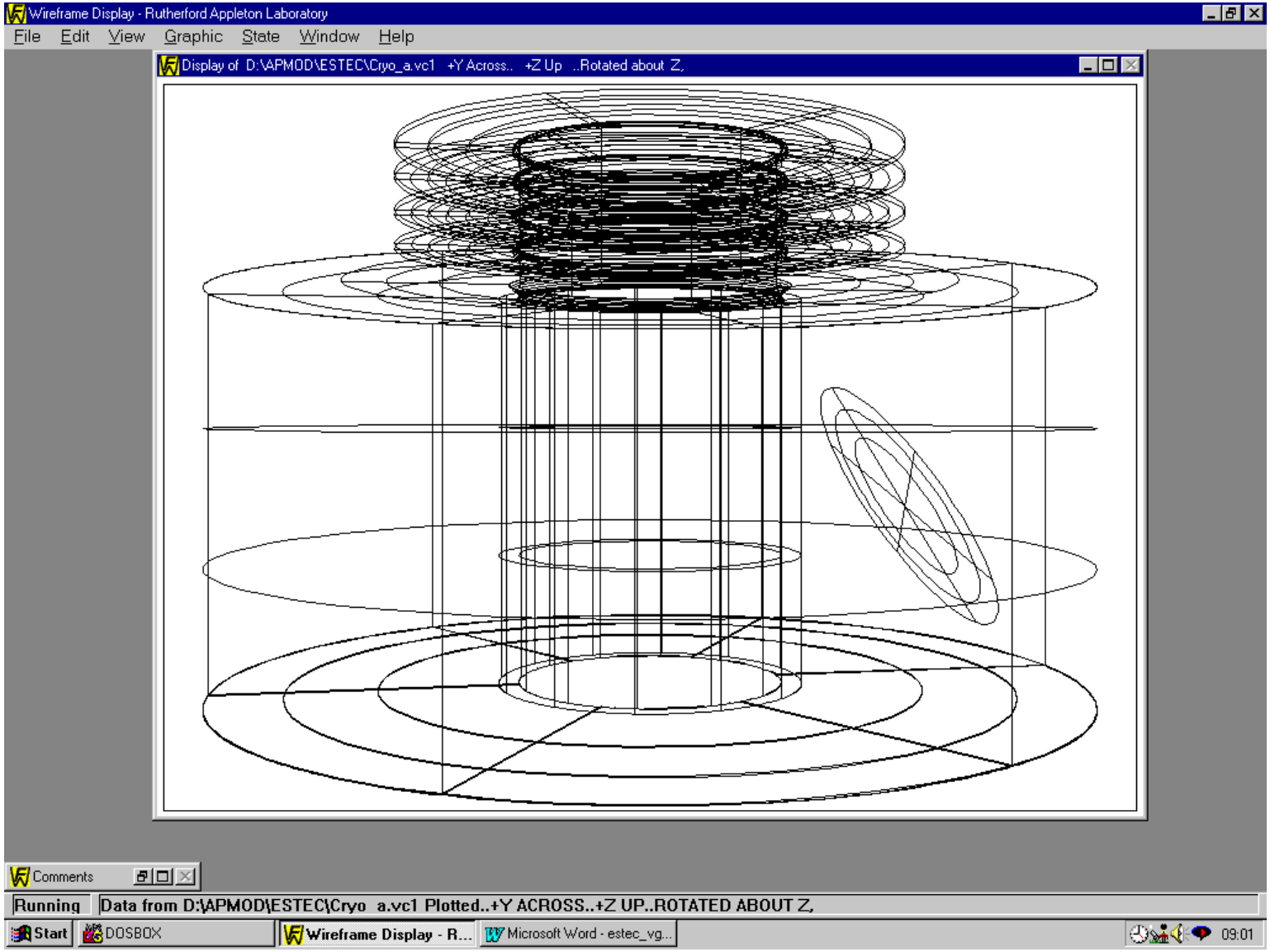

Figure 6.4-3 WIREFRAME display of the cryostat

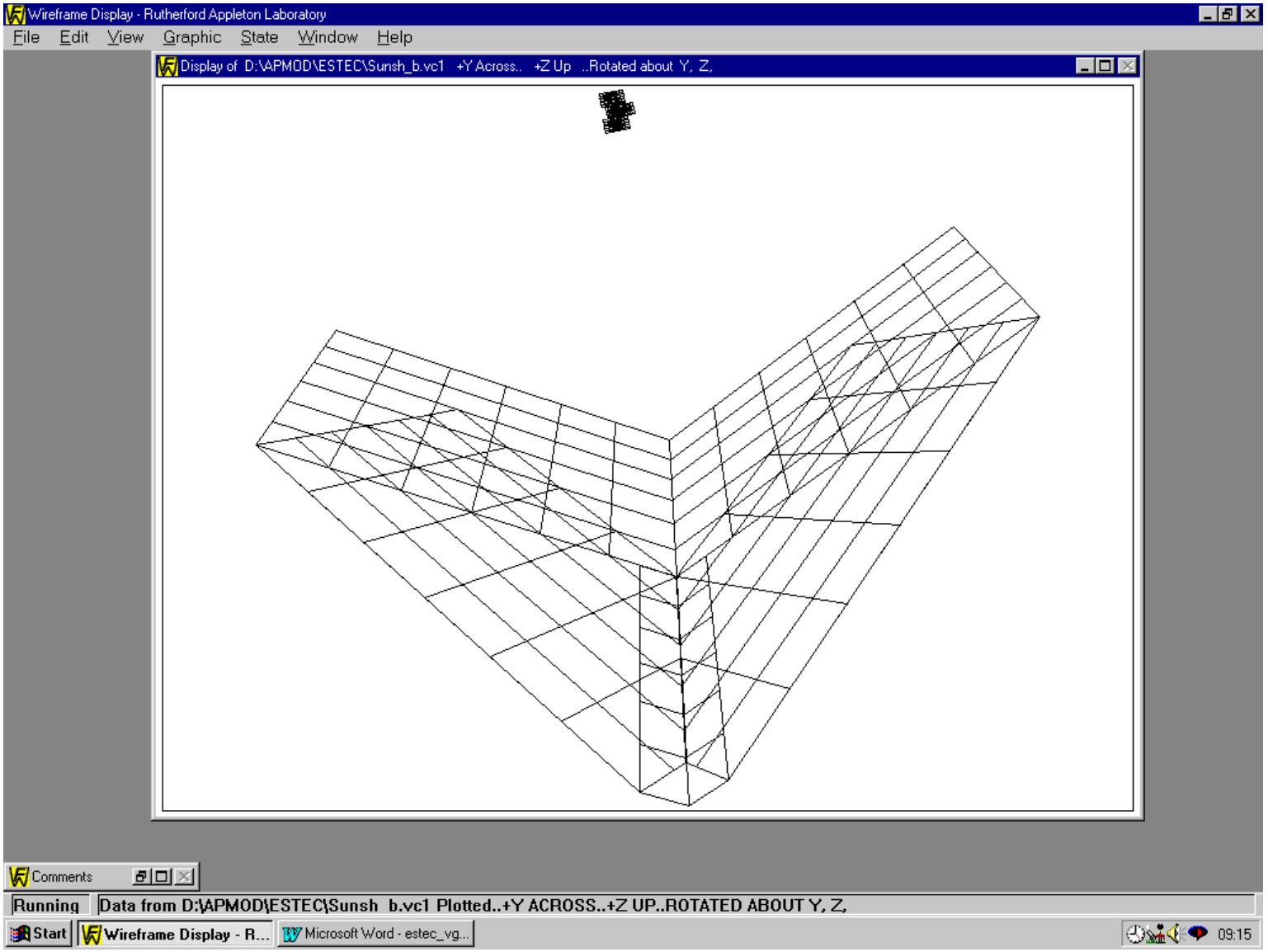

Figure 6.4-4 WIREFRAME display of the sun shield surfaces and the FPU apertures

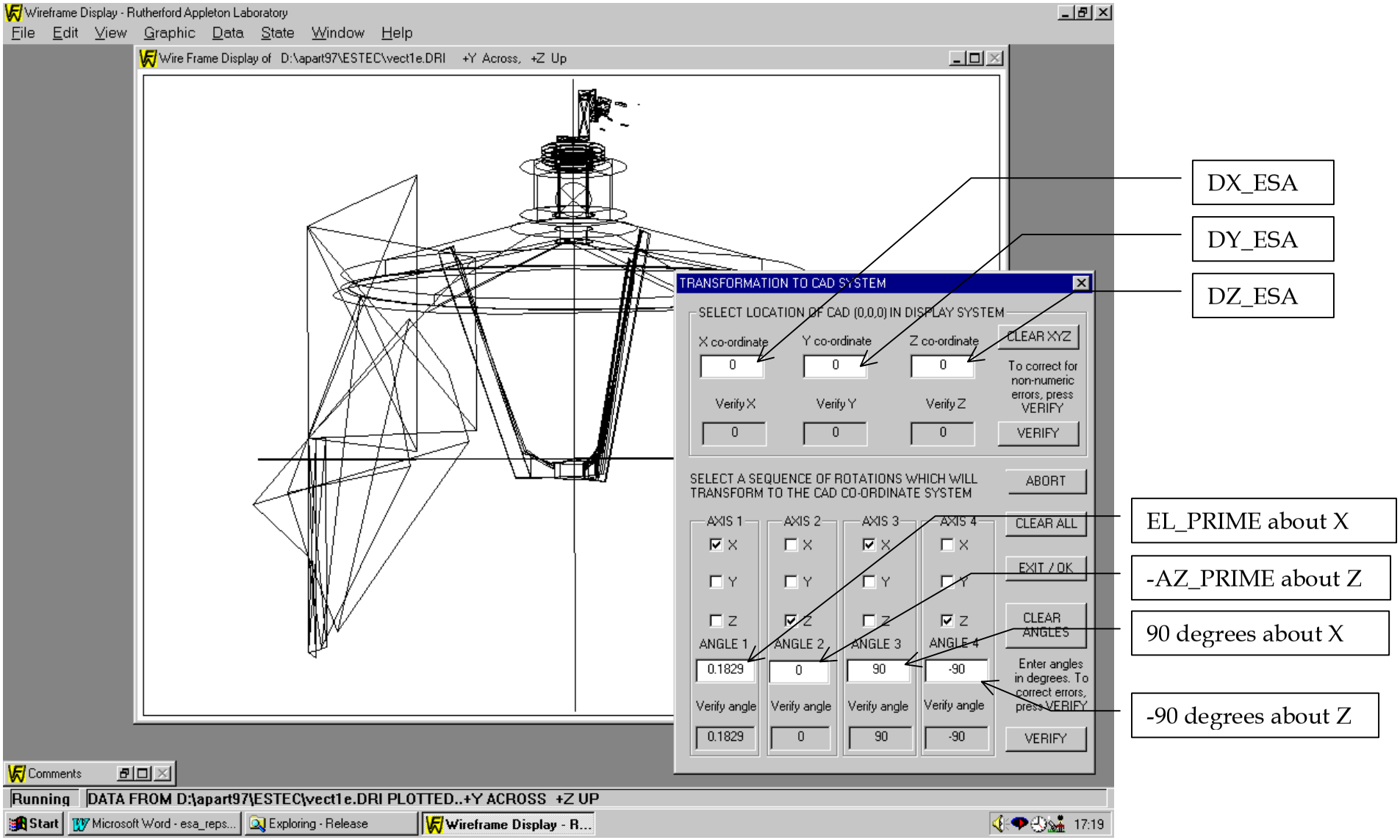

Figure 6.4-5 Using the APART to CAD system transformation program

6.4.2 Exporting the geometry to a CAD platform

Although visual display of the system in the APART co-ordinate frame is very useful for spotting errors made in locating or orienting an object, it does not permit the integration of the APART modelled geometry with other structure that may be described in another co-ordinate frame. If there exists structure that has been entered into a 3-D CAD model which uses the ESA-specified co-ordinate system for FIRST, then the only way to compare this with the APART model will be to transform the APART model into a form which can be read by the CAD system.

The APART package supplies a program called VECT2DXF.EXE which will transform a 3-D vector plot data file (VECT1E.*) into .DXF format, but no co-ordinate transformation is carried out. It is therefore necessary for the CAD system to be able to read .DXF formatted files and to move and orient every single entity represented in the DXF file into its correct place in the CAD co-ordinate system. This will require knowledge of the relationship between the APART and the CAD co-ordinate systems.

An alternative route is to transform the 3-D vector plot data into the CAD co-ordinate system and then to export the transformed data in a format such as IGES which is known to be acceptable to the majority of CAD systems. Because a specially developed APART to IGES format translator was available within the Optical Systems Group, this route is feasible. The application outputs only line entities. In order to use the program, the data required to transform the 3-D vector plots from the APART reference frame to the CAD system must be available. This data must be in the form of up to four distinct rotations about X, Y or Z-axes and translations along the three co-ordinate axes.

If the CAD system uses the ESA-specified co-ordinate system for FIRST, then the CAD origin is located a distance SPACMIRR+TEL_FIX mm along +Z ‘natural’ in figure 3.2-3 (where TEL_FIX=125, see table 5.1-1). The shifts and rotations needed to orient the APART system to coincide with the CAD co-ordinate axes can be derived using the parameters given in table 3.2-1 and they are presented in table 6.4-1.

AXIS	**X**	**Y**	**Z**	
SHIFT	0.0	PS- SIN(EL_PRIME)*{SPACMIRR+TEL_FIX}	PC+ COS(EL_PRIME)*{SPACMIRR+TEL_FIX}	
AXIS	**X**	**Z**	**X**	**Z**
ANGLE	EL_PRIME	-AZ_PRIME	+90	-90

Table 6.4-1 Shifts and rotations needed to transform from APART to ESA co-ordinates

The shift values are computed in the macro GUTRAY, which is executed when the prime FPU has been selected and the gut ray through the optical system must be found. The shift values are listed as variables DX_ESA, DY_ESA and DZ_ESA in the DRIVER.OT1 listing that is output when the system geometry is built by running APART program 1. Figure 6.4-5 shows how the IGES translator will make use of the shifts and rotations in order to do the transformation.

6.5 Listing the objects in the new model

The file FIRST_SURFACE_NUMBERS_NEW.DOC contains a full listing of the object numbers and types used in the new model. An excerpt is reproduced in table 6.5-1.

Object#	Type	Object Label	SUN SHADE	TRIPOD	SECNDRY	PRIMRY	CRYO STAT	OPTIC	FPU
1→2		(NOT USED)							
3	DISK	SM holder rear face		*					
4	CONE	SM side		*					
5	RECT	LEG#1 TOP		*					
6	RECT	LEG#2 TOP		*					
7	RECT	LEG#3 TOP		*					
8	EDGE	SM EDGE OBSC.			*				
9		(NOT USED)							
10	PYRAMID	LEG#1 BODY		*					
11	PYRAMID	LEG#1 INSERT		*					
12	FLAT	LEG#1 EDG.FAC#1		*					
13	FLAT	LEG#1 EDG.FAC#2		*					
14	PYRAMID	STRUT#1.INNER SECT		*					
15	PYRAMID	STRUT#1.OUTER SECT		*					
16	FLAT	STRUT#1 EDG.FAC1#		*					
17	FLAT	STRUT#1.EDG.FAC2#		*					
18	FLAT	INSERT#1EDG.FAC1#		*					
19	FLAT	INSERT#1EDG.FAC2#		*					
20	PYRAMID	LEG#2 BODY		*					
21	PYRAMID	LEG#2 INSERT		*					
22	FLAT	LEG#2.EDG.FAC#1		*					
23	FLAT	LEG#2.EDG.FAC#2		*					
24	PYRAMID	STRUT#2.INNER SECT		*					
25	PYRAMID	STRUT#2.OUTER SEC T		*					
26	FLAT	STRUT#2.EDG.FAC1#		*					
27	FLAT	STRUT#2.EDG.FAC2#		*					
28	FLAT	INSERT#2EDG.FAC1#		*					
29	FLAT	INSERT#2EDG.FAC2#		*					
30	PYRAMID	LEG#3 BODY		*					
31	PYRAMID	LEG#3 INSERT		*					
32	FLAT	LEG#3.EDG.FAC#1		*					
33	FLAT	LEG#3.EDG.FAC#2		*					
34	PYRAMID	STRUT#3.INNER SECT		*					
35	PYRAMID	STRUT#3.OUTER SECT		*					
36	FLAT	STRUT#3.EDG.FAC1#		*					
37	FLAT	STRUT#3.EDG.FAC2#		*					
38	FLAT	INSERT#3EDG.FAC1#		*					
39	FLAT	INSERT#3EDG.FAC2#		*					
40	CONE	Z-AXIS							
41	CONE	X-AXIS							
42	CONE	Y-AXIS							
43	RECT	SUNSH.MAIN +X+Y	*						
44	RECT	SUNSH.MAIN -X+Y	*						
45	RECT	SUNSH.BIG+X+Y	*						
46	RECT	SUNSH.SMALL+X+Y	*						
47	RECT	SUNSH.MID+X+Y	*						
48	STREDGE	SUNSH.RHEDGE+X+Y	*						
49	STREDGE	SUNSH.TOPEDGE+X+	*						
50	STREDGE	SUNSH.SLOPE+X+Y	*						
51	RECT	SUNSH.BIG-X+Y	*						
52	RECT	SUNSH.SMALL-X+Y	*						
53	RECT	SUNSH.MID-X+Y	*						
54	STREDGE	SUNSH.SIDEEDGE-X	*						
55	STREDGE	SUNSH.TOPEDGE-X+	*						
56	STREDGE	SUNSH.SLOPE-X+Y	*						
57	RECT	SS.LOWER.+X+Y	*						
58	RECT	SS.LOWER.-X+Y	*						
59									
60	RECT	OUT.DUM.PHOC.APE							*

Table 6.5-1 Excerpt from FIRST_SURFACE_NUMBERS_NEW.DOC

7. VERIFICATION OF TRANSFERS

7.1 List of transfers

Figure 7.1-1 shows a grid of all the types of transfers that are theoretically possible between the major modules of the APART model. The entry where the row labelled 'SS1' meets the column labelled 'TR2' shows transfers from the sun shield in space 1 to the tripod in space 2 etc. Sources label the rows and collectors label the columns.

The greyed out boxes in the grid indicate transfers that are either not feasible (e.g. transfers from one optical space to one of lower space number) or transfers that are equivalent to other transfers (e.g. transfers from space 1 to space 1 are equivalent to transfers from space N to space N where N>1.

The lightly shaded boxes indicate transfers that perhaps should be computed for the model. Those that have numbers inside them indicate the number of non-zero transfers found involving objects for combination of source and collector. Those that have an empty pair of brackets indicate the transfers that were felt to be initially unimportant and so they were not computed.

The total number of non-zero transfers that APART can sustain in any model is 900. This total is actually exceeded quite quickly if all the possible transfers covered by the transfer grid are considered. It is therefore necessary to consider groups of transfers in any subsequent analysis in order to remain below the APART transfer limit.

7.2 Tripod obscuration

It is frequently necessary, when computing transfers involving sources or collectors located above the primary mirror, to include obscurations that account for the shadowing effect of the tripod structure. Since this is a relatively complicated structure, some in-line macros were written to permit easy inclusion of obscurations by parts or all of the tripod surfaces. The in-line definition commands for these macros are collected together in the file TRIPOBSC.IN2 and they can be made available during program 2 runs by adding the following command to the start of all program 2 input files:

```
$IO INPUT TRIPOBSC.IN2 -3
```

Alternatively, the contents of TRIPOBSC.IN2 can be edited into the body of any or all program 2 input files so that the macro definition commands are the first commands executed before any references to them occur. Both the above methods have been used in testing the latest model. The arguments required for each macro are explained in the body of the Macro file.

STRUC/ SPACE	SS 1	SS 2	SS 3	PM 1	PM 2	PM 3	SM 1	SM 2	SM 3	TR 1	TR 2	TR 3	H0 1	H0 2	H0 3	H0 4	CR 1	CR 2	CR 4	FP 1	FP 2	FP 4	FP 5+	DE T
SS1	2	2	0	32		2	12	8		128	47	0	8			0	23		0					
SS2			0			16						10				4			52					
SS3																								
PM1	8						8			44														
PM2			0			14						9				4			52				2	1
PM3																								
SM1	2	2	0	8		4		4		21	16	15	2			2	13		25				2	2
SM2																								
SM3																							4	1
TR1	44	24	4	44									21											
TR2			8																					
TR3																								
H01	( )												1											
H02			( )													1							2	2
H03																								
H04																							2	0
CR1	( )									( )														
CR2			( )			( )						( )											17	19
CR4																							21	0
FP1	( )						( )			( )			( )				( )							
FP2			( )			( )						( )												
FP4																								
FP5+																								
PS																								

SS=sun shield, PM=primary+rim+edges, SM=secondary+edge, TR=tripod, H0=primary hole, CR=cryostat, FP=focal plane unit optics+structure, PS=point source, DET=detector. () indicates transfers that may or can be ignored.

Table 7.2-1 Grid of all possible transfers between modules and spaces. See text for explanation.

7.3 Primary optic obscurations

The vagaries of the APART co-ordinate system have been explained in detail in section 3. One of the consequences is the fact that the optical surface representing the primary is centred on the point where the gut ray intersects the primary mirror. Because at least two of the Focal Plane Units used in FIRST (SPIRE and PACS) have off-axis gut ray directions, the first APART reflecting optic will be centred at a point such as that labelled P in figure 3.2-3. This optic will be modelled as a sagged disk. It can be given a central hole but unfortunately this hole is forced to be concentric with the centre of the optical surface which, as explained above, is centred in general at an off-axis point such as P. This means that a hole in the APART optical surface cannot be made exactly coincident with the actual hole in the primary mirror. Neither can the edge of the optical surface be made to coincide with the edge of the real primary mirror. The solution was to define two primary mirrors. The first mirror, identified as object 120, is the real primary centred on the axis of the telescope with a concentric hole. The second mirror, object 123, is a dummy optical surface centred at the off-axis point P, with no central hole and with a radius that permits it to extend to the edge of the real primary farthest away from P.

The dummy optic, object 123, is made reflective but the surface properties are applied to the real primary mirror, object 120. Because the dummy primary cannot have a hole or an outer boundary exactly coincident with that of the real primary mirror, transfers involving passage through the primary optical surface must include obscurations that limit the area of the primary optic that can be used. This is done by calling out the outer edge of the real primary, object 122, as a hole obscuration and either calling out its inner edge, object 118, as a disk obscuration or calling out object 117 as a disk obscuration. Object 117 is a disk located at the front of the hole in the primary mirror added for this express purpose.

7.4 Program 2 input files

Because of the large number of transfers which are theoretically feasible in the present system, it was decided to create one program 2 input file for each time that a set of transfers covered by the transfer grid in table 7.2-1 was required. In this way a set of files would eventually be built up which would cover all the transfers in the transfer grid. The input files were in most cases named using the row and column identifiers so that, for example, transfers from sun shield surfaces in space 1 to cryostat surfaces in space 4 are contained in input file SS1CR4.IN2. Not all transfers indicated in the transfer table could be covered in the time allotted.

A set of program 2 input files were generated which were used to compute the transfers entered into the transfer grid in table 7.2-1. These files are listed in table 7.4-1. The transfer file FPUCRDET.IN2 marked '✳' is the only one which is not an UPDATE, so was normally the first transfer file used.

The file POINT.IN2 was used to test transfers from a point source to various objects, including objects inside the cryostat. The file LP1HC1 was used to generate transfers from the lower sections of the sun shield panels to the hole in the primary and to cryostat objects. The files labelled with a '✪' were used to produce transfers for the verification runs of program 3.

POINT.IN2	PM1SS1.IN2	SM1CR1.IN2	
SS1SS1.IN2	PM2SS3.IN2	SM1CR4.IN2	
SS1SS2.IN2	PM2PM3.IN2	TR1SS1.IN2	
SS1SS3.IN2	PM1SM1.IN2	TR1SS2.IN2	
SS2SS3.IN2	PM1TR1.IN2	TR1SS3.IN2	
SS1TR1.IN2 ✪	PM2TR3.IN2	TR2SS3.IN2	
SS1TR2.IN2 ✪	PM2HO4.IN2	TR1PM1.IN2	
SS1TR3.IN2 ✪	PM2CR4.IN2	TR1PM3.IN2	M3TRANS.IN2
SS2TR3.IN2 ✪	PMSMFPU.IN2 ✪	TR2PM3.IN2	
SS1PM1.IN2 ✪	SM1SS1.IN2	TR1SM1.IN2	
SS1PM3.IN2 ✪	SM1SS2.IN2	TR1SM2.IN2	
SS2PM3.IN2 ✪	SM1SS3.IN2	TR1HO1.IN2	TRIPOBSC.IN2
SS1SM1.IN2 ✪	SM1PM1.IN2	TR1FPU.IN2 ✪	
SS1SM2.IN2 ✪	SM1PM3.IN2	TR2FPU.IN2 ✪	
SS1HO1.IN2 ✪	SM1SM2.IN2	TR3FPU.IN2 ✪	
SS1HO4.IN2	SM1TR1.IN2	HC1HC1.IN2	
SS2HO4.IN2 ✪	SM1TR2.IN2	CR2FPU.IN2 ✪	
SS1CR1.IN2 ✪	SM1TR3.IN2	CR4FPU.IN2 ✪	
SS1CR4.IN2	SM1HO1.IN2	FPUCRDET.IN2 ✴	
SS2CR4.IN2 ✪	SM1HO4.IN2	LP1HC1.IN2 ✪	

Table 7.4-1 APART program 2 transfer files

7.5 Some Critical transfers

When APART program 2 was executed using transfer file CR2FPU.IN2 as input, it found non-zero transfers between the wall of the hole in the primary and some internal cryostat surfaces as sources, and various FPU surfaces as collectors. The FPU surfaces in question include the field mirror M3, object 210 in space 5, and the FPU detector, object 299 in space 15. These transfers go via the secondary mirror, so they involve cryostat surfaces facing the secondary. Similar transfers to the edge of the cold stop inside the FPU failed. This showed that APART had found an optical path from cryostat surfaces direct to the detector involving optical reflections from a region close to the centre of the secondary mirror. These transfers will eventually be shown be potentially able to contribute significant straylight to the FPU detector. Some of the transfers found are shown in tables 7.5-1 and 7.5-2, which are extracted from summary files produced by running APART program 2 with CR2FPU.IN2 as the input file. The wall of the primary hole is object 119. The forward edge of the primary hole is object 118. The other surfaces are cryostat surfaces, as examination of figure 5.4-1 will confirm.

TRANSFER		SOURCE	COLLECTOR	SOURCE PI Z	COLLECTOR PI Z	TRANSFER TIME	SOURCE SMALL AVERAGE	COLLECTOR SMALL AVERAGE	TOTAL GCF	AZIMUTH
403	TRANSFR	173.02	210.05	12 -10	12 -10	2.73 S	0.000	0.000	1.869E-09	0.000
404	TRANSFR	174.02	210.05	9 -9	12 -10	1.27 S	0.000	0.000	6.406E-09	0.000
405	TRANSFR	171.02	210.05	12 -10	12 -10	2.83 S	0.000	0.000	1.072E-09	0.000
406	TRANSFR	148.02	210.05	9 -9	12 -10	2.75 S	0.000	0.000	8.715E-09	0.000
407	TRANSFR	166.02	210.05	9 -9	12 -10	1.33 S	0.000	0.000	4.530E-09	0.000
408	TRANSFR	146.02	210.05	9 -10	12 -10	2.20 S	0.000	0.000	5.169E-09	0.000
409	TRANSFR	147.02	210.05	9 -9	12 -10	1.27 S	0.000	0.000	4.358E-09	0.000
410	TRANSFR	144.02	210.05	9 -10	12 -10	2.05 S	0.000	0.000	3.777E-09	0.000
411	TRANSFR	145.02	210.05	9 -9	12 -10	1.28 S	0.000	0.000	4.243E-09	0.000
412	TRANSFR	142.02	210.05	9 -10	12 -10	2.02 S	0.000	0.000	3.676E-09	0.000
413	TRANSFR	143.02	210.05	9 -9	12 -10	1.25 S	0.000	0.000	4.125E-09	0.000
414	TRANSFR	140.02	210.05	9 -10	12 -10	1.94 S	0.000	0.000	2.573E-09	0.000
415	TRANSFR	141.02	210.05	9 -9	12 -10	1.26 S	0.000	0.000	4.029E-09	0.000
416	TRANSFR	152.02	210.05	9 -5	12 -10	0.86 S	0.000	0.000	6.898E-10	0.000
417	TRANSFR	155.02	210.05	9 -5	12 -10	0.83 S	0.000	0.000	7.163E-10	0.000
418	TRANSFR	158.02	210.05	9 -5	12 -10	0.82 S	0.000	0.000	7.454E-10	0.000
419	TRANSFR	161.02	210.05	9 -5	12 -10	0.80 S	0.000	0.000	7.770E-10	0.000
420	TRANSFR	118.02	299.15	9 1	12 -10	1.48 S	0.000	0.000	5.176E-09	0.000
421	TRANSFR	119.02	299.15	9 -9	12 -10	10.62 S	0.000	0.000	3.759E-10	0.000
422	TRANSFR	173.02	299.15	12 -10	12 -10	7.98 S	0.000	0.000	4.222E-10	0.000
423	TRANSFR	174.02	299.15	9 -9	12 -10	6.26 S	0.000	0.000	1.434E-09	0.000
424	TRANSFR	171.02	299.15	12 -10	12 -10	7.90 S	0.000	0.000	2.399E-10	0.000
425	TRANSFR	148.02	299.15	9 -9	12 -10	11.74 S	0.000	0.000	1.950E-09	0.000
426	TRANSFR	166.02	299.15	9 -9	12 -10	6.46 S	0.000	0.000	1.012E-09	0.000
427	TRANSFR	146.02	299.15	9 -10	12 -10	8.30 S	0.000	0.000	1.155E-09	0.000
428	TRANSFR	147.02	299.15	9 -9	12 -10	6.21 S	0.000	0.000	9.734E-10	0.000
429	TRANSFR	144.02	299.15	9 -10	12 -10	7.56 S	0.000	0.000	8.435E-10	0.000
430	TRANSFR	145.02	299.15	9 -9	12 -10	6.21 S	0.000	0.000	9.479E-10	0.000
431	TRANSFR	142.02	299.15	9 -10	12 -10	7.56 S	0.000	0.000	8.212E-10	0.000
432	TRANSFR	143.02	299.15	9 -9	12 -10	6.29 S	0.000	0.000	9.216E-10	0.000
433	TRANSFR	140.02	299.15	9 -10	12 -10	7.01 S	0.000	0.000	5.744E-10	0.000
434	TRANSFR	141.02	299.15	9 -9	12 -10	6.26 S	0.000	0.000	9.002E-10	0.000
435	TRANSFR	152.02	299.15	9 -5	12 -10	5.61 S	0.000	0.000	1.541E-10	0.000
436	TRANSFR	155.02	299.15	9 -5	12 -10	5.57 S	0.000	0.000	1.600E-10	0.000
437	TRANSFR	158.02	299.15	9 -5	12 -10	5.56 S	0.000	0.000	1.666E-10	0.000
438	TRANSFR	161.02	299.15	9 -5	12 -10	5.53 S	0.000	0.000	1.734E-10	0.000

Table 7.5-1 APART-calculated transfers from the primary hole and cryostat forward facing surfaces to SPIRE M3 and detector

TABLE OF CALCULATED TRANSFERS FROM FORWARD-FACING FPU APERTURES AND APERTURE SURROUNDS TO THE SPIRE DETECTOR

TRANSFER		SOURCE	COLLECTOR	SOURCE PI	SOURCE Z	COLLECTOR PI	COLLECTOR Z	TRANSFER TIME	SOURCE SMALL AVERAGE	COLLECTOR SMALL AVERAGE	TOTAL GCF	AZIMUTH
6	TRANSFR	109.02	299.15	9	-9	12	-10	11.28 S	0.000	0.000	2.440E-09	0.000
7	TRANSFR	199.02	299.15	9	-9	12	-10	11.27 S	0.000	0.000	2.437E-09	0.000
8	TRANSFR	209.02	299.15	9	-3	12	-10	3.29 S	0.000	0.000	2.455E-09	0.000
9	TRANSFR	60.02	299.15	9	-6	12	-10	7.41 S	0.000	0.000	2.600E-09	0.000
10	TRANSFR	100.02	299.15	9	-6	12	-10	7.34 S	0.000	0.000	2.438E-09	0.000
11	TRANSFR	191.02	299.15	9	-6	12	-10	7.30 S	0.000	0.000	2.432E-09	0.000
12	TRANSFR	200.02	299.15	9	-6	12	-10	7.30 S	0.000	0.000	2.456E-09	0.000

TABLE OF CALCULATED TRANSFERS SPIRE MIRORS TO THE SPIRE DETECTOR

TRANSFER		SOURCE	COLLECTOR	SOURCE PI	SOURCE Z	COLLECTOR PI	COLLECTOR Z	TRANSFER TIME	SOURCE SMALL AVERAGE	COLLECTOR SMALL AVERAGE	TOTAL GCF	AZIMUTH
13	TRANSFR	210.06	299.15	12	-10	12	-10	3.68 S	0.000	0.000	1.373E-06	0.000
14	TRANSFR	266.08	299.15	12	-10	12	-10	7.16 S	0.000	0.000	6.456E-05	0.000
15	TRANSFR	268.10	299.15	12	-10	12	-10	8.65 S	0.019	0.000	3.544E-06	0.000
16	TRANSFR	270.12	299.15	12	-10	12	-10	3.96 S	0.000	0.000	2.182E-05	0.000
17	TRANSFR	273.14	299.15	12	-10	12	-10	2.80 S	0.000	0.000	1.129E-05	0.000
18	TRANSFR	274.15	299.15	12	-10	12	-10	1.24 S	0.000	0.000	3.821E-05	0.000

Table 7.5-2 APART-calculated transfers from forward facing FPU surfaces and SPIRE mirrors to the SPIRE detector

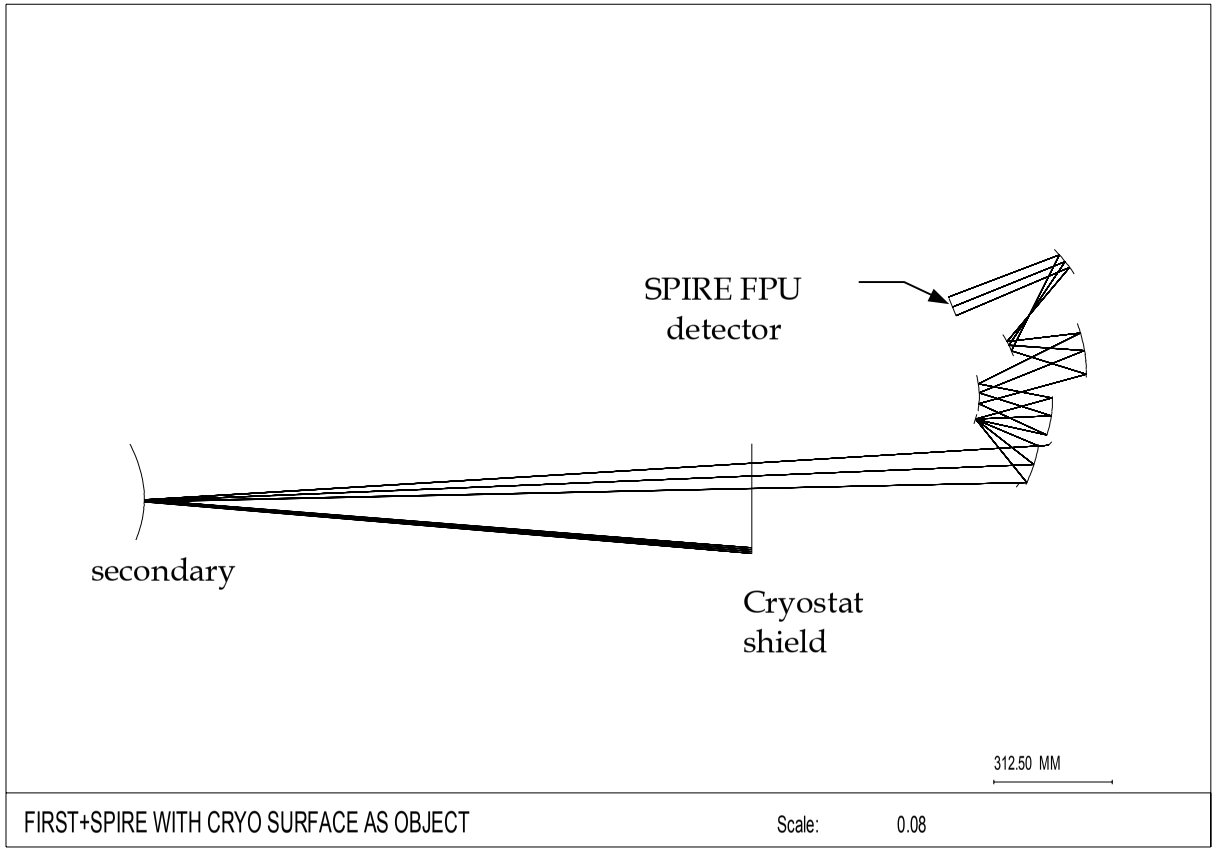

Figure 7.5-1 An example of the SPIRE detector's view of a cryostat surface illustrated using CODEV

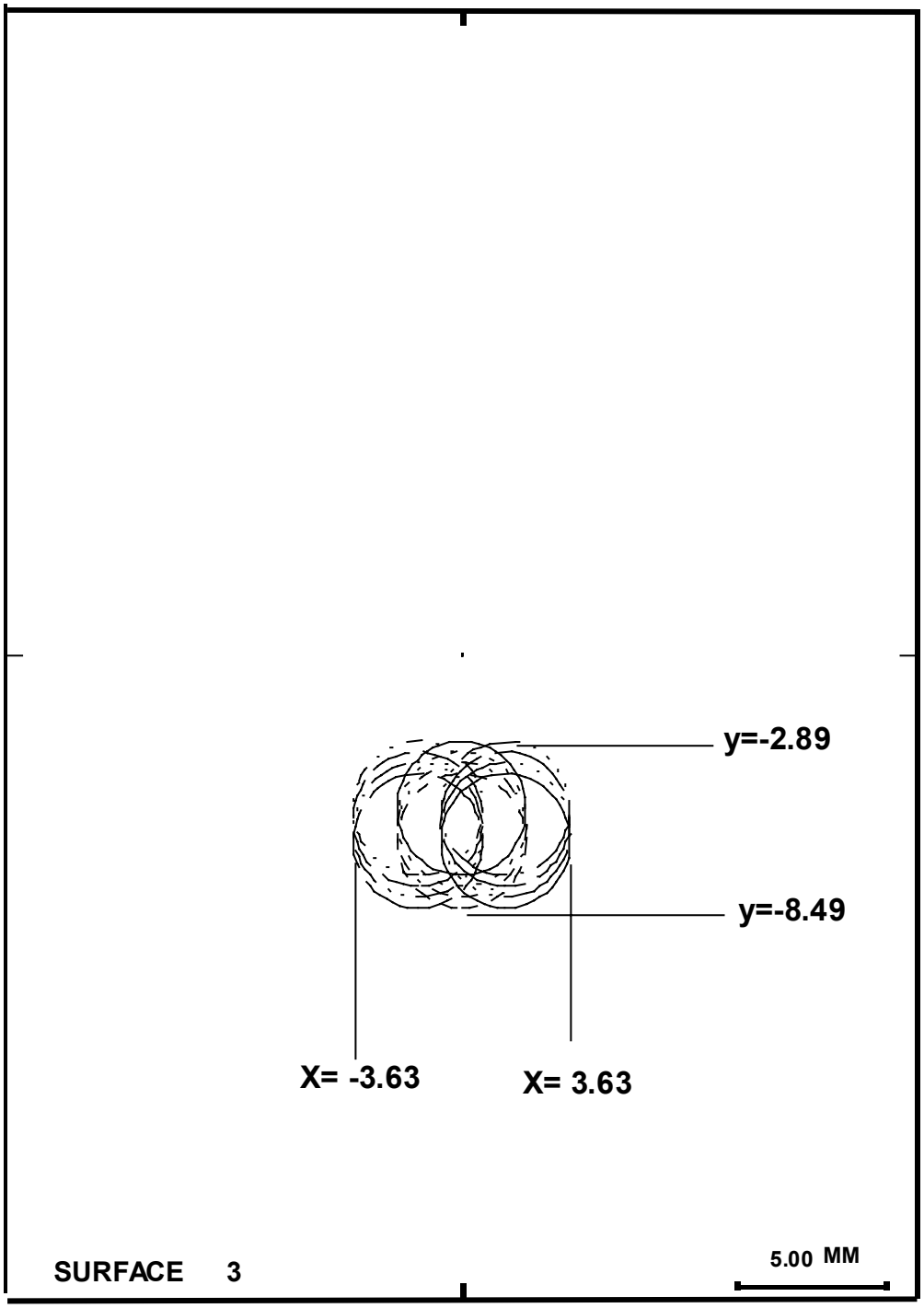

Figure 7.5-2 Region of the secondary mirror used to image cryostat surface onto the FPU detector.

The optical path that APART found has been confirmed using CODEV modelling. Figure 7.5-1 shows a CODEV plot of rays leaving several points located on an object close to the

inner edge of one of the cryostat shields. The rays are traced through the secondary and onwards to the FPU, eventually terminating within the detector boundary. Figure 7.5-2 shows the footprint of the beam on the secondary mirror, which covers a rectangle about 6 mm by 7 mm with its centre offset about 5.5 mm from the centre of the secondary mirror. This footprint size will increase as more locations inside the cryostat and the hole in the primary are considered for the objects.

8. VERIFICATION OF STRAYLIGHT PROPAGATION TO THE FPU DETECTOR

8.1 Surface properties and temperatures – original model

The file FIRST_SURF_TEMP_EMISS_COAT_OLD.DOC summarises the surface properties that were applied to the objects in the original model. An extract from this file is shown in table 8.1-1.

Object#	Type	Object Label	Object #	COATING NUMBER	COATING TYPE	TEMPERATURE	EMISSIVITY
1	EDGE	ENTR.WINDOW	1				
2	CONE	SUNSHADE	2	5	Mirror/8/-2	180	0.2
3	DISK	SMOBSCURATION	3				
4	CONE	SMBACKSIDECONE	4	5	Mirror/8/-2	130	1.000
5	RECT	TRIPOD1RECT	5				
6	RECT	TRIPOD2RECT	6				
7	RECT	TRIPOD3RECT	7				
8	EDGE	M2EDGEOBSC.	8	2	Edge/Kirch		
9	EDGE	SUNSHADEEDGE	9	2	Edge/Kirch		
10	PYRAMID	LEG#1 BODY	10	3	Harv/1.9/-2	117	0.04
11	PYRAMID	LEG#1 INSERT	11				
12	FLAT	LEG#1 EDG.FAC#1	12	3	Harv/1.9/-2		
13	FLAT	LEG#1 EDG.FAC#2	13	3	Harv/1.9/-2		
14	PYRAMID	STRUT#1.INNER SECT	14	3	Harv/1.9/-2		
15	PYRAMID	STRUT#1.OUTER SECT	15	3	Harv/1.9/-2		
16	FLAT	STRUT#1 EDG.FAC1#	16	3	Harv/1.9/-2		
17	FLAT	STRUT#1.EDG.FAC2#	17	3	Harv/1.9/-2		
18	FLAT	INSERT#1EDG.FAC1#	18				
19	FLAT	INSERT#1EDG.FAC2#	19				
20	PYRAMID	LEG#2 BODY	20	3	Harv/1.9/-2	117	0.04
21	PYRAMID	LEG#2 INSERT	21				
22	FLAT	LEG#2.EDG.FAC#1	22	3	Harv/1.9/-2		
23	FLAT	LEG#2.EDG.FAC#2	23	3	Harv/1.9/-2		
24	PYRAMID	STRUT#2.INNER SECT	24	3	Harv/1.9/-2		
25	PYRAMID	STRUT#2.OUTER SEC T	25	3	Harv/1.9/-2		
26	FLAT	STRUT#2.EDG.FAC1#	26	3	Harv/1.9/-2		
27	FLAT	STRUT#2.EDG.FAC2#	27	3	Harv/1.9/-2		
28	FLAT	INSERT#2EDG.FAC1#	28				
29	FLAT	INSERT#2EDG.FAC2#	29				
30	PYRAMID	LEG#3 BODY	30	3	Harv/1.9/-2	117	0.04
31	PYRAMID	LEG#3 INSERT	31				
32	FLAT	LEG#3.EDG.FAC#1	32	3	Harv/1.9/-2		
33	FLAT	LEG#3.EDG.FAC#2	33	3	Harv/1.9/-2		
34	PYRAMID	STRUT#3.INNER SECT	34	3	Harv/1.9/-2		
35	PYRAMID	STRUT#3.OUTER SECT	35	3	Harv/1.9/-2		
36	FLAT	STRUT#3.EDG.FAC1#	36	3	Harv/1.9/-2		
37	FLAT	STRUT#3.EDG.FAC2#	37	3	Harv/1.9/-2		
38	FLAT	INSERT#3EDG.FAC1#	38				
39	FLAT	INSERT#3EDG.FAC2#	39				
40→104		(NOT USED)	40→104				
105	EDGE	SHIELD0:	105				

Table 8.1-1 Excerpt from FIRST_SURF_TEMP_EMISS_COAT_OLD.DOC

Notice that not all surfaces were assigned temperatures and emissivities, only a relatively small subset of tripod surfaces being considered for emission calculations. The data were extracted from the *.IN3 data files extracted from DSS97MODEL.ZIP containing the APART scripts from previous analyses.

8.2 Surface properties and temperatures – new model

The data extracted from the original files and recorded in summary form in the document FIRST_SURF_TEMP_EMISS_COAT_OLD.DOC formed the basis for the surface properties to be used in verification runs of program 3. The data used in the verification runs is summarised in FIRST_SURF_TEMP_EMISS_COAT_NEW.DOC.

8.3 Input files for verification runs – new model

Several APART program 3 input files were generated in order to exercise and test the new model. Thermal emission was modelled from the sun shield, the tripod and secondary mirror, the primary mirror and primary mirror hole and the cryostat front and internal surfaces. Emission from FPU apertures and aperture surrounds was also included following the identification of transfer paths from these surfaces direct to the SPIRE FPU detector. Thermal emission was modelled in the three SPIRE wavebands, these being 200 –300 μ, 300 –400 μ, and 400 –650 μ. The APART program 3 data file names are listed in table 8.3-1. Typical temperatures and emissivities used are listed in table 8.3-2.

Input file name	Comments
TH250A.IN3	200 –300 μ waveband
TH250C.IN3	200 –300 μ , but no primary or secondary mirror or primary hole emission
TH350A.IN3	300 –400 μ waveband
TH350C.IN3	300 –400 μ , but no primary or secondary mirror or primary hole emission
TH500A.IN3	400 –650 μ waveband
TH500C.IN3	400 –650 μ , but no primary or secondary mirror or primary hole emission

Table 8.3-1 Program 3 input files used for verification runs

Temp °K	APART parameter	Applied to	Emissivity	APART parameter	Applied to surfaces associated with
170	TSSUP	Upper sun shield	0.04	ESS	Sun shield
250	TSSLOW	Lower sunshield	0.01	EPM	Primary mirror
74	TPM	Primary mirror	0.01	ESM	Secondary mirror
74	TSM	Secondary	0.02	EHOLE	Primary hole wall
74	TSMCELL	Secondary support cell	0.04	ESMCELL	Secondary support cell
74	TTRIPOD	Tripod surfaces	0.04	ETRIPOD	Tripod struts and legs
74	TCAVITY	Upper cryostat cavity	0.05	ECAVITY	Walls of cryostat upper cavity
77	TCVV	CVV surfaces	0.05	ECVV	CVV plate
64	THS3	Cryostat shield 3	0.15	EHS3	Cryostat shield 3
49	THS2	Cryostat shield 2	0.15	EHS2	Cryostat shield 2
32	THS1	Cryostat shield 1	0.15	EHS1	Cryostat shield 1
14	THS0	Cryostat shield 0	0.15	EHS0	Cryostat shield 0
14	TFPUBOX	FPU aperture and surround	0.5	EFPUBOX	FPU aperture and surround
14	TFPUM3	FPU mirror M3	0.02	EFPUMIRR	FPU mirror M3
4	TFPUMIRR	Other FPU mirrors	1.0	EBLACK	

Table 8.3-2 Temperatures and emissivities used in verification runs

8.4 Results of verification runs – new model

Some results of APART modelling of the levels of telescope/PLM thermal radiation reaching the SPIRE detector are presented here. The results for the shortest SPIRE waveband is typical of all three wavebands so only those will be shown.

The results are presented with (TH250A.IN1) and without (TH250C.IN1) thermal emission modelled from the primary and secondary mirror surfaces. The results without radiation from the main mirrors are used to get more detail on the minor sources of background radiation.

The tables show that, as expected, thermal radiation from the primary and secondary mirrors dominates. The next most important contribution is not M3, but object 173, the outside surface of the cryostat cavity. This contributes because of the transfer path from the object via the secondary that was found during program 2 verification runs.

Comparing the results for runs done with and without the major contributions from the telescope mirrors, it would appear that the minor contribution is about 6.5% of the total. This figure satisfies the ESA requirement for stray thermal emission power reaching the detector, that it be less than 10% of the total direct (i.e. no scattering) contribution from the telescope and FPU optics. However, the margin appears small, given the uncertainties, so more detailed APART modelling is merited.

OBJECTS/		LEVEL 0	1
10	LEG#1 BODY	0.05	0.01
12	LEG#1,EDG.FAC#1	0.28	0.00
13	LEG#1,EDG.FAC#2	0.28	0.00
14	STRUT#1,INNER SE	0.00	0.00
15	STRUT#1,OUTER SE	0.00	0.00
16	STRUT#1,EDG.FAC#	0.10	0.00
17	STRUT#1,EDG.FAC#	0.10	0.00
20	LEG#2 BODY	0.06	0.00
22	LEG#2,EDG.FAC#1	0.23	0.05
23	LEG#2,EDG.FAC#2	0.26	0.00
24	STRUT#2,INNER SE	0.00	0.00
25	STRUT#2,OUTER SE	0.00	0.00
26	STRUT#2,EDG.FAC#	0.08	0.01
27	STRUT#2,EDG.FAC#	0.09	0.00
30	LEG#3 BODY	0.06	0.00
32	LEG#3,EDG.FAC#1	0.26	0.00
33	LEG#3,EDG.FAC#2	0.23	0.05
34	STRUT#3,INNER SE	0.00	0.00
35	STRUT#3,OUTER SE	0.00	0.00
36	STRUT#3,EDG.FAC#	0.09	0.00
37	STRUT#3,EDG.FAC#	0.08	0.01
60	OUT.DUM.PACS.APE	0.03	0.00
69	PACS APERT.SURRN	0.05	0.03
100	OUT.DUM.HIFI.APE	0.04	0.00
109	HIFI APERT.SURRN	0.05	0.03
119	PM HOLE WALL	0.07	6.72
120	PRIMARY MIRROR	44.57	38.33
129	SECONDARY MIRROR	49.52	43.79
140	SHLD0 TO TEL	0.00	0.00
141	SHLD0 EDGE	0.00	0.00
142	SHLD1 TO TEL	0.03	0.00
143	SHLD1 EDGE	0.00	0.00
144	SHLD2 TO TEL	0.06	0.00
145	SHLD2 EDGE	0.00	0.00
146	SHLD3 TO TEL	0.13	0.00
147	SHLD3 EDGE	0.00	0.00
148	CVV UPPER CONE	0.08	0.00
166	CVV INNER EDGE	0.00	0.00
171	CVV OUTER SURF	0.55	0.00
173	CAVITY CAP OUT.S	1.41	0.00
174	CRYOCOVER HOLEED	0.00	0.00
191	OUT.DUM.DUMMY.AP	0.01	0.00
199	DUMMY APERT.SURR	0.02	0.00
200	OUT.DUMMY FPU.AP	0.03	0.00
209	FPU APERT.SURROU	0.05	0.03
210	M3 MIRROR	1.05	10.92
266	M4,ASTOP1	0.00	0.02
268	M5	0.00	0.00
270	M6	0.00	0.00
273	M7	0.00	0.00
274	M8	0.00	0.00
TOTAL POWER(WATT)		2.40E-9	3.6E-11

Table 8.4-1 % power contributed by each object as a function of each scatter level

Top 10 propagation paths and their percent contributions

```
1  48.69%  129.03-->299.15
     *SECONDARY MIRR* DETECTOR *

2  43.90%  120.02-->299.15
     *PRIMARY MIRR *  DETECTOR *

3   1.39%  173.02-->299.15
     *CRYO.OUT.FACE*  DETECTOR *

4   1.04%  210.06-->299.15
     *SPIRE.M3 MIRR*  DETECTOR *

5   0.54%  171.02-->299.15
     *CVV.OUT.FACE *  DETECTOR *

6   0.33%   44.01-->129.01 129.03-->299.15
         *SUNSHADE*SECONDARY MIRRO* DETECTOR*

7   0.33%   43.01-->129.01 129.03-->299.15
         *SUNSHADE*SECONDARY MIRRO* DETECTOR*

8   0.28%   43.01-->120.01 120.02-->299.15
         *SUNSHADE*PRIMARY MIRRO* DETECTOR*

9   0.28%   44.01-->120.01 120.02-->299.15
         *SUNSHADE*PRIMARY MIRRO* DETECTOR*

10   0.16%   12.01-->299.15
   *TRIPOD LEG EDGE* DETECTOR*
```

Table 8.4-2 Top 10 propagation paths for the 200μ - 300μ waveband

PERCENT OF POWER CONTRIBUTED BY EACH OBJECT AS A FUNCTION OF EACH LEVEL

OBJECTS/	LEVEL 0	1	2
10 LEG#1 BODY	1.10	0.01	0.00
12 LEG#1,EDG.FAC#1	5.75	0.00	0.00
13 LEG#1,EDG.FAC#2	5.75	0.00	0.00
14 STRUT#1,INNER SE	0.01	0.00	0.00
15 STRUT#1,OUTER SE	0.00	0.00	0.00
16 STRUT#1,EDG.FAC#	2.03	0.00	0.00
17 STRUT#1,EDG.FAC#	2.03	0.00	0.00
20 LEG#2 BODY	1.13	0.00	0.00
22 LEG#2,EDG.FAC#1	4.80	0.05	0.00
23 LEG#2,EDG.FAC#2	5.39	0.00	0.00
24 STRUT#2,INNER SE	0.05	0.00	0.00
25 STRUT#2,OUTER SE	0.01	0.00	0.00
26 STRUT#2,EDG.FAC#	1.74	0.01	0.00
27 STRUT#2,EDG.FAC#	1.79	0.00	0.00
30 LEG#3 BODY	1.13	0.00	0.00
32 LEG#3,EDG.FAC#1	5.39	0.00	0.00
33 LEG#3,EDG.FAC#2	4.80	0.05	0.00
34 STRUT#3,INNER SE	0.05	0.00	0.00
35 STRUT#3,OUTER SE	0.01	0.00	0.00
36 STRUT#3,EDG.FAC#	1.79	0.00	0.00
37 STRUT#3,EDG.FAC#	1.74	0.01	0.00
60 OUT.DUM.PACS.APE	0.63	0.00	0.00
69 PACS APERT.SURRN	1.10	0.00	0.00
100 OUT.DUM.HIFI.APE	0.75	0.00	0.00
109 HIFI APERT.SURRN	1.02	0.00	0.00
119 PM HOLE WALL	1.41	6.86	100.00
120 PRIMARY MIRROR	0.00	39.09	0.00
129 SECONDARY MIRROR	0.00	44.66	0.00
140 SHLD0 TO TEL	0.03	0.00	0.00
141 SHLD0 EDGE	0.01	0.00	0.00
142 SHLD1 TO TEL	0.52	0.00	0.00
143 SHLD1 EDGE	0.00	0.00	0.00
144 SHLD2 TO TEL	1.25	0.00	0.00
145 SHLD2 EDGE	0.00	0.00	0.00
146 SHLD3 TO TEL	2.66	0.00	0.00
147 SHLD3 EDGE	0.00	0.00	0.00
148 CVV UPPER CONE	1.64	0.00	0.00
166 CVV INNER EDGE	0.00	0.00	0.00
171 CVV OUTER SURF	11.38	0.00	0.00
173 CAVITY CAP OUT.S	29.05	0.00	0.00
174 CRYOCOVER HOLEED	0.00	0.00	0.00
191 OUT.DUM.DUMMY.AP	0.13	0.00	0.00
199 DUMMY APERT.SURR	0.34	0.00	0.00
200 OUT.DUMMY FPU.AP	0.58	0.00	0.00
209 FPU APERT.SURROU	1.01	0.00	0.00
210 M3 MIRROR	0.00	9.24	0.00
266 M4,ASTOP1	0.00	0.00	0.00
268 M5	0.00	0.00	0.00
270 M6	0.00	0.00	0.00
273 M7	0.01	0.00	0.00
274 M8	0.01	0.00	0.00
TOTAL POWER(Watt)	1.2E-10	3.6E-11	1.1E-16

Table 8.4-3 % power contributed by each object as a function of each scatter level (no primary, secondary or M3 emission)

TOP 10 PROPAGATION PATHS AND THEIR PERCENT CONTRIBUTIONS

```
1  22.23%  173.02-->299.15
     *CRYO.OUT.FACE*  DETECTOR *

2   8.71%  171.02-->299.15
     *CVV.OUT.FACE *  DETECTOR *

3   5.23%   44.01-->129.01 129.03-->299.15
          *SUNSHADE*SECONDARY MIRRO* DETECTOR*

4   5.23%   43.01-->129.01 129.03-->299.15
          *SUNSHADE*SECONDARY MIRRO* DETECTOR*

5   4.51%   43.01-->120.01 120.02-->299.15
          *SUNSHADE*  PRIMARY MIRRO* DETECTOR*

6   4.51%   44.01-->120.01 120.02-->299.15
          *SUNSHADE*  PRIMARY MIRRO* DETECTOR*

7   2.54%   12.01-->299.15
   *TRIPOD LEG#1 EDGE* DETECTOR*

8   2.54%   13.01-->299.15
   *TRIPOD LEG#1 EDGE* DETECTOR*

9   2.49%   32.02-->299.15
   *TRIPOD LEG#1 EDGE* DETECTOR*

10   2.49%   23.02-->299.15
   *TRIPOD LEG#1 EDGE* DETECTOR*
```

Table 8.4-4 Top 10 propagation paths for the 200μ - 300μ waveband (no primary, secondary or M3 emission)

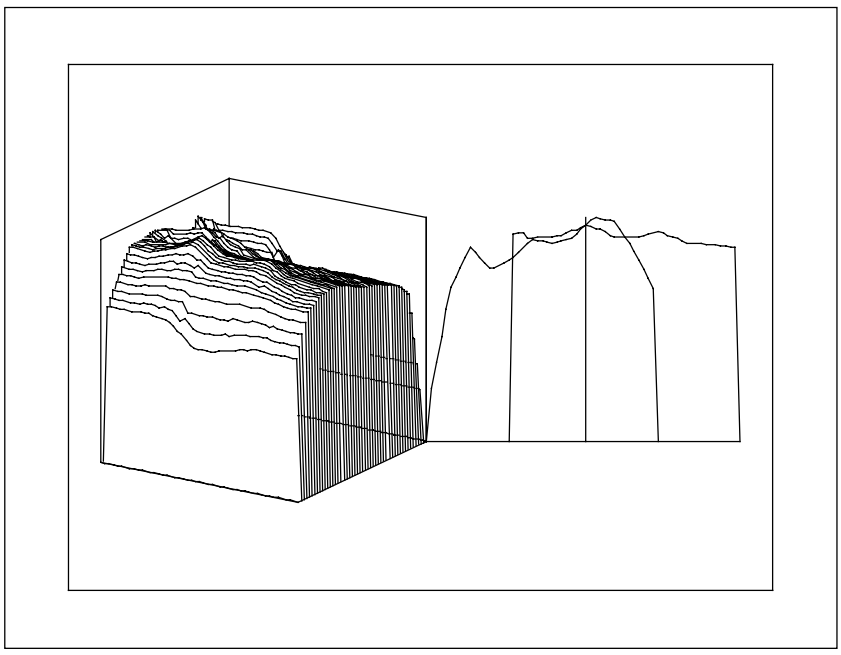

Table 8.4-5 Typical Stray Energy Distribution on the SPIRE detector

9. ASAP BEAM PATTERNS IN THE SPIRE-PHOT INSTRUMENT & THE FIRST TELESCOPE

9.1 System analysed

The optical system analysed is detailed in the ASAP input file BOLPHT80.inr. The wavelength λ at which the analysis was carried out was 0.5mm, i.e. the centre of the longest-wavelength SPIRE channel. The beam patterns were analysed at each component in the FPU and the telescope, using the ASAP©-based method published elsewhere (ASAP references 1, 2). Previously the possible choices of beam shape (detector type) were analysed in the telescope alone (ASAP reference 3), and here we use the edge-diffraction worst-case of a 'top-hat' beam, i.e. a bare detector, with zero spatial size and infinite angular size (fully incoherent).

The optical prescription, as translated into ASAP, uses 'object' numbers to label each component (see the BOLPHT80.inr file). The system is illustrated in the ASAP ray-traces given in figures 9.1-1 and 9.1-2. Table 9.1-1 gives the key to linking the main components to the ASAP object numbers given in the figures.

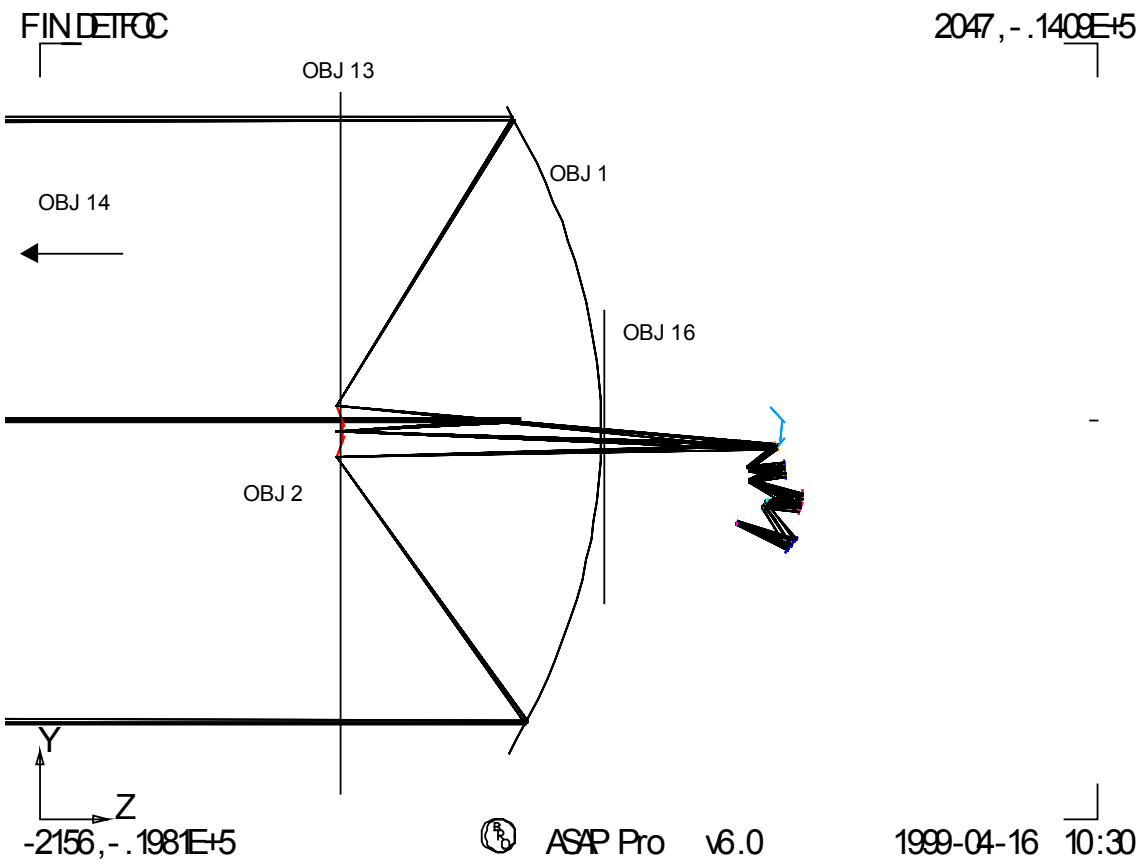

Figure 9.1-1 ASAP ray-trace of all objects in the analysed system.

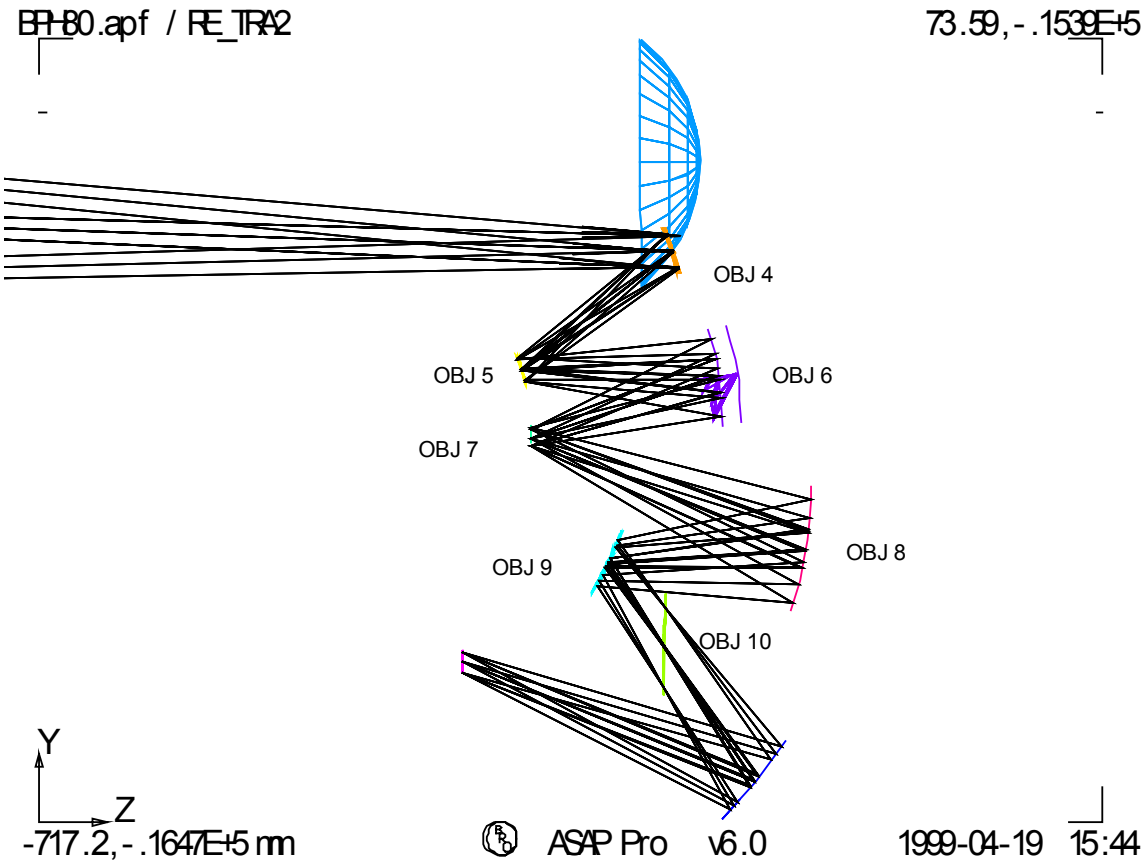

Figure 9.1-2 ASAP ray-trace of all FPU objects in the analysed system.

Component name	ASAP object number	Aperture radius, mm (see BOLPHT80.INR)
Detector	12	
Mirror	11	
Cold stop	10	
Mirror M8	9	
	8	
Pick-off M6	7	
Mirror M5	6	
Chopper M4	5	
SPIRE input mirror M3	4	
Telescope FP sphere	3	
M1 cut-out	16	139.9
M2	2	139.9
M1	1	1750
Telescope centre obscuration	13	
Sky	14	

Table 9.1-1 Components of the ASAP model linked to ASAP object numbers

9.2 Method

The beam is propagated stepwise through the system, and is analysed at each component to give the beam profile. This is given in terms of optical intensity, i.e. flux per unit area. In this version all patterns show relative intensity only.

Any clipping which occurs is implemented at the component and the clipped beam is then propagated onwards.

The propagation is outwards from the detector (time-reversed).

9.3 Spatial resolution of clipping edges

As for any finite-element based numerical model, spatial resolution limits arise, and in this optical case these are that the element size must be > λ. The beam propagation algorithm requires that the spacing between rays is always much greater than the wavelength. In the results this limitation gives errors which increase during the reverse ray-trace and so are largest at the telescope mirrors.

As a result the diffraction actually modelled is that from a 'soft-edged' aperture, rather than the real 'hard-edged' aperture (a top-hat function energy transmission). As to the consequences of this, from the principles of Fourier optics we can say that the limited spatial resolution of the beam limits the angular range of the energy pattern in the far-field. Therefore the energy at larger diffraction angles is underestimated in the present analysis. The far-field angular range at which this effect is significant is estimated as roughly (λ/d) where d is the pupil ray spacing (spatial resolution).

The patterns shown here are accurate in the far-field up to approximately N times the Airy disc equivalent angular radius (λ/D where D is the pupil diameter), for N spatial samples across the beam.

The beam within the instrument is defined by the cold stop edge (object 10, D=55mm), where 32 spatial samples are used (giving a spatial step size of 55mm/32 = 1.7, which is approximately. 3λ), and so is accurate in the far-field out to approximately the 30th Airy ring. In the telescope, the larger apertures allow a bigger value for N to be used and here it is limited, by the computation times possible to date, to N=200.

9.4 Plane of analysis

The plane at which the beam is analysed should ideally lie close to the component surface. The orientation of the analysis plane is parallel to the component aperture and is situated at a position close to this aperture (this is not necessarily on the vertex of the component surface except in the case of planar objects).

For simplicity here we make the analysis only as a one-dimensional profile across the 2-D beam. The direction of the profile is in X or Y, and this is labelled at bottom left of each plot. For X this refers to the direction perpendicular to the plane of incidence (which for a system

folded within the Y-Z plane only is also the global X-axis) whereas for Y it refers to direction parallel to plane of incidence.

9.5 Results

All plots show the normalised beam flux versus position in mm. The object number is displayed at the top left and the plot direction (X or Y) is shown at the right of the horizontal axis. The plots are here presented in the order of outward propagation (as per the list in the above table).

Because a top-hat beam shape is used (mimicking the case of a 'bare', point-like detector), the beam pattern from the detector is first defined at the system exit pupil location (determined from the geometric ray-trace), where it is given uniform amplitude & spherical wavefront (centred on detector position). The edge-clipping is described at limited resolution as explained above.

9.5.1 ASAP Beam patterns inside the FPU

The beam described above is propagated into the system, and the pattern is first analysed at the cold stop (the System Pupil Stop).

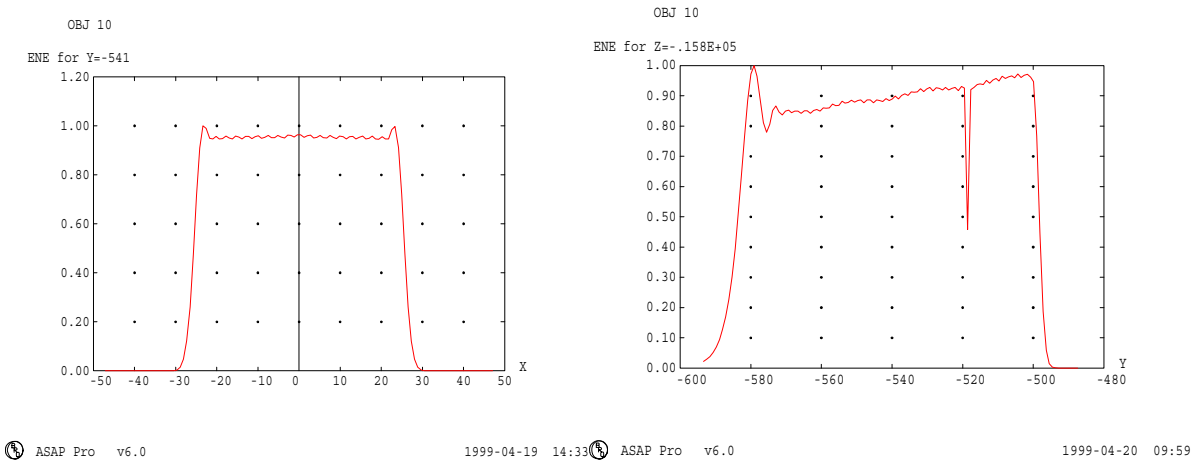

Figure 9.5-1 ASAP Beam pattern at the cold stop (object 10)

Here the pattern has a nearly top-hat shape, but with rounded edges due to the limited edge-resolution, and some fringing caused by the cold stop edges not corresponding exactly to the exit pupil edges (i.e. pupil aberration). The slope in the Y-direction plot is due to the effect of the non-collimated beam incident on a tilted component, and this tilt also leads to the beam appearing to be wider in this plot. . The single drop-out data point near 520mm in the Y-plot is due to ray-trace errors which begin to arise when working close to the spatial resolution constraint of section 9.3.

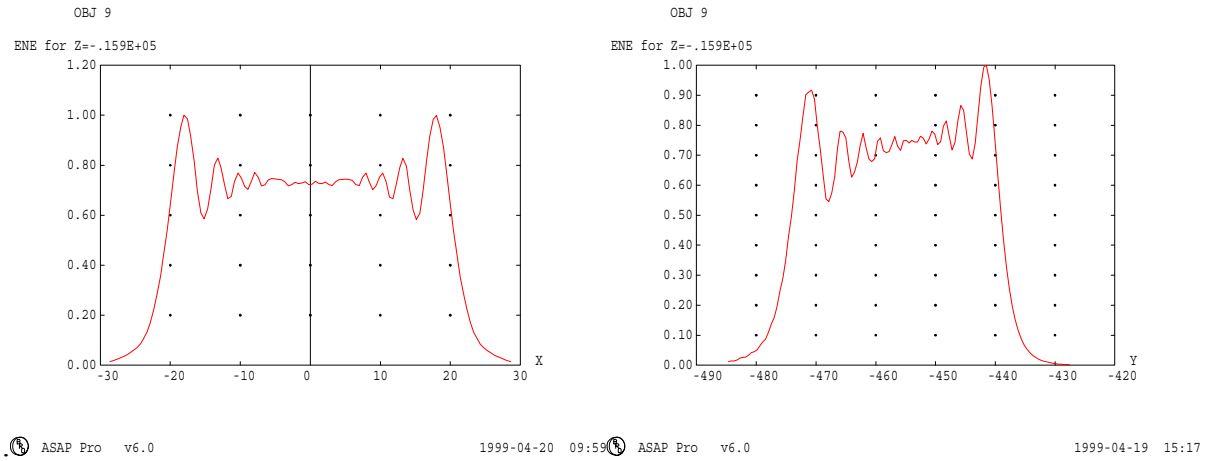

Figure 9.5-2 ASAP Beam pattern at mirror M8 (object 9)

At mirror M8 (object 9, figure 9.5-2) fringes begin to appear in the beam and these fringes are stronger at mirror M7 (object 8, figure 9.5-3).

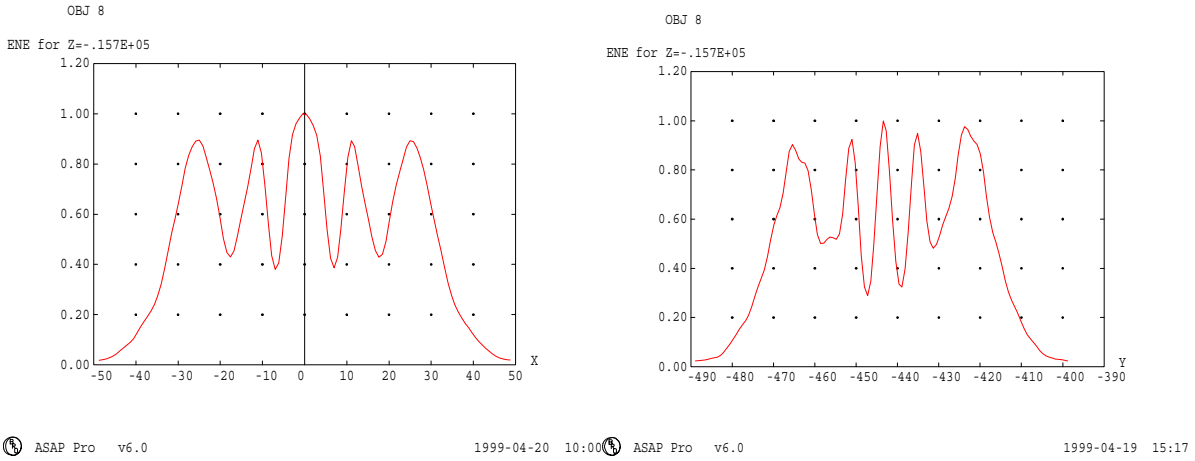

Figure 9.5-3 ASAP Beam pattern at mirror M7 (object 8)

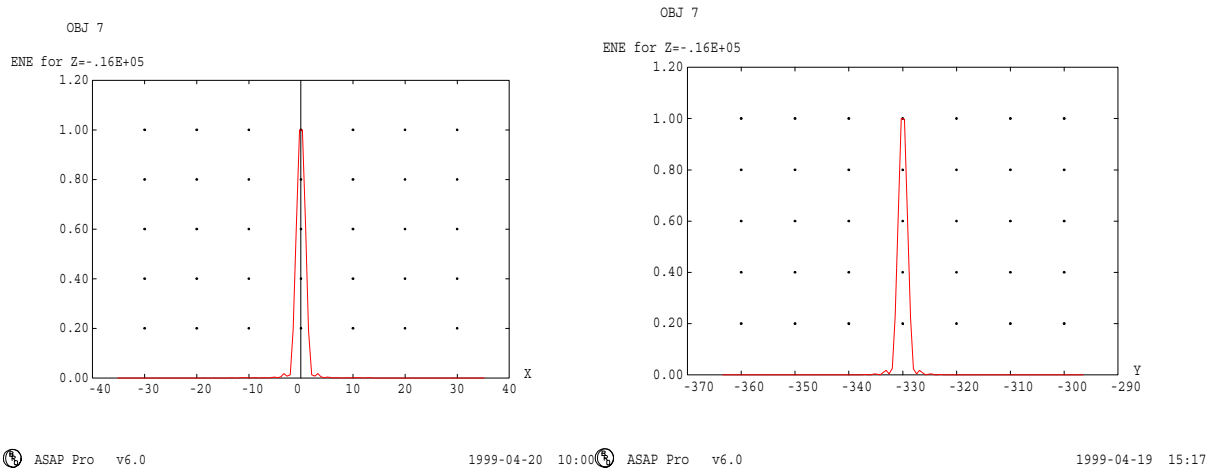

Figure 9.5-4 ASAP Beam pattern at mirror M6 (object 7)

M6 is located at a focal plane and here the beam has a form like an Airy-pattern.

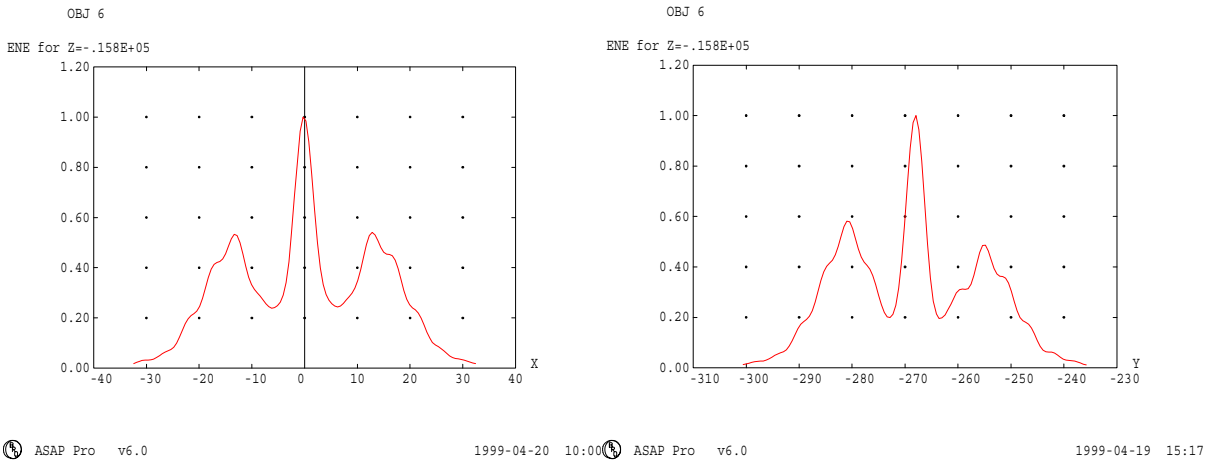

Figure 9.5-5 ASAP Beam pattern at mirror M5 (object 6)

Mirror M5 (object 6, figure 9.5-5) is relatively close to an image plane, so the pattern has a mixed far/near-field shape.

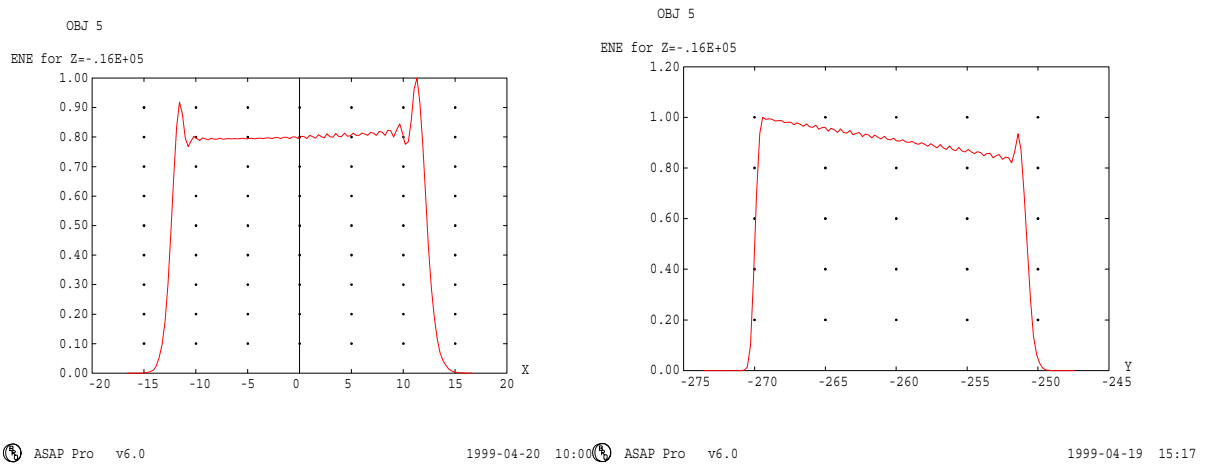

Figure 9.5-6 ASAP Beam pattern at mirror M4 (object 5).

The chopper mirror M4 (object 5, figure 9.5-6) is at a pupil plane (conjugate to the cold stop), and so here the beam again has a top-hat shape.

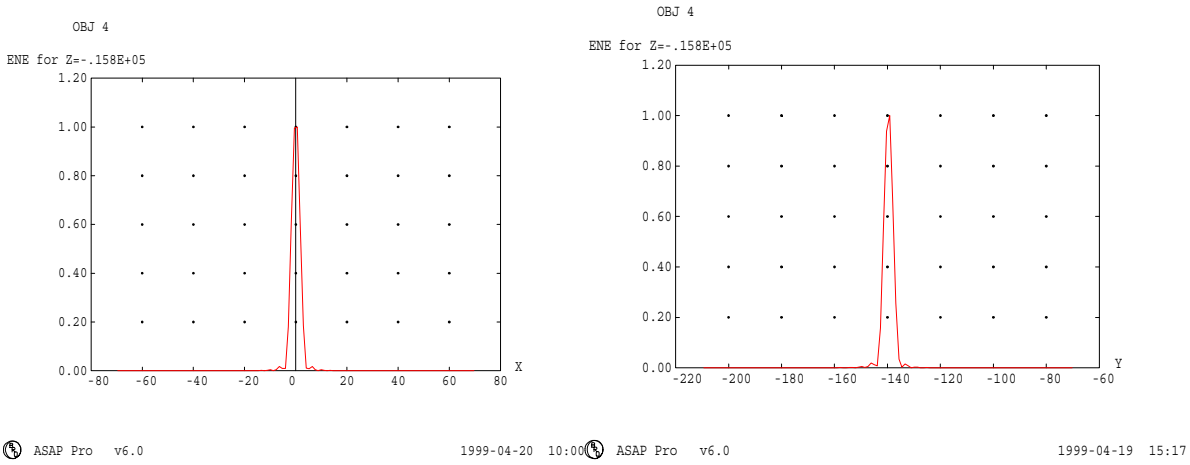

Figure 9.5-7 ASAP Beam pattern at mirror M3 (object 4) at the telescope focal surface.

At this component, the patter is affected by spatial filtering (field stop beam clipping). Although this is here described as occurring only at the telescope image plane (M3 mirror, object 4), in the final design it will probably be applied at an earlier focal plane. The pattern as clipped by this component is shown below. The plot is in energy units, with a logarithmic vertical scale extending from log (10^{-6} to 10^{0}).

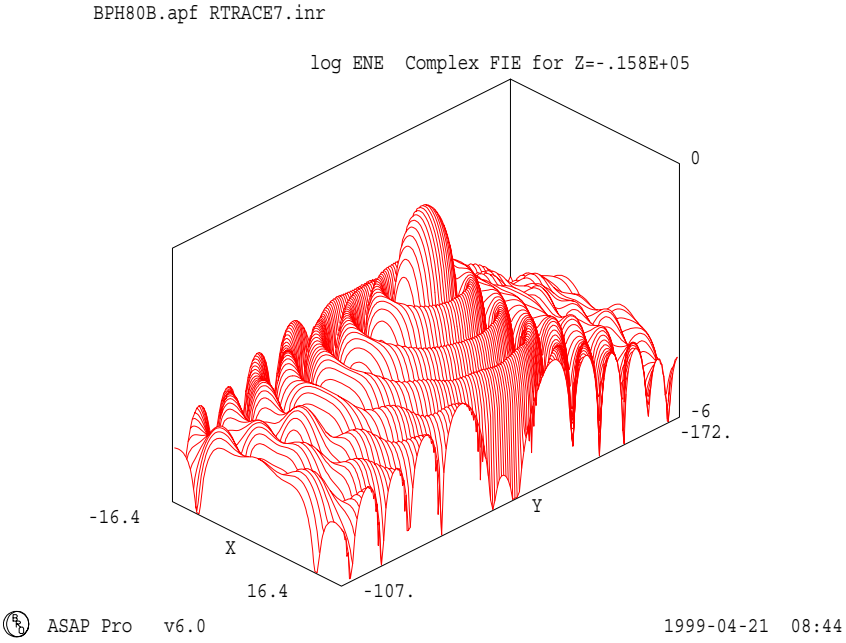

Figure 9.5-8 ASAP Beam pattern as clipped at M3.

9.5.2 ASAP Beam patterns in the Telescope

For the beam in the telescope, because of the larger size of the components in the telescope (larger relative to λ), the beam-clipping can be described at higher spatial resolution and so the relevant patterns appear with sharper edges.

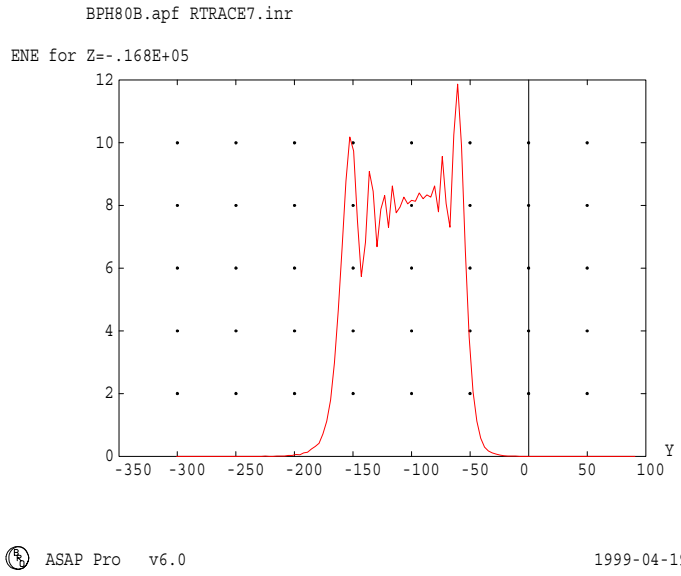

Figure 9.5-9 ASAP Beam pattern at the primary mirror (M1, object 16) hole.

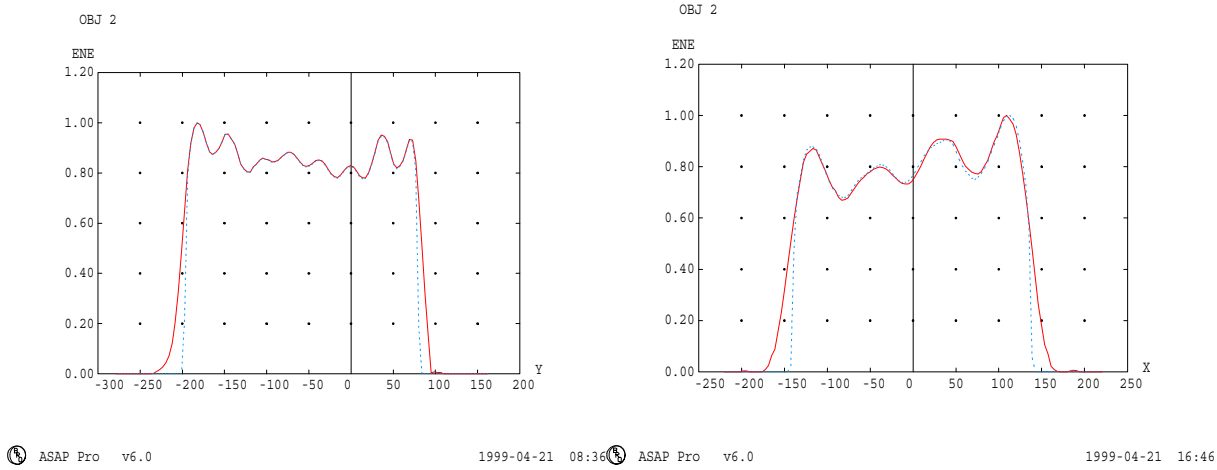

Solid line = incident beam, dotted line = clipped reflected beam.

Figure 9.5-10 ASAP Beam pattern at the secondary mirror (M2, object 2)

At the secondary mirror M2, the reduced edge-resolution of the beam arising from spatial filtering is evident. Because by design the FPU instrument pupil is not undersized with respect to that of the telescope (no Lyot stop action), the beam has some spill over at M2, and so is clipped by the M2 edges as shown by the dotted line profile in figure 9.6-2. The onward propagation is of the clipped beam. The spatial resolution used is N=120.

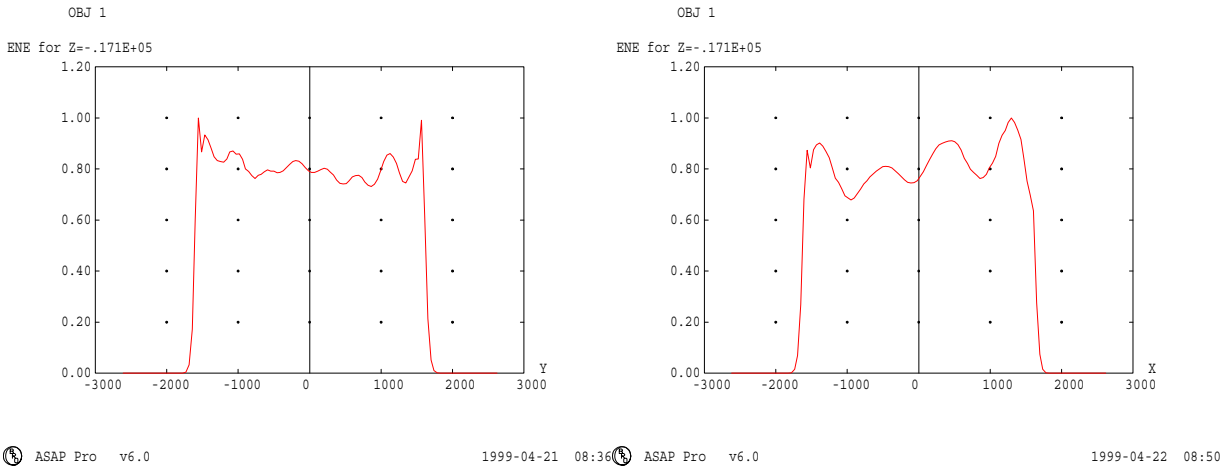

Figure 9.5-11 ASAP Beam pattern at the primary mirror (M1, object 1).

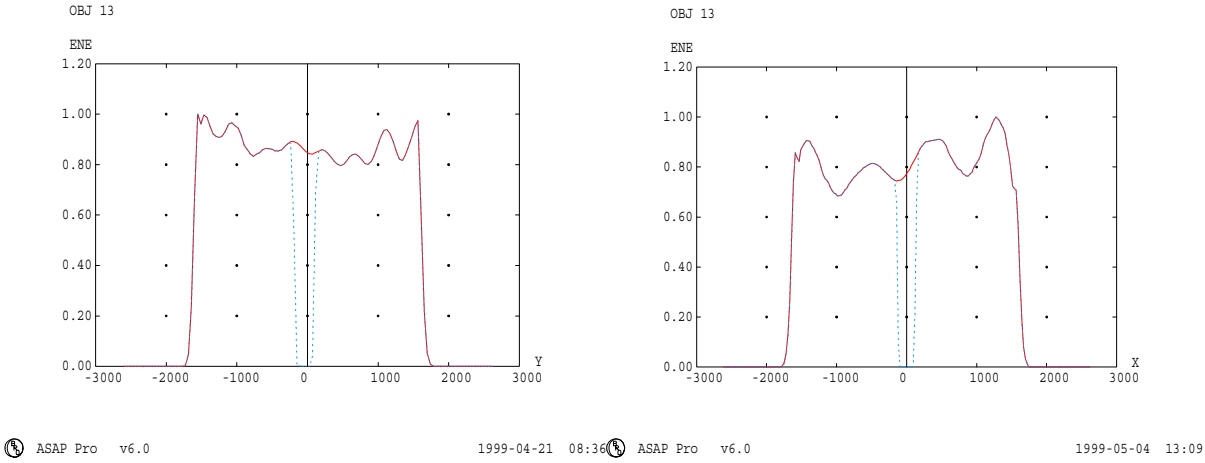

Figure 9.5-12 ASAP Beam pattern at the plane of the central obscuration (object 13).

Here the clipping by the central obscuration (same size as M2) is applied, shown in figure 9.6-4 by the dotted lines. The limited resolution of the central obscuration is due to the spatial resolution (pixel size) which is 2500mm/200 points = 25mm, as compared to the obscuration diameter of 280mm.

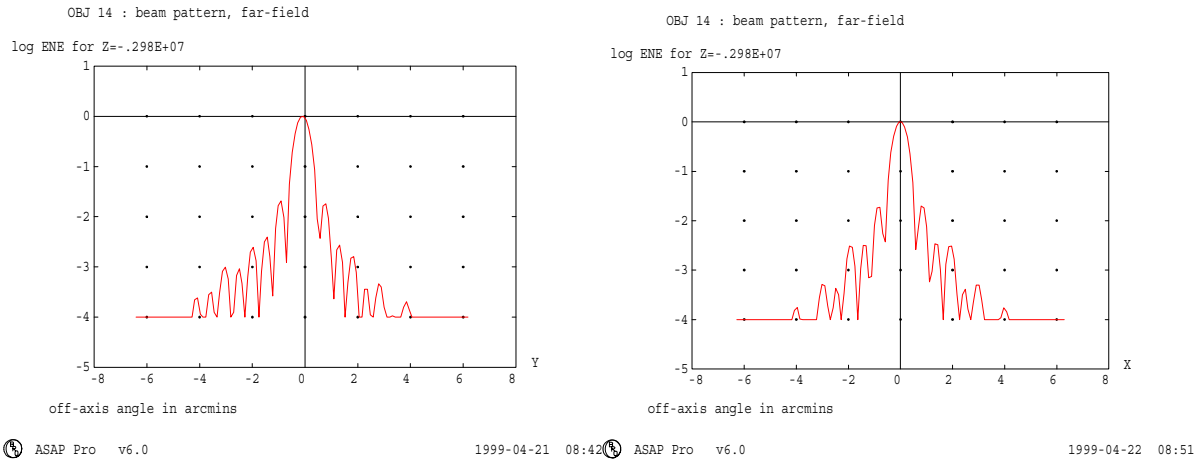

Figure 9.5-13 ASAP Far field beam pattern on the sky.

The far field beam pattern on the sky represents the point-source-transmittance (PST) response function of the instrument as modelled. For the case of a 'bare' detector of finite spatial size, the PST may be obtained as the convolution of the above response with the detector geometric footprint, providing that the following assumptions apply over the FOV angular range of analysis:

1. The change in aberration is negligible.
2. The change in clipping by components is negligible.

The second assumption should hold well for detectors near the centre of the arrays (as here), but becomes invalid for those close to the array edge, where clipping by components other than the pupil and field stops is added, and that by the field stops becomes severe.

9.6 ASAP References

1. "Multiple beam clipping in far infrared & sub-millimetre space instruments: ISO-LWS and FIRST-SPIRE." M Caldwell, P F Gray & B Swinyard. SPIE. Vol. 3426. Stray-light & system optimisation. (July 1998).
2. "Test of a ray-trace method for antenna systems design" M Caldwell & P F Gray. Int. J. IR & MM-waves. Vol.20, No.2, pp.279-303 (Feb.1999).
3. "Trade-off in beam shape & size in telescope" SPIRE tech note RAL-NOT-000118.

10. SUPPLEMENTARY ELECTRONIC FILES

This report for ESA is supplemented by electronic copies of all the APART files mentioned within the text, plus copies of all other WORD documents (*.DOC) and MATHCAD documents (*.MCD) mentioned. All of these files will be made available to ESA on 3 ½ inch disks or by anonymous FTP from the following address: TBD.

10.1 APART model files

These are text files written using the APART (© BRO) command and macro language.

Program 1 input files required to build the geometry are listed in table 6.1-1.
Program 2 input files used to generate transfers are listed in table 7.4-1.
Program 3 input files used to test thermal emission calculations are listed in table 8.3-1.

10.2 APART model summary files

The following text files referred to in the report summarise the APART object numbers and their surface properties and temperatures for both the new APART model and the model as received at the start of the study. The files are in Microsoft © WORD 97 format:

FIRST_SURFACE_NUMBERS_OLD.DOC
FIRST_SURFACE_NUMBERS_NEW.DOC
FIRST_SURF_TEMP_EMISS_COAT_OLD.DOC
FIRST_SURF_TEMP_EMISS_COAT_NEW.DOC

10.3 MATHCAD files

The following text file, in MATHCAD format, was used to produce the sun shield shadow diagrams in figure 5.1-4.

SUNSHADOW.MCD

10.4 ASAP files

The following text file, written using the ASAP (© BRO) command and macro language, was used to produce the ASAP analysis data in section 9:

BOLPHT80.INR

11. A NOTE ON DIMENSIONS USED

All linear dimensions specified in the figures are in millimetre units. All angles are specified in degrees.